REPORT DOCUMENTATION PAGE

Form Approved
OMB No. 0704-0188

1. AGENCY USE ONLY (Leave blank)	2. REPORT DATE	3. REPORT TYPE AND DATES COVERED
	2/25/98	Final 9/30/90 - 3/31/98

4. TITLE AND SUBTITLE
MIT Microwiggler for Free Electron Laser Application
Non-perturbative Electron Beam Characterization with a Microwiggler

5. FUNDING NUMBERS
N00014-90-J-4130
s400091scu01

6. AUTHOR(S)
Prof. Hermann A. Haus for Prof. George Bekefi

7. PERFORMING ORGANIZATION NAME(S) AND ADDRESS(ES)
Research Laboratory of Electronics
Massachusetts Institute of Technology
77 Massachusetts Avenue
Cambridge, MA 02139

8. PERFORMING ORGANIZATION REPORT NUMBER

9. SPONSORING/MONITORING AGENCY NAME(S) AND ADDRESS(ES)
Office of Naval Research
800 North Quincy Street
Arlington, VA 22217

10. SPONSORING/MONITORING AGENCY REPORT NUMBER

11. SUPPLEMENTARY NOTES
The view, opinions and/or findings contained in this report are those of the author(s) and should not be construed as an official Department of the Army position, policy, or decision, unless so designated by other documentation.

12a. DISTRIBUTION/AVAILABILITY STATEMENT
Approved for public release; distribution unlimited.

12b. DISTRIBUTION CODE

13. ABSTRACT

The potential of undulators to provide beam diagnostic information has been cited in the literature for many years. We demonstrate that while important parameters describing the beam - the energy, energy spread, divergence, spot size, matching and bunchlength - are convolved together in the synchrotron emission, a careful experimental setup can extract divergence, energy spread and bunchlength from this convolution.

The MIT microwiggler is uniquely suited for the development and testing of electron beam diagnostic techniques. A pulsed electromagnet with long length and extensive tunability, it provides flexibility and high quality at a period short enough to produce visible radiation at moderate beam energies (40-55 MeV). We have achieved a field uniformity of 0.08% in rms peak amplitudes and have performed measurements to test this claim against a comprehensive set of criteria, thus marking the first time this figure of merit has been reduced below 0.1% in any sub-cm period wiggler. Studies with electron beam were performed at the Accelerator Test Facility at BNL. The long term statistics collected of the wiggler performance under full operation will be documented.

The production of visible radiation, where numerous diagnostics are readily available, makes single shot techniques a special strength of the microwiggler. We have developed a family of beam diagnostic techniques with the wiggler, making use of the spectrum, spatial profile, and fluctuational characteristics of its emissions. Cone measurements are used to characterize divergence and energy spread. The systematic diagnosis and understanding of the spontaneous emission characteristics is important in determining when Self Amplified Spontaneous Emission begins. This is discussed in the context of measurements of SASE at 1.064 microns. Studies were performed of the fluctuational characteristics of the spontaneous emission and experiments motivated by the potential of the fluctuations to provide beam diagnostic information were carried out. Systematic measurements of the fluctuations in the wiggler emission spectrum from a single micropulse were performed as a function of beam bunchlength and an effective bunchlength monitor was demonstrated.

19980303 095

14. SUBJECT TERMS

15. NUMBER OF PAGES

16. PRICE CODE

17. SECURITY CLASSIFICATION OF REPORT	18. SECURITY CLASSIFICATION OF THIS PAGE	19. SECURITY CLASSIFICATION OF ABSTRACT	20. LIMITATION OF ABSTRACT
UNCLASSIFIED	UNCLASSIFIED	UNCLASSIFIED	UL

Grant No. N00014-90-J-4130
September 30, 1990 – March 31, 1998

Final Technical Report
MIT Microwiggler for Free Electron Laser Applications

Non-perturbative Electron Beam Characterization with a Microwiggler

Submitted by:

PI: Professor Hermann A. Haus, MIT
for PI: Professor George Bekefi, MIT
Co-thesis supervisor: Professor Jonathan S. Wurtele, U. of CA at Berkeley

on February 12, 1998

Abstract

The potential of undulators to provide beam diagnostic information has been cited in the literature for many years. We demonstrate that while important parameters describing the beam - the energy, energy spread, divergence, spot size, matching and bunchlength - are convolved together in the synchrotron emission, a careful experimental setup can extract divergence, energy spread and bunchlength from this convolution.

The MIT microwiggler is uniquely suited for the development and testing of electron beam diagnostic techniques. A pulsed electromagnet with long length and extensive tunability, it provides flexibility and high quality at a period short enough to produce visible radiation at moderate beam energies (40-55 MeV). We have achieved a field uniformity of 0.08% in rms peak amplitudes and have performed measurements to test this claim against a comprehensive set of criteria, thus marking the first time this figure of merit has been reduced below 0.1% in any sub-cm period wiggler. Studies with electron beam were performed at the Accelerator Test Facility at BNL. The long term statistics collected of the wiggler performance under full operation will be documented.

The production of visible radiation, where numerous diagnostics are readily available, makes single shot techniques a special strength of the microwiggler. We have developed a family of beam diagnostic techniques with the wiggler, making use of the spectrum, spatial profile, and fluctuational characteristics of its emissions. Cone measurements are used to characterize divergence and energy spread. The systematic diagnosis and understanding of the spontaneous emission characteristics is important in determining when Self Amplified Spontaneous Emission begins. This is discussed in the context of measurements of SASE at 1.064 microns. Studies were performed of the fluctuational characteristics of the spontaneous emission and experiments motivated by the potential of the fluctuations to provide beam diagnostic information were carried out. Systematic measurements of the fluctuations in the wiggler emission spectrum from a single micropulse were performed as a function of beam bunchlength and an effective bunchlength monitor was demonstrated.

Table of Contents

CHAPTER 1: INTRODUCTION

The MIT Microwiggler is a 70 period, planar, pulsed electromagnet which is unique for its short period, its extensive tunability and its rigorous design, through which record field precisions have been reached for sub-cm period wigglers. A microwiggler, a wiggler with period less than 1 cm, permits higher frequency radiation to be generated at a given beam energy than wigglers of the usual design (3-10 cm period). This report will

describe work continuing the technological development of the wiggler, and will report on a growing family of single shot beam diagnostic techniques which have been demonstrated with the wiggler. The results from an FEL program of experiments will be documented.

In this chapter, we define the main areas in which research was performed and explain the motivation for the new directions of the research. A succinct statement of the experimental results is contained in Chapter Five.

1.1 Microwiggler technology

1.1.1 ***Motivation***. Microwiggler-based experiments depend critically on high field precision. Field errors translate into angular errors in the electron trajectory and culminate in walkoff of the beam from the desired line of travel and phase errors in the periodic motion. Considerable theoretical effort has been delegated to determining acceptable levels of field errors by studying reduction in spontaneous emission peak power and small signal gain for large collections of non-ideal profiles. The correlation between field error and performance is not straightforward unless the field error is sufficiently small[i]. Furthermore, it is especially important to solve the problem of high field precision as the wiggler period is shortened, because the tradeoffs involved in achieving higher frequencies work against the other parameters required for good gain and spontaneous emission power, such as field strength.

The attainment of high field precision in a microwiggler is a difficult engineering problem and can be costly to implement. At this length scale, typical machining tolerances are large enough compared with the wiggler period to cause significant field errors. The seriousness of the problem compounds with wiggler length; a design for a high precision short wiggler prototype may not necessarily scale to its longer descendant. For instance, there are manufacturing limitations on the machining of long lengths of a material. This has led a number of groups to implement the full-length wiggler as a concatenation of separate sections, which creates its own problems. Another difficulty is the achievement of accuracy in the measurement of fields over long distances.

1.1.2 ***Previous work.*** Various technologies for microwiggler construction were under investigation at the start of this work. Since then, experimental programs using a few of these wigglers have reported results, ranging from at least one successful infrared FEL (10 microns) to at least one abandoned technology (slotted tube pulsed wigglers).

The former is the design of Professor Pantell[ii] and graduate students, and is based on the staggered array principle. In this structure, immersing an alternating array of magnetic pole pieces in a strong longitudinal solenoidal field produces the transverse periodic magnetic field. A large longitudinal magnetic field component remains, available for beam confinement. Thus, the design is particularly suited for lower beam energies (1-10 MeV). Very high field strengths (1 Tesla) were achieved through small gap design. However, the field uniformity, at 1.2% rms spread, was not high.

The slotted tube microwiggler[iii] is the work of Roger Warren at Los Alamos National Laboratory, and was a novel idea for overcoming by a unique construction the

reduction in field strength which plagues short period wiggler design. Large pulses of current (25 kA) were passed through a single copper tube, with slots machined periodically along the length of the tube to produce the transverse field along axis. Wiggler of 5 mm period were constructed with field strengths as high as 1 Tesla. The difficulty which the authors cite as the reason they discontinued development was the presence of large bending and defocussing field error components. The intense currents required for the high field strengths created time dependent, heating-induced resistance changes near the slots. This resulted in field errors which were highly time-dependent, and narrowed the operating window to about 1 microsecond, which is too small for practical use.

At CREOL, an 8 mm period permanent magnet wiggler[iv] has been constructed, culminating in an 185 period microwiggler with a 0.2% field uniformity. Field errors were reduced through sorting and shimming techniques. This wiggler is particularly notable for its long length and good field uniformity. However, the peak field strength is limited to 0.2 Tesla.

1.1.3 ***The device.*** The MIT microwiggler provides a unique answer to the engineering challenges of short period wiggler design. It provides a high field strength (0.45 Tesla) over a long length (70 periods) at a very short period (8.8 mm), giving 0.37 for the wiggler parameter, $a_w = \frac{eB_w\lambda_w}{2\pi m_e c}$. This figure of merit is a measure of the angular kick to the electron created by the flux of each pole of the wiggler, being proportional to the pole integral through the product of peak field strength B_w and wiggler period λ_w. m_e is the electron rest mass and c is the speed of light. When a_w is 0.37 and γ=100, the

radiation wavelength is 532 nm and the amplitude of the electron oscillation in the wiggler is about 5 microns. The wiggler parameter is thus large enough to provide an experimentally useful number of photons in 70 periods but the movement of the electron is small compared with a typical electron beam radius of 200 microns. As an aside, note that this is a convenient attribute for a non-perturbative beam diagnostic.

1.1.4 ***New directions.*** Unlike its counterparts, extensive tunability and a novel tuning algorithm designed for real-time control of the 140 available degrees of freedom characterize the MIT microwiggler. We will describe a comprehensive set of field measurements made to investigate the limits of tunability of the microwiggler and to support a claim of 0.08% rms in peak amplitude variation. Following the description of the wiggler and magnetic measurements, some proposals for future work are made. The scaling of this wiggler design to even shorter periods is discussed. A bottleneck lies in the errors not in the longitudinal direction, but the transverse direction, that is, in the position of the magnetic centers.

Finally, simply from the point of view of microwiggler technology, it is important to know how a completed microwiggler performs in the long term. There has been very little reported on the long-term evolution and survival of the initial field characteristics of either microwigglers or larger period wigglers, although questions on this topic have been raised frequently at Conferences. Radiation damage to permanent magnets is one cause for wiggler deterioration on installation in a beamline. Simple mechanical shifting is another. After several years of intensive operation of this microwiggler at a Users Facility, we can now provide information about these statistics for this microwiggler.

1.2 Non-destructive beam characterization with a microwiggler

1.2.1 ***Motivation.*** It has long been recognized, in theoretical studies[v,vi], that wiggler spontaneous emission has the potential to serve as an important non-perturbative beam diagnostic. Until recently, it was difficult to infer beam parameters such as emittance and energy spread because of resolution limitations, exacerbated by numerous inherent spontaneous emission broadening sources and there was an absence of a practical system which can execute such a measurement in a single shot. Experimental work has been performed in storage rings and a 100 MeV linac and proposed. In particular, electron beam divergence has been extracted from the spatial profile of 31.1 Å spontaneous emission at the ALS. However, work at these beam energies generally occurs with long period wigglers (up to 5 cm period), while at 50 MeV setting the wavelength in an optimal range requires a wiggler with far shorter period which has high field quality over a large number of periods.

With the MIT Microwiggler, we have the opportunity to develop techniques to resolve beam characteristics, making use of a wide range of optical diagnostics which are available in the wavelength range of the emissions. We have emphasized the development of single shot techniques.

1.2.2 ***Previous work.*** Comprehensive descriptions of the effect of beam parameters on wiggler spontaneous emission can be found in the literature. K.-J. Kim[v]

has derived an expression for the full spectral angular dependence of spontaneous emission, including harmonics, and has proceeded to analyze a variety of special cases which are experimentally useful, with special emphasis on the forward emissions. Examples are spontaneous emission power in the forward opening angle integrated over frequency, spectral dependence at a fixed angle, width of emissions at the on-axis resonant frequency, and so forth. He includes the effects of inhomogeneous broadening by postulating Gaussian distributions in beam energy spread, divergence, and transverse shape, and calculates their effect on spectral width by convolving with the natural lineshape. Dattoli[vi] *et al.* have written a Monte-Carlo spontaneous emission code in which the Lienard-Wiehert integrals are evaluated for a given initial phase space distribution of electrons and wiggler field profile. They have performed detailed comparisons of simulations with their analytic expressions for various length wigglers and field strengths, at the fundamental and at harmonics. They comment in their work on the difficulty of extending their theory to experiment because of complications from realistic wiggler errors.

Alex Lumpkin at the Advanced Photon Source has performed a body of work in the area of beam diagnosis with undulator radiation and his publications, which include a comparative review[vii] of present beam diagnostic techniques, are an excellent source of information on experimental work in the area. In 1990, he performed time resolved measurements of spontaneous emission at 650 nm generated by the 2.18 cm period, 5 meter Boeing wiggler at a beam energy of 110 MeV with a streak/spectrometer with the purpose of studying the electron beam properties at the wiggler location[viii]. The spatial profile, spatial position, and energy of the electron beam were extracted from the

measurements. Their streak camera was capable of resolving not only submacropulse time-scales but submicropulse. Micropulse length and spectral shifts across the macropulse were recorded. Their studies of the spontaneous emission, both at the fundamental and 2nd harmonic, led to techniques which debugged problems in the FEL setup which were preventing first observations of lasing.

In 1995, A. Lumpkin and co-workers published new work detailing an approach for quantitative measurements of emittance and energy spread directly from spontaneous emission[ix]. In this case, the target beam for analysis was at 7 GeV, with nominal emittance of 8×10^{-9} mm.mrad. Design studies were performed for two possible configurations: the single pass undulator and the optical klystron. Harmonics are chosen to increase sensitivity to changes in the beam characteristics. For the single pass undulator, while the authors suggest emission power and spectral content as measured parameters. They performed simulations of the spatial profile of the harmonic and spectral characteristics off-axis. For the optical klystron configuration, simulations were done for harmonics with and without nominal beam emittance, and with and without 0.1% energy spread and excellent sensitivity was observed. Emphasis was placed on keeping the cone angle considerably smaller than the opening angle of the beam divergence in this article.

Experiments in undulator-based beam diagnosis have taken place at the ALS at LBL, also in the GeV beam energies, using both the fundamental and the harmonic of undulator radiation[x]. This group has estimated beam emittance from narrow bandwidth measurements of the red-shifted spatial profile and theoretical knowledge of the storage ring beta function. The undulator radiation was centered in the X-ray wavelengths for the

5 cm period wiggler used. A. Lumpkin has also applied this technique in storage rings at the APS at 7 GeV using red-shifted third harmonic radiation from a 3.3 cm period wiggler. Unlike the previous work, which required point-by-point repositioning of the detector, a two-dimensional image was recorded by using a crystal to up-convert the radiation to the visible wavelengths.

Experimental work in extracting beam emittance using wiggler radiation has been performed in France at the ESRF on a storage ring[xi]. In this technique, which occurs in the X-ray regime, Bragg reflection is used to select a narrow bandwidth portion of the spontaneous emission, and to relate the emission spot size to beam parameters. Care is taken to restrict the measurement to the on-axis frequency alone, so that cones of spontaneous emission are avoided. The image size, in combination with knowledge of the beta function of the beam, gives beam emittance. The measurement has been incorporated into the control system of the accelerator.

An intriguing proposal exists in the literature for the use of a very short period undulator as a beam diagnostic. John Madey's group at Duke is constructing a five period wiggler which has the unique property of transparent sides to allow for measurement of emissions at large angles (up to 90 degrees)[xii]. While a short period prototype can be constructed faster than a high precision, longer wiggler, a number of tradeoffs exist which favor longer wigglers for the purpose of beam diagnosis.

1.2.3 ***New directions.*** We will describe a family of single shot beam characterization techniques demonstrated during the course of the work. We will discuss extraction of beam divergence, Twiss parameters, energy spread and bunchlength from

the wiggler emissions and present systematic studies of the emissions as a function of a variety of beam and wiggler parameters.

We performed experiments on narrow-bandwidth emission cones in the spatial profile[xiii]. These are the first measurements of this kind performed with a beam produced by an S-band linac, and as a result our analysis included issues which could be ignored in the storage ring experiments[xiv]. For example, in the parameter regime in which the on-axis null first appears, the contribution from energy spread and divergence are comparable for our machine parameters, and we would not have been able to separate out divergence from a single cone measurement similar in form to that in Figure 5 in reference [xv]. They are also the only such measurements performed with a microwiggler. These experiments also differ from other work in being single shot measurements without the need for up- or down-conversion to reach the visible wavelengths. Photon production was sufficient for recording a narrow bandwidth portion of a 2nC total macropulse charge in a single shot with a garden variety CCD camera. Single micropulse cones at much lower charge were easy to capture with an intensifier.

The usefulness of the wiggler as a beam diagnostic is greatly enhanced if the measurements do not require averaging, over many shots, or over many micropulses. One motivation for reducing the number of shots required to monitor beam quality is the move toward computer automation of operations of accelerator facilities. Currently, one of the user groups at ATF, Vista Corporation, is designing a new generation control system for the facility. The time for such a system to receive feedback about the beam can influence its success. In the case of the work at the ALS, which makes use of X-ray emissions, a large number of shots are averaged. An emphasis on a minimum-shot

technique will be included in the design on diagnostic techniques with the wiggler. In particular, one of our goals is to extract a figure for both beam divergence and energy spread from a single shot.

A possible avenue of development unique to a tunable wiggler is highlighted by a comment in reference [xvi]. Theoretical work, which had the purpose of determining the optimum choice of wiggler configuration for beam diagnosis, was limited by a computation time of 20 hours per grid point. A wiggler which offers speed in going from configuration to configuration is a useful design tool. A few possible profiles which could be tuned into the wiggler in the future for diagnostic research are discussed.

1.3 Fluctuation-based bunchlength monitor

1.3.1 ***Motivation and previous work.*** One way to expand the diagnostic repertoire of the wiggler is to consider a wider class of e-beam signatures in the emissions than only broadening by distributions in parameters. Such a signature is the fluctuation in the emitted radiation that originates from shot noise of the electron bunch.

Bunchlength diagnostic procedures which are put to use in practice have some common disadvantages. They are usually invasive, requiring significant adjustments to the beam tune. They can also be time consuming, at best multi-shot and at worst completed on a time-scale comparable to drifts in the machine. Furthermore, if the trend to produce shorter and shorter microbunches continues, current techniques will not provide the required resolution at less than 1 ps, particularly during developmental stages

when charge and power levels are not optimal. Single shot parameters only make the problem more difficult.

A common solution to the diagnostic problem is to transfer the bunch profile to a more easily measurable parameter, by deliberately introducing a calculable correlation between time and the desired output parameter. At Jefferson Lab[xvii], a time-height correlation has been chosen, enabling time slices to be selected by a collimating slit. At the ATF, a time-energy correlation is induced by adding an energy chirp to the beam, dispersing it with a bending dipole, and again selecting time slices with a slit. The resolution limitation in the latter case, which is 1 ps, arises from the betatron size of the electron beam cross section at the high energy slit, and the unmeasured intrinsic energy spread. Both of these must contribute negligibly to the beam size at the slit compared with the energy chirp in order for an accurate measurement to take place.

The need for new techniques to measure bunchlength is indicated in a recent surge of publications which propose or test new procedures. Additional discussion and a list of collections of related articles is contained in reference xv. Transition radiation, a well-proven diagnostic for numerous beam parameters[xviii,xix], is a favored choice, and its sibling, diffraction radiation, is attracting interest because it does not scatter or stop the electron beam.[xx] Some bunchlength techniques are based on interferometry, usually with transition radiation[xxi,xxii] and a tomographic approach has been demonstrated[xxiii]. Others make use of the bunchlength-dependent form-factor associated with coherent enhancement. Krafft *et al.*[xxiv] have sped up the bunchlength measurements for their experiments by calibrating the quadratic variation of coherently enhanced synchrotron radiation power against an independent measure of the bunchlength. D. Nguyen has

proposed the use of the intensity distribution of off-axis Smith Purcell radiation. This distribution is related to bunchlength through the form factor for coherent enhancement, which takes on an angular dependence because of phase matching. Note that for bunchlengths typical of most machines, the latter techniques are best tested in the infrared or far infrared wavelengths. Streak cameras, although costly, are a favored solution, and can be operated in single-shot mode, as well as synchroscan. Picosecond resolutions are common, while state-of-the-art units currently advertise resolution of about 200 fs. The minimum detectable power and useful wavelength range is limited by the quantum efficiency of the MCP photocathodes. For all of these techniques, when scaling to shorter bunchlengths, the resolution requirement and radiation levels are difficult obstacles to surmount.

1.3.2 ***Proposed technique.*** The fluctuation-based bunchlength detector we hope to demonstrate is based on the techniques proposed by M. Zolotorev and described in references [xxv] and [xxvi]. It is attractive because it is expected to work well at bunchlengths below 200 fs. In fact, a beneficial tradeoff exists which is intrinsic to the theory and says that the spectral resolution requirements become less strict as the bunchlength becomes shorter. The method can be implemented at low power levels (less than 1 pJ), and is non-invasive. The additional equipment requirement beyond the source of incoherent radiation is relatively simple. It is inherently a single shot method, and the immediate feedback it would provide avoids the nagging questions which arise when machine parameters have been altered in order to make a measurement, or a significant length of time elapses before the data taking can be completed. The method is not

wiggler-specific, requiring only incoherent emission from an electron beam, but it was suggested that a demonstration of the technique with this microwiggler was possible[xxvii].

1.5 The search for stimulated emission.

1.5.1 ***Previous work.*** Understanding the physics of self amplified spontaneous emission has been a subject of considerable theoretical effort in recent years. However, experimental work has until now been limited to long wavelengths, the most recent reported results being those of CLIO at 10 and 5 microns[xxviii,xxix,xxx,xxxi,xxxii]. Moving studies toward shorter wavelengths is technically challenging because of tighter demands on the quality of the system. Furthermore the longer wavelength experiments are favored by higher gain and a larger ratio of wavelength to bunchlength, which can provide coherent enhancement of spontaneous emission without gain. Several groups working in the far infrared have reported levels of coherent enhancement of four orders of magnitude, which provided beneficial reductions in the startup requirements for their experiments.

1.4.2 ***New directions.*** Our experiments in single pass gain differed from previous work in the wavelength of emission (1.064 μm) and compactness of the wiggler. This permitted searches for SASE at 1.064 μm and even 632 nm to occur at a lower beam energy than the recent studies[xxviii] at 5 microns.

We observed evidence of self amplified spontaneous emission at 1.064 μm of a factor of about two enhancement over spontaneous emission. The details of the experiments and modelling which support this claim are documented in the report. Similar trends were observed at 632 nm and the differences in the setup between the

experiments at these two wavelengths raise some important modelling issues, which are discussed.

The original experimental efforts of the project concentrated on a proof of principle demonstration of a microwiggler-based free electron laser operating in the green, and ultimately UV wavelengths, but were not successful. Later, attempts were made to turn on the FEL at 1 micron, which also failed. This raises the question of how SASE could be observed at a wavelength at which multi-pass lasing was not observed, and there are some possible reasons. A brief chronology of the FEL experiment is included.

1.5 Summary:

In sum, we performed experiments in three areas: the microwiggler, the quantitative wiggler-based beam characterization, and the search for stimulated emission. Magnetic measurements performed with the microwiggler will be discussed in Chapter 2. The beam diagnostic work is organized by single macropulse techniques (Chapter 3), and single micropulse techniques (Chapter 4). The former includes spatial profile and spectral measurements. The single micropulse feature, on the other hand, is an intrinsic requirement to the proposed fluctuation-based bunchlength technique. The enhancements over spontaneous emission will be discussed in Chapter 3 and to some extent in Chapter 4 with emphasis on the understanding which can be provided by the demonstrated wiggler-based diagnostic techniques. Chapter 5 closes with a concise statement of the experimental results and conclusions, as well as a discussion of future work.

Many people have influenced and contributed to this work in a variety of ways and their expertise and support are appreciated. Please refer to the acknowledgments for more detail about their contributions.

The recent technical work and measurements on the wiggler described in Chapter 2 were performed by the author. The responsibility for the use of beamtime, the preparation of the setups and the accuracy of the wiggler emission data and analysis rests on the author for the work on non-perturbative diagnosis. The author worked on all shifts involving measurements of wiggler emissions related to the studies of self amplified spontaneous emission and raised the described modelling issues.

References (Chapter 1)

[i] B. L. Bobbs, G. Rakowsky, P. Kennedy, R. A. Cover and D. Slater, "In search of a meaningful field-error specification for wigglers," *Nucl. Instr. & Meth A* **296**, 574-8, (1990)

[ii] Y. C. Huang, H. C. Wang, R. H. Pantell, J. Feinstein, and J. Harris, "Performance characterization of a far-infrared, staggered wiggler," *Nucl. Instr. & Meth A*, **341**, 431, (1994)

[iii] C. M. Fortgang and R. W. Warren, "Measurement and correction of magnetic fields in pulsed slotted-tube microwiggler," *Nucl. Instr. & Meth A*, **341**, 436, (1994)

[iv] P. Tesch, J. Gallagher and L. Elias, "Final construction of the CREOL 8 millimeter period hybrid undulator," *Nucl. Instr. & Meth. A*, **375**, 504, (1996)

[v] Kim, Kwang-Je, "Characteristics of synchrotron radiation," *AIP Conference Proceedings* **184**, Vol. 1, 565-632, (1989)

[vi] R. Barbini, F. Ciocci, G. Dattoli and L. Giannessi, "Spectral properties of the undulator magnets radiation; analytical and numerical treatment," *Rivista del Nuovo Cimento*, **13**(6), 1-65, (1990)

[vii] A. H. Lumpkin, "On the path to the next generation of light sources," *Nucl. Instr. & Meth. A*, **393**, 170-177, (1997)

[viii] A. Lumpkin, "Comprehensive, nonintercepting electron-beam diagnostics using spontaneous-emission characteristics," *Nucl. Instr. & Meth. A*, **296**, 134, (1990)

[ix] A. Lumpkin, B. Yang, Y. Chung, R. Deju, G. Voykov and G. Dattoli, "Preliminary Calculations on the Determination of APS Particle-Beam Parameters Based on Undulator Radiation," Proceedings of the 1995 Particle Accelerator Conference, (1995), 2598.

[x] P. Heimann, D. Mossessian, A. Warwick, C. Wang, S. Marks, H. Padmore, B. Kincaid and E. M. Bullikson, "Experimental characterization of ALS undulator radiation," *Rev. Sci. Instrum.* **66**(2), 1885, (1995)

[xi] E. Tarazona and P. Elleaume, "Emittance measurements at the ESRF," *Rev. Sci. Instrum.* **66**(2), 1885, (1995)

[xii] M. L. Ponds, Y. Feng, J. M. Madey and P. G. O'Shea, "Non-destructive diagnosis of relativistic electron beams using a short undulator," *Nucl. Instr. & Meth. A*, **375**, 136, (1996)

[xiii] X. Qiu, P. Catravas, M. Babzien, I. Ben-Zvi, J.-M. Fang, W. Graves, Y. Liu, R. Malone, I. Mastovsky, Z. Segalov, J. Sheehan, R. Stoner, X.-J. Wang, J. S. Wurtele, "Experiments in nonperturbative electron beam characterization with the MIT microwiggler at the accelerator test facility at BNL," *Nucl. Instr. & Meth. A*, **393**, 484-9 (1997)

[xiv] We learned of the storage ring work in this area after submission of the draft in the previous reference to the publisher.

[xv] A. H. Lumpkin, "On the path to the next generation of light sources," *Nucl. Instr. & Meth. A*, **393**, 170-177, (1997)

[xvi] A. Lumpkin, B. Yang, Y. Chung, R. Deju, G. Voykov and G. Dattoli, "Preliminary Calculations on the Determination of APS Particle-Beam Parameters Based on Undulator Radiation," Proceedings of the 1995 Particle Accelerator Conference, 2598, (1995)

[xvii] Discussion with David Keane, Jefferson Lab.
[xviii] R. B. Fiorito and D. W. Rule, "Optical transition radiation beam emittance diagnostics," *AIP Conference Proceedings*, **319**, 21-37 (1994)
[xix] R. Govil, P. Volfbeyn and W. Leemans, "UV laser ionization and electron beam diagnostics for plasma lenses," *Proceedings of the 1995 Particle Accelerator Conference,* vol. 2, 776-8 (1995)
[xx] D. W. Rule, R. B. Fiorito and W. D. Kimura, "Noninterceptive beam diagnostics based on diffraction radiation," *AIP Conference Proceedings*, **390**, 298 (1997).
[xxi] P. K. Kung, H. C. Lihn, H. Wiedemann and D. Bocek, *Phys. Rev. Lett.* 73 (1994) 967.
[xxii] R. Lai and A. J. Sievers, *Phys. Rev. E* **50**, 50, (1994)
[xxiii] E. R. Crosson, K. W. Berryman, B. A. Richman, T. I. Smith, R. L. Swent, "The determination of an electron beam's longitudinal phase space distribution through the use of phase-energy measurements," *Nucl. Instr. & Meth. A*, **375**, 87-90, (1996)
[xxiv] G. A. Krafft, D. Wang, E. Price, and E. Feldl, "Coherent synchrotron radiataion for a non-invasive subpicosecond bunch length monitor," *Proceedings of the 1995 Particle Accelerator Conference*, 2601-2603, (1995)
[xxv] M. S. Zolotorev and G. V. Stupakov, "Fluctuational interferometry for measurement of short pulses of incoherent radiation," SLAC-PUB-7132 (March, 1996)
[xxvi] M. S. Zolotorev and G. V. Stupakov, "Spectral fluctuations of incoherent radiation and measurement of longitudinal bunch profile," submitted to the 1997 Particle Accelerator Conference.
[xxvii] Suggestion from J. S. Wurtele, LBL (March, 1996; Sept. 1996)
[xxviii] R. Prazeres, J. M. Ortega, F. Glotin, D. A. Jaroszynski and O. Marcouille, "Ovservation of self-amplified spontaneous emission in the mid-infrared in a free-electron laser," *Phys. Rev. Lett.* **78**(11), 2124-7 (1997)
[xxix] T. Orzechowski et al., *Nucl. Instr & Meth. A* **250,** 144 (1987)
[xxx] D. A. Kirkpatrick, G. Bekefi, A.C. Dirienzo, H. P. Freund and A. K. Ganguly, "A high power, 600 mu m wavelength free electron laser," *Nucl. Instr. & Meth. A* **285,** 43-46 (1989)
[xxxi] S. Okuda, J. Ohkuma, N. Kimura, Y. Honda, T. Okada, S. Takamuku, T. Yamamoto and K. Tsumori, "Self-amplified spontaneous emission at wavelengths of 20 and 40 mu m from single-bunch electron beams," *Nucl. Instr. & Meth. A* **331,** 76-8 (1993)
[xxxii] D. Bocek, M. Hernandez, P. Kung, Hung-chi Lihn, C. Settakorn and H. Wiedemann, "Observation of coherent undulator radiation from sub-picosecond electron pulses," *AIP Conference Proceedings*, **367**, 381-90 (1996)

CHAPTER 2: THE MICROWIGGLER

In this chapter, we review work performed on the microwiggler during the course of the thesis, including comprehensive magnetic measurements to support a new claim of

field uniformity: 0.08% rms spread in peak amplitudes. This is the first time a field profile spread of less than 0.1% has been reported for a sub-cm period wiggler. We investigate the limits of tunability provided by the system.

2.1 The microwiggler

2.1.1 ***Description and previous work.*** The MIT microwiggler is a pulsed electromagnet with a period of 8.8 mm and a length of 70 periods. The wiggler gap is 4.2 mm, and nominal operating point is 4.2 kG peak on-axis field strength, which corresponds to a wiggler parameter of 0.34. A complete description of the design, construction, and measurement apparatus are contained in references 1 and 2, from which one can see how the problem of generating the experimentally useful parameters of Table 1 was solved in detail. An idea of the mechanical construction of the wiggler can be obtained from the photograph in Figure 1. A precision-machined Aluminum matrix houses the 280 coils, and closes on either side of a stainless steel bore. Each coil consists of 50 turns of AWG32 Formex wire with a core of Microsil laminates, a material commonly used in transformer manufacturing, which was chosen for low hysteresis and remanent field.

An electrical schematic for the pulser and wiggler internal connections is shown in Figure 2. The pulser for the wiggler is configured as a rectified LRC circuit. It produces 1 ms pulses at a rep rate of 0.5 Hz and supplies an output current of about 10 kA to the load. Each pair of magnets which creates a half period is wired in parallel. Each half period is connected between the high voltage buss and ground in series with an adjustable

resistance. Because the L/R time constant of the coils is about 80 microseconds, which is much shorter than the current pulse, the wiggler equivalent circuit simplifies to a resistive network at the time of maximum field strength. In this way, the field strength of each half period is controlled independently by the adjustable series resistance, in practice a length of manganin wire chosen to have a resistance of about 10% of the coil resistance. This adjustment provides an additional 140 degrees of freedom compared to most wiggler designs, a blessing or a curse, depending on how well it is controlled.

PARAMETER	VALUE
On-axis magnetic field, B_w	4.2 kG
Wiggler period, λ_w	8.8 mm
Wiggler parameter, a_w	0.34
Wiggler gap, G	4.2 mm
Number of periods, N_w	70
Rms spread in peak amplitudes, $(\delta B/B)_{RMS}$	0.08%
Rms spread in pole integrals, $(\delta I/I)_{RMS}$	0.14%
Rep rate	0.5 Hz

Table 1. MIT microwiggler parameters

In response, a tuning algorithm was developed by R. Stoner, as well as a rigorous procedure for field profile characterization. The rms spread in peak amplitudes and pole positions was measured carefully as a matter of routine, and the error in pole integrals

estimated from these measurements. Other basic measurements, required less frequently, were the full dependence of the magnetic field on longitudinal position, from which the content of the spatial harmonics present in the field was computed, the variation from coil to coil in the time to maximum field caused by coil-to-coil differences, and the error in magnetic centers. This tuning regimen led to the original result: a demonstration of a field profile of 0.12% rms spread in peak amplitudes, 0.18% rms spread in pole integrals, and 17 micron rms spread in magnetic centers. It was the first demonstration of this level of performance for any sub-cm period wiggler.

2.1.2 ***New work.*** Unfortunately, this achievement was marred by one coil in the profile, which did not have characteristics identical to its neighbors; the highest field strength achievable in this coil was at best 0.7% too low. To correct this problem required a disassembly of the wiggler and subsequent full recharacterization of the field properties. Because the device is a sufficiently complex prototype, and precision a hallmark issue, appropriate care is required to perform the mechanical task successfully. It was, however, an excellent way to acquire the familiarity with the system needed to provide the wiggler in working condition under the constraints of a tight running schedule, and a real test of whether the prior excellent performance results could be reproduced with both the wiggler and measurement system reassembled from scratch subsequent to the departure of the original author. Once done, it possible to test the limits of the system for the first time. A claim of better than 0.1% field uniformity requires discussion, as the sources of error erupt in number and in relative importance as the figure of merit improves. These issues are discussed in detail below.

2.2 New measurements

The description of field measurements which follow were performed for the full 70 period wiggler, excluding the end tapers, operating at a rep rate of 0.5 Hz and a field strength of 0.45 Tesla. Before discussing the detailed measurements of the profile of the magnetic field, we include a description of how the absolute calibration of the magnetic field was done. This value is important, not only from the point of view of experiments, in which magnetic fields of sufficient strength are a prerequisite, but because field errors become more prominent as the field strength increases.

2.2.1 ***Absolute calibration of the wiggler magnetic field.*** In previous work[1], several independent methods were used to determine the absolute calibration of the strength, and show a variation of about 10%, which is a realistic uncertainty for absolute measurements in high current pulsed systems.

We added an additional calibration method to this collection, by concentrating on an area measurement for the $\dot{B}$ loop – the pickup coil used to measure the field strength. This was done by inserting the probe into a rotating DC magnetic field and deriving the area-turn product from measurements of the frequency of rotation and the DC field strength. A horseshoe magnet spun in a lathe about the probe[3], the stray field provided a healthy trigger signal, and the frequency and voltage of the induced signal in the $\dot{B}$ loop were measured with an oscilloscope. The DC field strength was measured with a Hall

probe. Nominal values were 1 Tesla magnetic field, 13 Hz rotation and 1 mV induced signal.

In the future, the setup could be improved by using a lighter magnet, which would enable the rotation to occur at a faster rpm setting, producing a stronger coil output voltage. Refrigerator type magnets are easily found in strip form and produce fields at the surface of over 1 Tesla.

2.2.2 ***Measurement of the peak amplitudes.*** The $\dot{B}$ loop used in the measurements of peak amplitudes and positions is mounted in a Teflon holder machined to have a resistive fit in the bore. The values for peak amplitudes are recorded in an automated process in which the $\dot{B}$ loop is pulled through the bore by a stepper motor, its signal integrated and then digitized with a 12-bit A/D board. The controlling program takes a series of points near the peak until it detects a change in the derivative, and then directs the stepper motor to skip directly to the next peak, while generating a parabolic fit to the acquired data, with numerical outputs field strength, peak position, and variance of the fit.[1]

A vigorous search for noise preceeded the field measurements, and specific criteria were used to determine the acceptable noise level. The measured spread in peak amplitudes is expected to contain two contributions: the true rms in peak field amplitudes, which is the quantity of interest, and the measurement error, which is the rms in the value of a fixed peak measured in consecutive runs. The measurement error could arise from a number of factors: undesired pickup, mechanical shock on the probe, and a variety of pulser problems. A system which produces a large measurement error is unacceptable for

high precision measurements. The contributions to the measurement error are divided between shot to shot problems and problems due to long term drifts in the system. To isolate the former, the variances computed by the controlling program during the fits to each peak during a complete field scan were examined and the system was improved until they were contained by an acceptable upper bound. Further search for noise proceeded until the measurement error over long periods of running – perhaps 12 hours - was reduced to about 1/3 of the measured rms in peak amplitudes. As the true noise and the measurement error are uncorrelated, they add in quadrature, and this ensures that the spurious random signal is less than 10% of the true signal. Systematic errors are harder to detect than random noise, as they may mistakenly be tuned out of the profile. Any flags of systematic errors, such as the existence of a ramp in the field profile, were probed until they were understood.

Additional tests followed. In order to check for errors due to imperfections in the probe construction, the Teflon probe holder was rotated about the wiggler axis. In order to find pickup inside the wiggler due to any loop area along the twisted leads leading to the outside of the wiggler, the B-dot loop itself was flipped by 180*. In order to check for pickup along the cable outside the wiggler, the leads to the cable leading to the data acquisition electronics were flipped. In order to check for some kinds of systematic errors, the direction in which the probe was pulled, usually downstream to upstream, was reversed to upstream to downstream. In order to weed out pickup from radiated noise from the pulser, the pulser was rotated relative to the wiggler and the scans repeated. It was possible to obtain the same value for spread in peak amplitudes under all of these perturbations of the system.

A final measurement of the field profile consisted of at least six scans of the full profile, which were averaged. The best measurement error obtained was 0.017%, an improvement by a factor of two over the best previous results[1]. Consecutive tunings brought the spread in peak amplitudes from the initial 0.5% after reassembly of the wiggler to 0.1% in 3 iterations. Field uniformities of 0.08% were consistently achieved with a time investment of a few days. Every test mentioned above was passed for this measurement.

2.2.3 ***When should you stop tuning?*** At some point, the question arises: when do you stop tuning? As will be described below, 0.08% was not the best result achieved. We consider below the factors involved in deciding when to stop. First, we demonstrate that the tuning system was by no means operating at its limit for this measurement. We further consider a variety of other measurements: error in magnetic centers, error in pole positions, and prior measurements of the effect of coil to coil differences on the time to maximum field, and explain the meaning of the reported measurement in the context of the entire family of measurements.

To determine the limit of the tuning and measurement system, a repeatable measurement of the field profile was set up, and iterations continued until improvement was small. The result: 0.042%. The tests of rotating the probe in the wiggler and of flipping the polarity of the leads exterior to the wiggler were passed. In Figure 2, this result is shown, along with the first field measured after construction of the wiggler[1] to give a sense of the improvement which could be implemented.

This is an unexpectedly fine control of a microwiggler field. The criterion for small errors in the beam trajectory the length of the wiggler is 0.2-0.3%, approaching an order of magnitude excess of the measured number, and the latter uniformity has not been achieved in many cases. To put this in perspective, the measured number matches the best number reported for a wiggler of any period, including long period wigglers, which was 0.04%, by the Santa Barbara wiggler[4]. The period of this wiggler was 7.14 cm - an order of magnitude larger. Thus, the reported results of 0.08% for peak amplitude spread were not taken anywhere near the limit of the measurement system.

2.2.4 ***Spread in pole integrals*** The spread in pole integrals, an important figure of merit for wigglers contains a contribution from the peak amplitudes and the peak positions. The latter can be extracted from the same data scans which produced the peak amplitude information. Both these data sets are plotted in Figure 4. The correlations in peak amplitude and position data were studied in previous work[1]; the errors add in quadrature. Current measurements yielded a value of 0.12% for the spread in peak positions; for a spread of 0.08% in the peak positions, the pole integral estimate is 0.14%. Here, therefore, is one of the answers to when one should stop tuning, at least with the current measurement technique. When the peak amplitudes dominate over peak positions, reducing the spread in peak amplitudes is identical to reducing the spread in pole integrals. When the peak positions dominate over the peak amplitudes, reducing the spread in peak amplitudes further is no longer effective. Therefore, with the present system one should balance the effort required to reduce the peak amplitudes with the effectiveness achieved

in reducing pole integrals. A field uniformity of 0.08% is typically easy to implement, and is still improves the pole integrals.

Note, however, that the measurement system could be converted so that the pole integrals are optimized directly, rather than the peak amplitudes, with the same kind of precision as that available with the original system. A very simple probe was designed to try out this idea. Instead of monitoring the peak field by placing a small loop at the peak position, a loop of area equal to one pole was used to integrate the flux of the entire pole. The effect of uncertainty in the length of this loop relative to the exact pole integral length was considered, and it was found that there would be an error introduced at pole integrals spreads were reduced much lower than 0.1%. However, it was such a simple way to beat the limit on pole integrals of 0.12% imposed by the error in peak positions, that some time was spent on it for fun. This probe was appealing because it could be substituted without modification of the original controlling programs in any way, as the pole integral would go through a maximum in exactly the same way as the peak amplitude.

In practical terms, this method has an advantage in terms of both speed and signal to noise over the common technique for measuring pole integrals which consists of measuring a dense set of points along the entire length of the wiggler and then integrating. The method is much faster because it reduces an enormous number of points to the minimum required to fit a curve to the peak with an appropriate error bar. The signal to noise is better because data is only taken at the largest field values, not at the zero crossings.

Some results are shown in Figure 5, where the pole integral probe signals are compared with a rough estimate of the pole integral obtained from the product of peak

amplitude and distance between zero crossings. The data is encouraging, showing the same contour and slightly different values. The work was ended at this point because there was no practical reason to justify spending additional time to further improve the field. A careful study of the precision of the method would have included systematic measurements and a comparison with an independent measurement of the same quantity, perhaps the estimate for pole integrals as usually performed and the pulsed wire method.

Such a probe might be considered for pulsed wigglers with periods shorter than 8.8 mm. More flux passes through its larger area than the peak amplitude B-dot loop, resulting in better signal to noise, which is a problem as the period gets smaller.

2.2.5 ***Spread in magnetic centers.*** The characterization of magnetic centers is important because it is a measure of what the field quality will be off of the central axis. This figure of merit is omitted from most wiggler characterization papers in the literature, exceptions being Verschuur and Warren[5] and earlier studies using Warren's pulsed wire method[6],[7]. High quality in this parameter is much easier to achieve in a long period wiggler than a microwiggler. The spread in magnetic centers increases in significance with short period wigglers because of the increasingly rapid variation of the cosh function with transverse position.

The position of the magnetic center with respect to the center of the bore was determined by monitoring the field with a longitudinally oriented $\dot{B}$ loop. The longitudinal field varies in the transverse direction like $\sinh k_w y \sim k_w y$ /2 for small displacements, so that the induced voltage is approximately proportional to the error in the magnetic center position with respect to the probe center. The experimental results

following reassembly are shown in Figure 6 and determine a spread in magnetic centers of 17 microns.

But because perfect cross gap symmetry produces no signal, the signal to noise becomes poor when the error is small. There is also some coupling to the probe from the transverse field, which is minimized because the transverse field goes through a null when the longitudinal field is maximum. This measurement is therefore an upper bound to the actual measurement. In previous work[1], mechanical measurements determined a lower bound of 10 microns for the spread in magnetic centers.

The limit which the spread in magnetic centers imposes on the final value for field uniformity was set by requiring that tuning improve the field quality over the full area of the optical mode. The relation between the spread $\sigma_{off-axis}$ in peak amplitudes at a distance y from the axis caused by a spread $\sigma_{\Delta y}$ in the magnetic center error Δy is

$$\sigma_{off-axis} \approx k_w^2 y \sigma_{\Delta y} \qquad \text{when} \quad \frac{(k_w y)^2}{2} << 1$$

Figure 7 contains a calculation of $\sigma_{off-axis}$ for the region lying between the measured upper and lower bounds in $\sigma_{\Delta y}$. It shows that the intrinsic spread in magnetic centers is sufficiently small that tuning to a uniformity of 0.08% along the axis is well worth the trouble for the entire transverse area of the optical mode. This is an excellent result. As will be shown later, such a good result for cross-gap symmetry is not an easy thing to achieve in microwiggler (less than 1 cm period) construction.

2.2.6 ***Coil-to-coil variations and timing issues.*** The effect of coil-to-coil variations was considered to determine whether the cited value of field uniformity was

available over a reasonably large window in time to be meaningful. It is possible for variations in impedance from coil to coil to create small differences in their temporal waveforms. These differences were quantified in previous work by measuring the variation in the time of maximum current for a collection of coils[1]. To put this in perspective, note that the pulser provides a rectified current pulse of 1 ms full width and the electron beam bunchlength is 1-10 ps. In the bulk of the wiggler, the variation was found to be 1 microsecond. The first pair of coils is operated at half the field of the bulk of the wiggler, so that its operating point, unlike its neighbors is not in the saturated regime of the core, and is therefore a good illustration an extreme case of coil-to-coil variation. Between the bulk of the wiggler and end coil pair the difference was 5 microseconds.

In order to evaluate the significance of coil to coil variations, the error for a time interval of 400 microseconds around the time of maximum field strength (a generous window) was computed for deviations in the time to maximum between the coils of 1, 3 and 5 microseconds. The calculation in Figure 8 shows that the cited value of 0.08% for spread in peak amplitudes is not exceeded in the bulk of the wiggler for this entire time window.

As an aside, we resurrect an observation which was raised in the previous thesis about the difference recorded between the temporal waveform at the end taper and the bulk of the wiggler. It was noted that in addition to the change in the waveform period that there was a ripple during the current rise. It had been hypothesized that this feature was caused by the bulk of the wiggler going into saturation and we took measurements to confirm that the ripple coincided exactly with this event. It is worth remarking that this

and the temporal variation measurements above indicate that any reduction in field quality of the bulk of the wiggler due to coil variations will occur at a much slower rate than deviations from ideal behavior at the end taper. This becomes relevant, for example, for wiggler timing scans and field strength scans with the electron beam.

2.3 Setup of the wiggler in the beamline

A few of the practical issues of setting up the wiggler in the beamline are described below, including alignment and environmental conditions.

2.3.1 ***The wiggler microenvironment.*** The wiggler was operated in a room which had large changes in the relative humidity: at times swinging from 20 to 70% humidity over the course of two weeks was routine. This is of practical concern because condensation forming on the surfaces of the wigger chilled to 40*F can lead to damaged coils. It is easy for experimenters concentrating during the course of a run with electron beam to be unaware of substantial weather changes and condensation could have caused a problem during the time that the Experimental Hall was interlocked without additional preventative measures.

To prevent such damage, the wiggler was operated within its own microenvironment, a homemade bubble fashioned from winter window insulation[8], with dry air piped in to control the humidity level[9]. This permitted continuous operation at 30-40% relative humidity in all types of weather, irregardless of the fact that the ambient

humidity was high enough that the cooler hoses feeding into the microenviroment were dripping with water for many months of the year.

2.3.2 ***Alignment procedure.*** The co-alignment of the wiggler and electron beam are important for successful experiments. Misalignments in the non-wiggle plane can broaden the emission spectra significantly, smearing out the effects of other parameters or reducing gain, as the trajectory of the electron beam will be modified by a restoring force toward the center of the wiggler. The misalignment is particularly critical if good overlap between the electron beam and an optical mode from an FEL cavity is required for many passes through the wiggler. A number of procedures were developed to ensure good alignment. The two mentioned below depended on co-alignment with a reference HeNe laser. The first was simple and robust. It worked well, but it required a vacuum break. The second was all-optical and performed under vacuum, and eventually was debugged to give results results consistent with the first method. For the former, two tight fitting plugs were machined, one with a number 80 hole (13 mils) for upstream side of the wiggler, and the other with a 110 mil through hole over which was placed a jagged piece of onion skin, for the downstream side. Some images of these plugs during alignment are shown in Figure 9. In the upper image, taken before alignment, one can see the 13 mil hole back-illumated, and the alignment HeNe next to it. Aligned, the HeNe produces a clear halo around the dark hole. In the lower right image, one sees the HeNe exiting from the through hole in the downstream side plug. This method allowed the HeNe to be placed with about 1 pixel of resolution (about 40 microns). The second alignment technique involved imaging the rectangular, back-illuminated bore, along with

the alignment HeNe, either in the forward direction or back-reflected from the cavity. Again, the precision was limited by the imaging, and was typically about 40 microns.

The stability of the alignment is a point of concern. Dial indicators (0.5 mil) on the wiggler indicated its position remained unchanged for many months. The efficacy of the alignment therefore depended on the HeNe pointing remaining stable, which was not always the case, and, since the beam was usually tuned using the HeNe spot, the absence undesired magnetic fields. This point was brought home by the discovery of four pieces of magnetic material in the beamline between the two targets on which the alignment HeNe was viewed (see figure 3 in Chapter 3), including the target assemblies themselves, which contained magnetized through holes measured at 20 Gauss on-axis after removal, which took them away from the bending dipoles, and affected the beam trajectory relative to the alignment HeNe. Some of the vacuum valves also showed signs of DC fields. The effect of radiated fields from the pulser is also an issue to consider, particularly in the presence of multiple grounds loops in the beamline, from ion pumps, steering coils which were grounded to the beamline, and so forth. We had hoped to check the effect of an electrical break in the beamline, but the opportunity to install the break was not available.

2.3.3 ***Results with electron beam.*** The effect of pickup in the beamline due to noise generated from the bussbar to the coils was checked. In particular, the worst candidate for noise is the area in which the manganin wires extended to the twisted pair and the return current goes to the bussbar, because this is the only section in which the currents flow in parallel, forming a loose solenoid[10]. The area of this "solenoid" was changed by at least a factor of 4, and some tests were done with μ metal. It was not

possible to see any effect on the beam. The only time that noise from the wiggler was seen to perturb the beam was during studies to determine the effect of the end coil strength on the beam trajectory in which a long string of resistors was hung, creating a giant loop which hung at the beam level. This was easy to correct.

A zero deflection of the electron beam downstream from the wiggler requires a high field quality, and may be significantly influenced by other sources, such as pulser coupling exterior to the wiggler through ground loops in the facility, the unintended presence of magnetic material near the wiggler, as discovered, and by the beam tune. The wiggler rep rate is one third that of the accelerator and images of the electron beam downstream from the wiggler were examined to monitor changes between wiggler-on and wiggler-off states. Best results are shown in Figure 10, which demonstrate negligable deflection between wiggler-on and wiggler-off states in both the wiggle or non-wiggle plane. Comparitive shots are included for two locations in the beamline, one 0.5 meters downstream from the wiggler ("finger 2"), and the other at the end of the beamline, some five meters downstream.

2.4 Long term statistics of the wiggler operation

2.4.1 ***Usage***. The wiggler began operation in the beamline in October, 1993. The total number of shots fired well exceeds one million. The wiggler was often operated for twelve hours at a time and during intensive running periods approached 24 hour operation.

It was possible to take a few data points in long term drift in field uniformity over the course of three years. This is important because the time required between retunings of the wiggler is hard to predict, and although changes in the profile may be quickly remedied by sending the wiggler through a tuning iteration, the time between the required iterations needed to be determined empirically. These changes could be due to mechanical shock on firing, or may depend on the environment in which it is operated. The first measurements in the bulk of the wiggler profile showed a change from 0.08% to 0.15% after several months. The best measurement was 0.12% over 40 periods after 9 months of storage and 6 months of running had accumulated since the tuning. During this session of running, a coil burned out at each end of the wiggler, which is why the last experiments are reported at 60 period length. One could speculate about an improvement in the bulk stability. However, these were not data points taken under well controlled conditions.

2.4.2 ***Long term coil-to-coil drifts.*** The long term drift in the coil behavior was monitored during the disassembly of the wiggler by comparing the profiles measured one year apart. Any coil which showed difference beyond an arbitrarily defined point was taken apart and examined in an effort to isolate the causes for any of these changes. Some of the coils examined showed no apparent defects; in this case, the sag was probably due to settling caused by the magnetic forces in this geometry, and the coils would probably have remained stable after an additional retuning. In one case, a flaw in the Formex wire was found, and dealt with before the coil failed. Since this coil was in the center of the wiggler, this probably prevented a repair at an unfortunate timing. The differences in resistance of all 280 coils were measured at this time, as some of the coils had one turn

more or less than the others. (Note that this is not expected to produce a difference in the field produced, as the increased resistance exactly compensates the increased inductance, if the stray series resistance is ignored.) There was no correlation found between the long term changes in coil efficiency and the number of turns, indicating that differences in coil heating on such a scale were probably not the cause of any drifts in field strength.

2.5 Future work with the wiggler

2.5.1 ***Non-uniform target profiles.*** An excellent area for future development with the wiggler is non-uniform target profiles. 140 new degrees of freedom must offer something far more powerful than just the ability to tune to a uniform field profile. A few possibilities are put forth below.

A tunable wiggler and an antenna array with individually controlled currents are analagous. From radar to optics, this configuration is put to practical use. In the former, the control of currents of individual elements is used to define the resulting direction and field profile of the array. Similarly, the tunability of the wiggler can be used like an apodizer to control the intensity profile of the spontaneous emission. We considered the possibility of a Gaussian profile briefly for diagnostic purposes, but remarked that the sinc function at 70 period length changes to Gaussian rather quickly (the lobes wash out) with broadening by realistic beam parameters and moreover, the analysis is not greatly simplified[11].

A few comments could be made about the practical details of implementation on

non-uniform profiles. The present tuning algorithm neglects non-linear effects in perturbations of the field profile. This is valid because the coils are well saturated. The linear approximation was used at the end taper, as well, but tuning requires some additional iterations. If a new tune were to take advantage of the entire tuning range, non-linear effects would have to be considered more carefully. In addition to non-linearities arising from the saturation curve of the magnetic material, there will be some contribution to the tuning matrix from temperature differential which will exist along the cores if adjacent cores are operating at very different currents. This means that sufficient time must be allowed for the wiggler to stabilize during measurements. Furthermore, one must take care when operating the wiggler in humid conditions that there are some new failsafes in the microenvironment. The operation in a room with better decoupling from the outside weather would trivialize this problem, though. It will be interesting to check stability issues of the wiggler when non-uniform tunes are applied. Mechanically, a uniform tune is the most likely to provide a balance of magnetic forces. These details are all manageable.

A few possibilities for useful non-uniform profiles are: the introduction of short gaps, the reversal of coil polarity in the wiggler, and square wave-type envelopes. Short gaps are under study theoretically at the moment to better understand concatenation of wiggler sections. A half period can be disconnected, and the adjacent coils tuned as desired. The reversal of coil polarity is a way in which a pulsed wigger can be converted to an optical klystron without the need for a long dispersive section. Experimental results have been reported, which were not as good as expected[12]. It may be that detailed control

over the field profile in the region of the reversed coils is essential. The optical klystron configuration produces spectral and spatial profiles with interesting properties, which are useful for beam diagnosis[13]. The beam diagnostic properties of more than two sections (square wave profiles of the field envelope) are something to consider.

2.5.2 ***Two-dimensional tuning.*** If microwigglers are scaled to periods much shorter than the present one, the field quality will be limited very quickly by the error in magnetic centers unless countermeasures are taken. As an example, the case of a 2.2 mm period wiggler is considered, a reduction by a factor of four. For the same bounds in spread in magnetic centers (10-17 microns), the error they contribute is plotted in Figure 11 along with the 8.8 mm case for transverse positions from 0 to 100 microns. Note that if the number of periods in the wiggler is the same, the resonant wavelength and Rayleigh length both decrease by a factor of four, and the optical waist decreases from 200 microns (compare Figure 7) to 50 microns. However, because high field strengths are difficult to achieve in short period wigglers, and one attempts to compensate by lengthening the wiggler, the optical waist increases, and the error rises quickly to levels of 1%.

This problem may be addressed with the present tunable design by adapting the tuning procedure to two dimensions, wiping out errors in both the longitudinal and transverse directions. Longitudinal tuning is presently done by using the resistance adjustment, $\overline{R}_{long}$, controlling the current flowing to each pair of coils. By adding a resistance, $\overline{R}_{Xverse}$, in one arm of the coil pair only as indicated in Figure 12, one imbalances the current density and shifts the magnetic center. This will increase the

efficacy of the longitudinal tuning enormously as long as the wiggler gap is not too small.

The following modification to the original wiggler tuning algorithm includes the second dimension.

$$\Delta\bar{B}_y = \frac{\partial\bar{B}_y}{\partial\bar{R}_{long}}\Delta\bar{R}_{long} + \frac{\partial\bar{B}_y}{\partial\bar{R}_{Xverse}}\Delta\bar{R}_{Xverse}$$

$$\Delta\bar{y} = \frac{\partial\bar{y}}{\partial\bar{R}_{long}}\Delta\bar{R}_{long} + \frac{\partial\bar{y}}{\partial\bar{R}_{Xverse}}\Delta\bar{R}_{Xverse}$$

where the strength of the magnetic field of each peak in the non-wiggle plane, $\bar{B}_y$, is controlled by the series resistances $\bar{R}_{long}$ and the transverse position of the magnetic center of each peak, $\bar{y}$, is controlled by the new parallel resistances $\bar{R}_{Xverse}$. $\frac{\partial\bar{B}_y}{\partial\bar{R}_{long}}$, $\frac{\partial\bar{B}_y}{\partial\bar{R}_{Xverse}}$, $\frac{\partial\bar{y}}{\partial\bar{R}_{long}}$ and $\frac{\partial\bar{y}}{\partial\bar{R}_{Xverse}}$ are matrices of size i x j = 140 x 140 generated by measuring the change produced in the ith half period by an intentional perturbation in $\bar{R}_{long}$ and $\bar{R}_{Xverse}$ in the jth half period. Only the first order terms of the Taylor expansion have been retained. The matrix $\frac{\partial\bar{B}_y}{\partial R_{long}}$ is identical to the one currently used in the longitudinal tuning. All the matrices will be sparse, facilitating implementation. Once they are determined, one sets $\Delta\bar{B}_y$ and $\Delta\bar{y}$ to the correction required to meet the target profile and solves for the required adjustment vectors $\Delta\bar{R}_{long}$ and $\Delta\bar{R}_{Xverse}$.

Several configurations for the measurement of the magnetic centers are possible. The current one produces an upper bound for the spread, but a precision measurement will be difficult since the signal one is interested in will approach zero as the system

improves. One example of an alternate configuration may be based on Warren's pulsed wire method. A set of three wires at different transverse positions would be pulsed simultaneously in peak amplitude mode and the deflection signals monitored with a diode array detector. A parabola would be fit to the data for each half period in order to calculate the position of the magnetic center. This determines the vector $\Delta\bar{y}$. To determine $\Delta\overline{B}_y$, one could use the same diagnostic. Another suggestion has also been made[14] for efficient noise reduction in which the perturbation resistance would be switched in and out repeatedly, and the alternating signal processed in a way similar to lock-in amplifier.

2.6 Summary

In sum, we have taken data to characterize the performance of the wiggler after a disassembly which made it possible to test the limits of the prototype. With these new measurements, we made a claim of the first demonstration of a typical microwiggler field uniformity of 0.08% and a best measurement of 0.042%. To support this claim, we have examined the sources of error which contribute to this measurement in great detail, through criteria on different types of acceptable noise, through searches for systematic errors and through tests of perturbations in the measurement system. Furthermore, we present measurements to show that the cited number retains its meaningfulness in light of the entire family of measurements made on the wiggler: the pole integral behavior, the cross-gap field symmetry figure of merit, and the temporal variations caused by coil-to-

coil differences. Over a period of several years, we demonstrated that this result could be obtained repeatedly, and with the rapidity necessary to be practical. Results obtained with the electron beam are consistent with the field measurements.

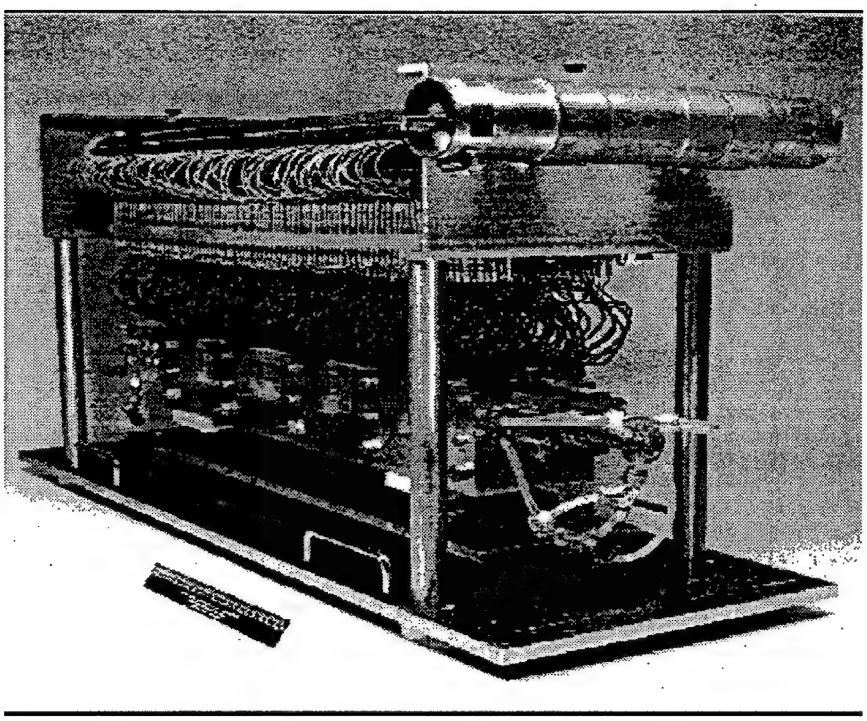

Figure 1. MIT Microwiggler

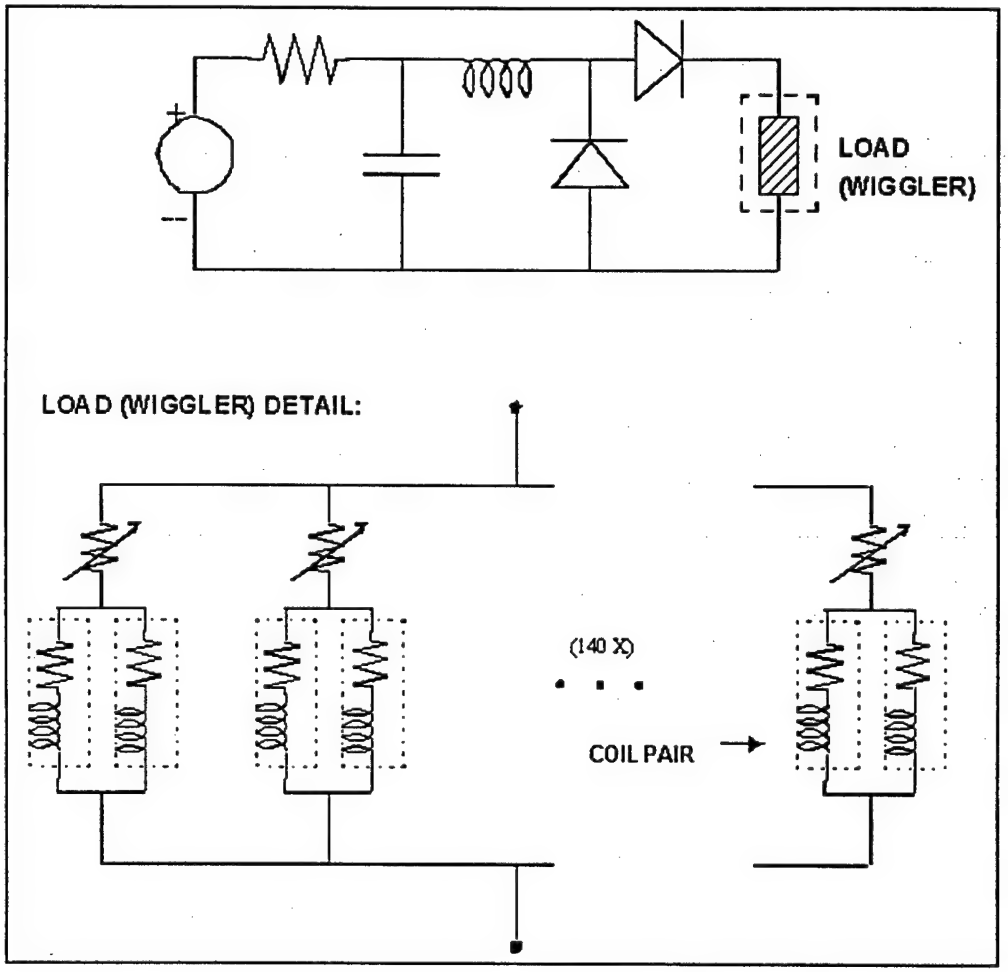

Figure 2. Electrical schematic of wiggler and pulser.

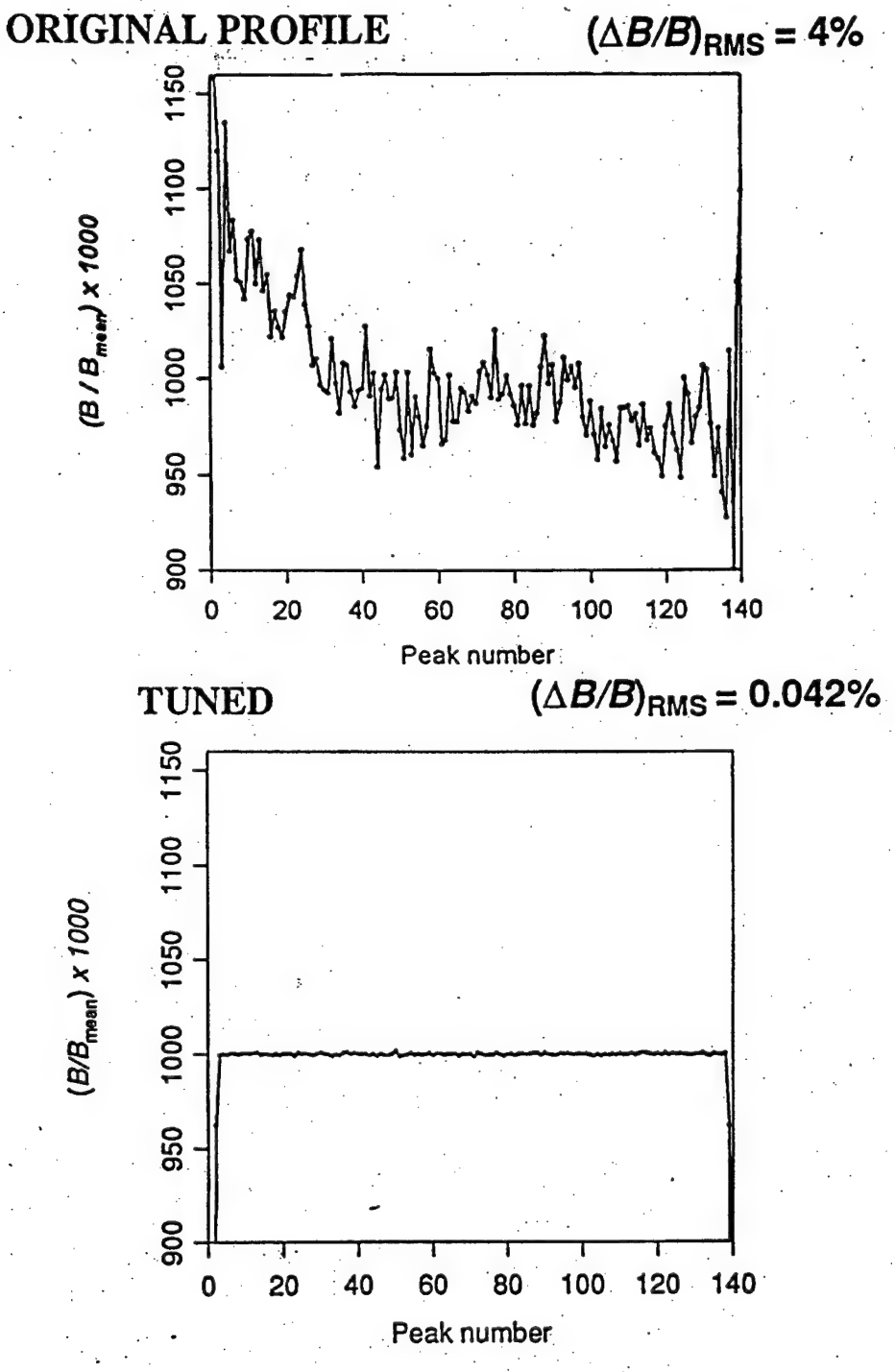

Figure 3 Results of tuning. *The upper profile of field amplitude vs. peak number is the original profile measured after first assembly of the wiggler [ ]. The lower profile is the best result obtained after repeated iterations of the tuning algorithm. This is the first time that any sub-cm period wiggler has achieved a field uniformity of better than 0.1%.*

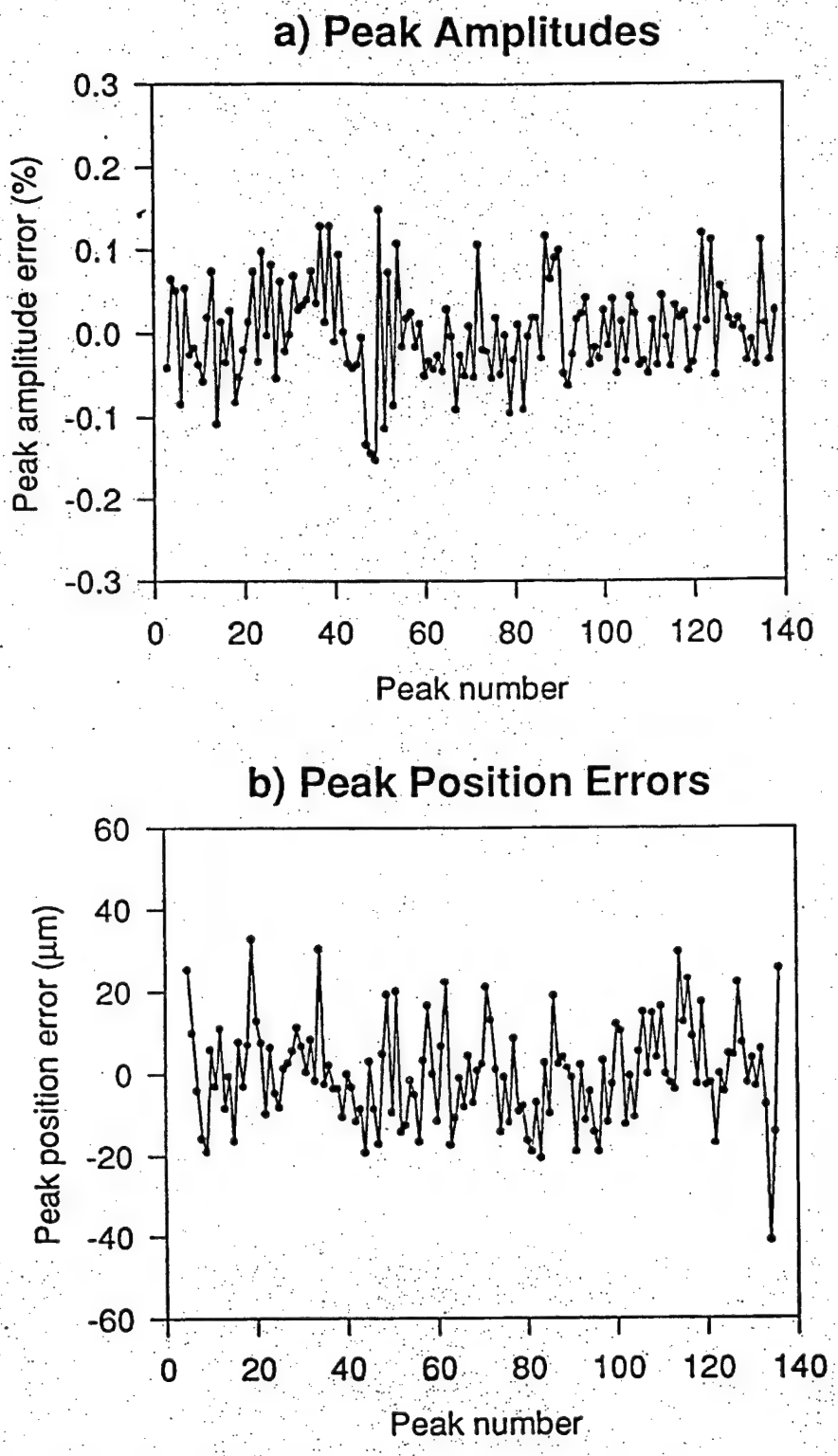

Figure 4. Peak amplitude profile and deviation in pole positions from the nominal period along the wiggler. *These results are typical field profiles obtained consistently over two years and satisfying the rigorous tests for accuracy described. After half a year of running, the wiggler could be returned to this state with a single tuning iteration.*

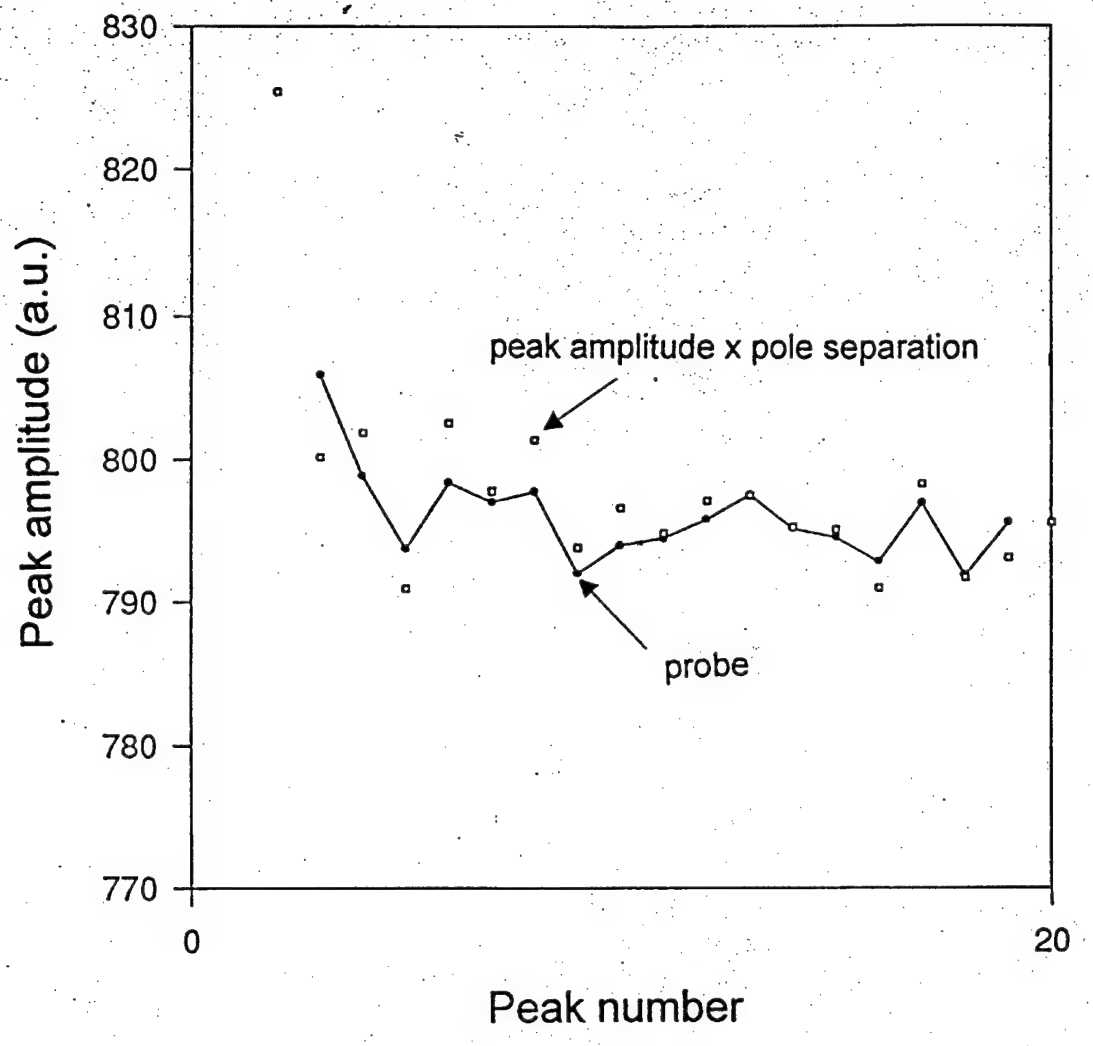

Figure 5. Pole integral probe results. *A probe was designed to convert the tuning algorithm from optimization of peak amplitudes to pole integrals. This is desirable for increased speed of tuning and the removal of the pole positions as the limiting factor in determining the pole integrals. The first results with this probe (joined by solid line) are compared with a rough estimate of the pole integral (single points), obtained from the product of the peak amplitude and the distance between adjacent poles positions.*

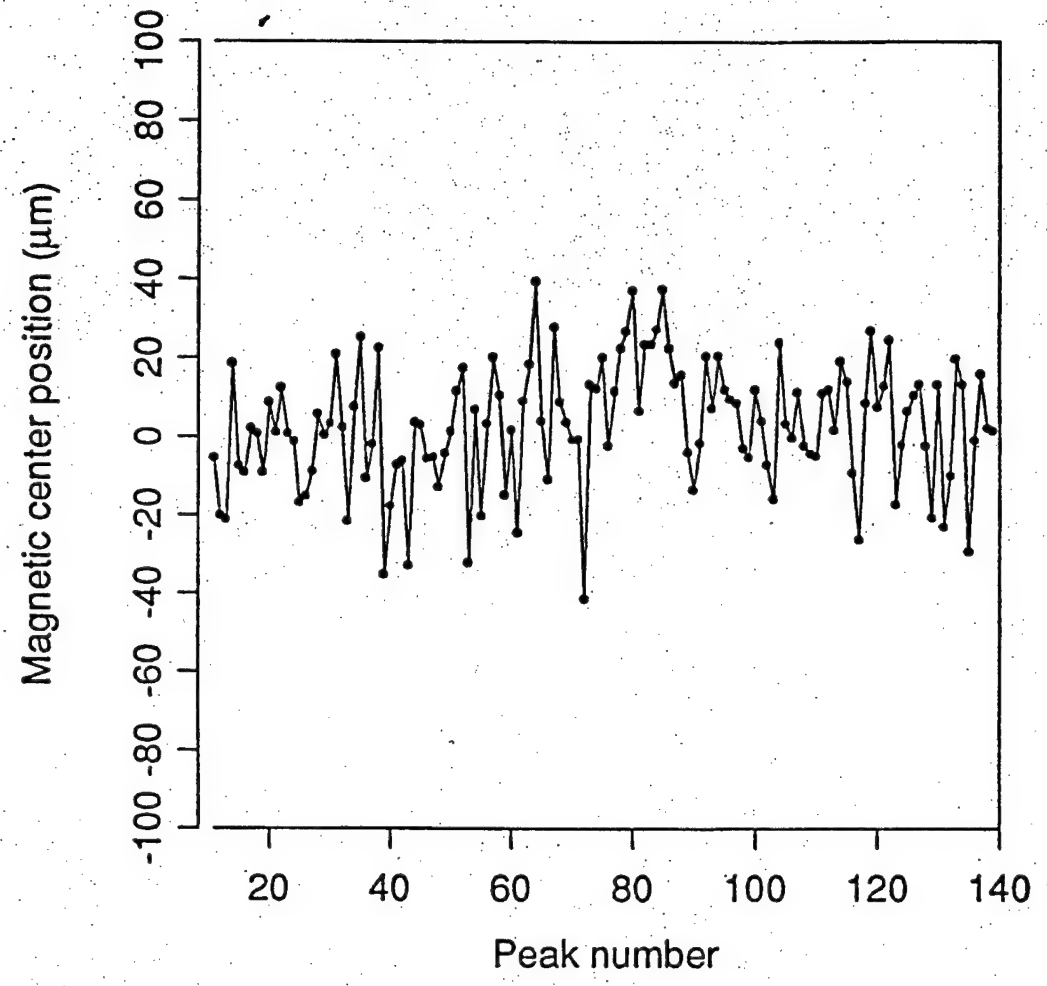

Figure 6. Measurement of magnetic center position along the wiggler. *The spread in magnetic centers is an important, and often omitted, figure of merit for a wiggler. The experimental results for deviation of the magnetic centers are plotted as a function of peak number, with an rms of 17 microns. The significance of this number is discussed in Figure 5.*

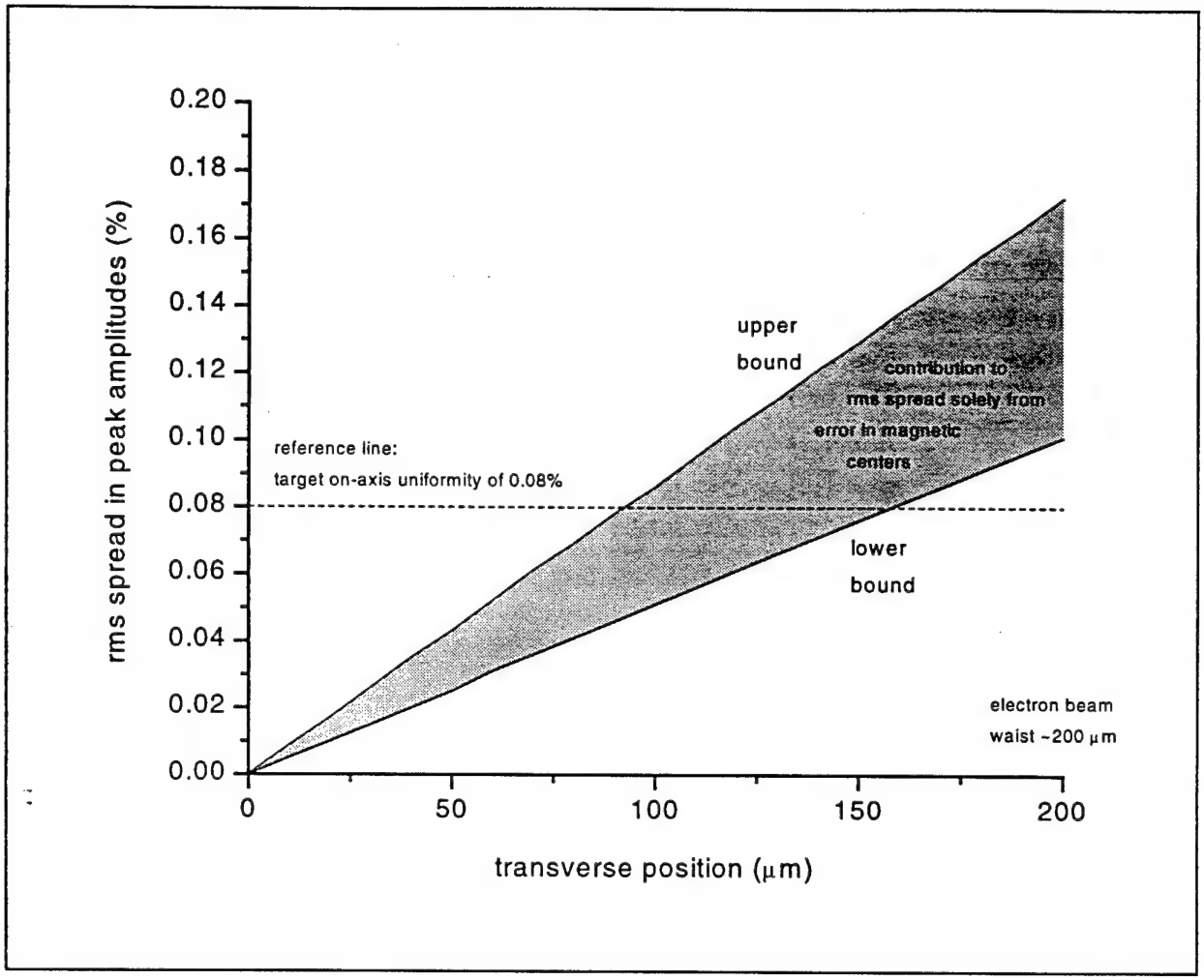

Figure 7. Off-axis field error due to spread in magnetic centers. *The off-axis field characteristics were used as one criterion for a meaningful minimum field error on-axis. The contribution to off-axis field errors given a perfect on-axis field was computed from two separate measurements of the spread in magnetic centers: the recent magnetic measurements (upper bound) and the original mechanical measurements [ ] (lower bound). These curves show that the cited value of 0.08% on-axis provides a significant improvement in the field uniformity not merely on-axis but over the full cross section of the electron beam.*

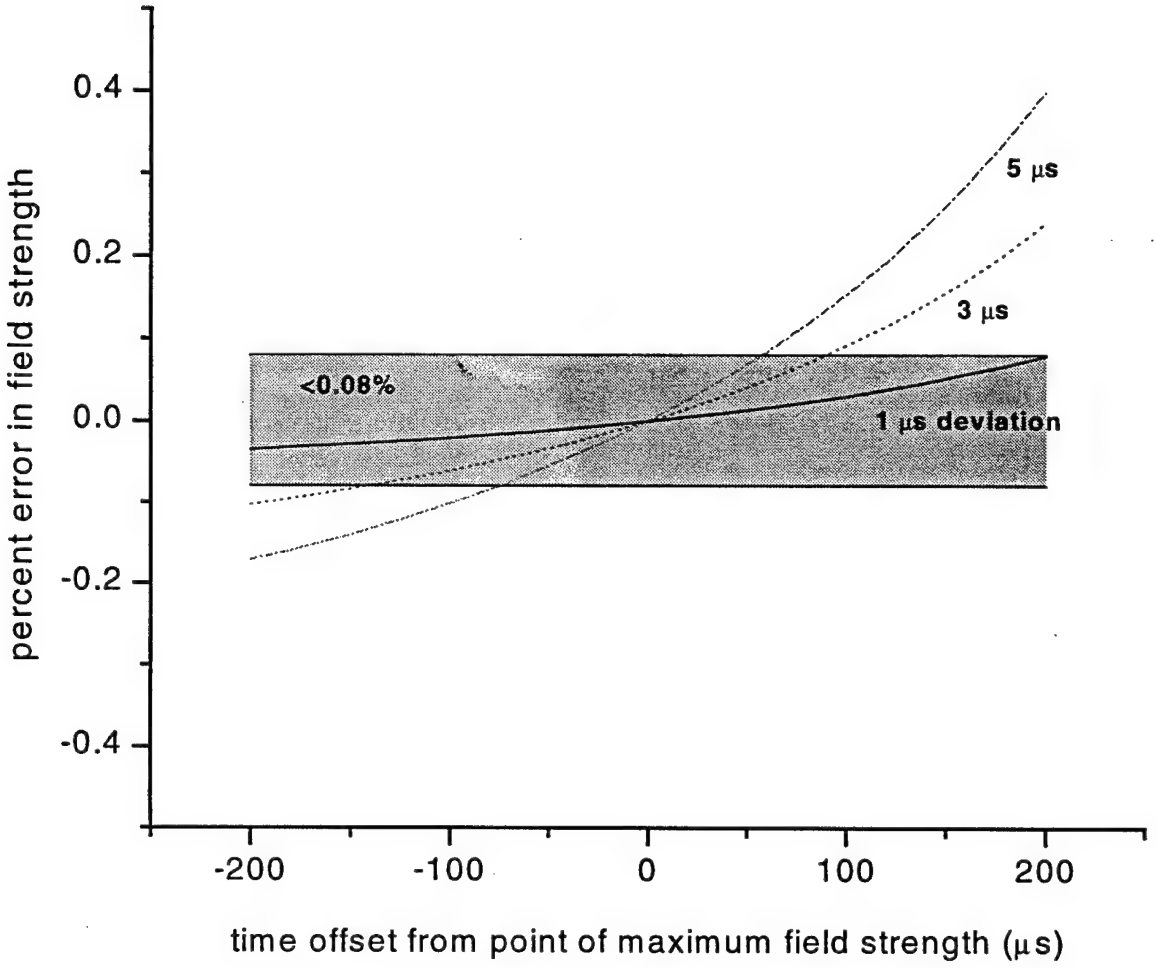

Figure 8. Estimated error in field strength due to coil-to-coil variations for a 400 microsecond time window around the field maximum. *Variations in coil to coil impedance create a 1 microsecond deviation in the time it takes different coils to reach maximum. The effect of changing the arrival of the 10 ps electron bunch relative to the time at which tuning was performed is determined by computing the field error arising from deviations between coils of 1, 3 and 5 microseconds. The cited value of 0.08% in peak amplitudes is meaningful for the entire time window, which is larger than needed in practice.*

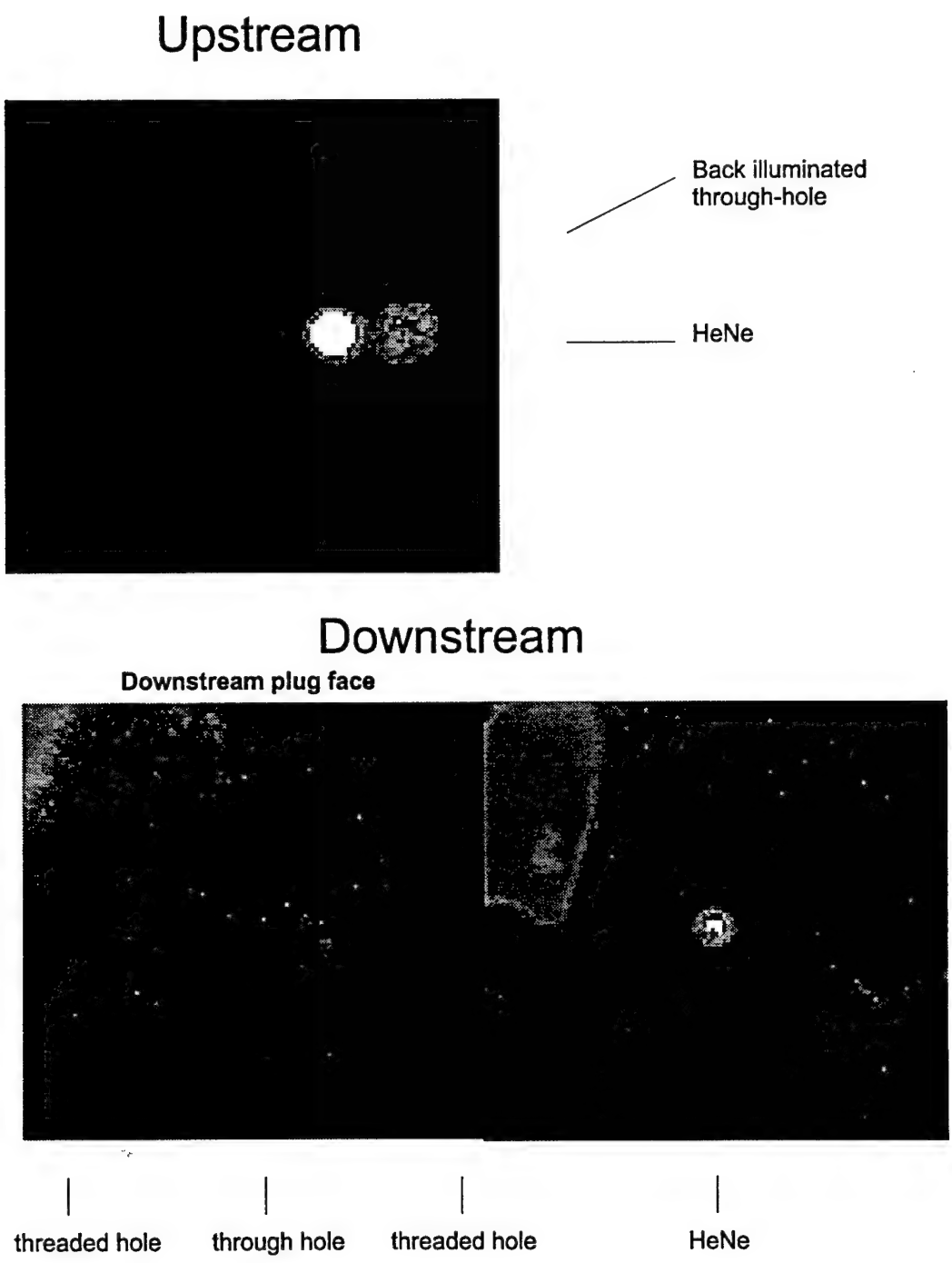

Figure 9. Wiggler mechanical alignment. *One of the wiggler alignment schemes relied on tight-fitting brass inserts which plugged the wiggler bore from either end. The upstream plug (upper image) contained a centered 13 mil through hole, which can be seen back-illuminated and unaligned to the left of the HeNe. The downstream plug (lower left image) contains a larger hole. (Flanking this through hole on the right and left are 2-56 threaded holes for plug removal.) The wiggler lateral position was adjusted until the HeNe was concentric with both through holes (lower left image).*

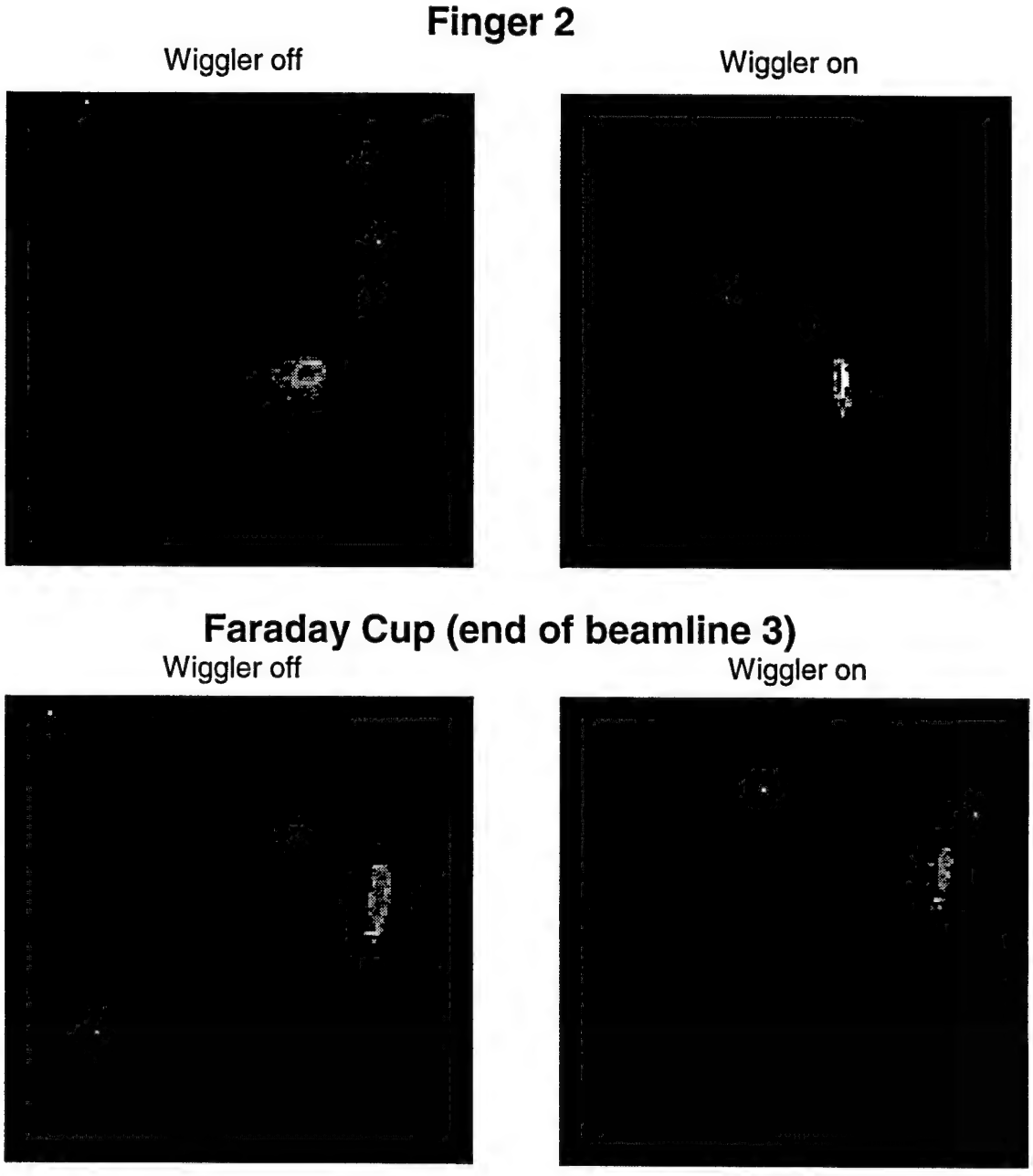

Figure 10. Comparison between the beam positions downstream from the wiggler with the wiggler on and off. *The upper pair of images was taken at the phosphor screen located about half a meter from the end of the wiggler. The "wiggler-on" shot on the right shows the strong focussing at this distance for the 48MeV tune as well as no visible deflection in either plane (Note that the wiggle plane is vertical for this wiggler). The lower pair of shots was taken at the end of the beamline, about 5 meters from the wiggler, and also shows no deflection. This negligable deflection at two locations was achieved with a careful setup and is not possible without a good quality field profile.*

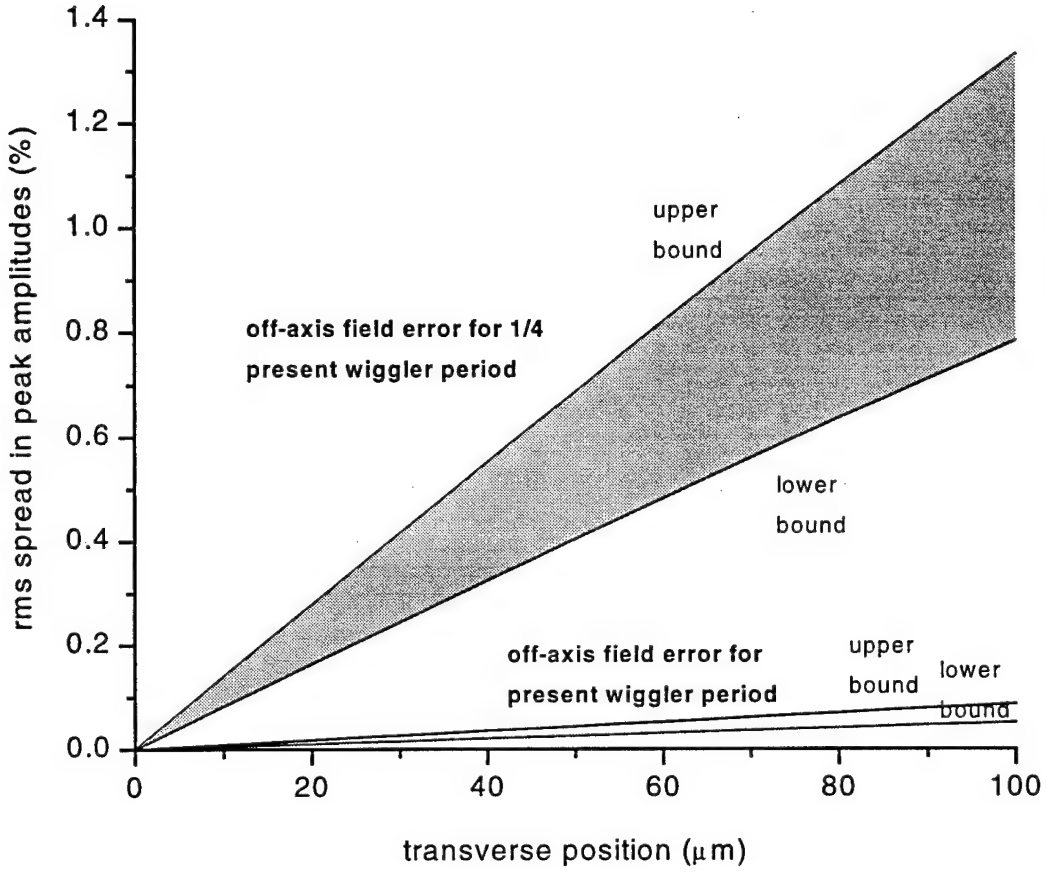

Figure 11. Comparison of off-axis field error due to spread in magnetic centers for two wiggler periods. *This source of field error becomes more significant as the wiggler period becomes shorter because of the scaling of the tranverse field variation with* k_w. *Shown are the marked increase in contribution to off-axis field errors for 10-17 μm spread in magnetic centers for a microwiggler with a 2.2 mm period (shaded region) compared with the present period of 8.8 mm (lower two curves).*

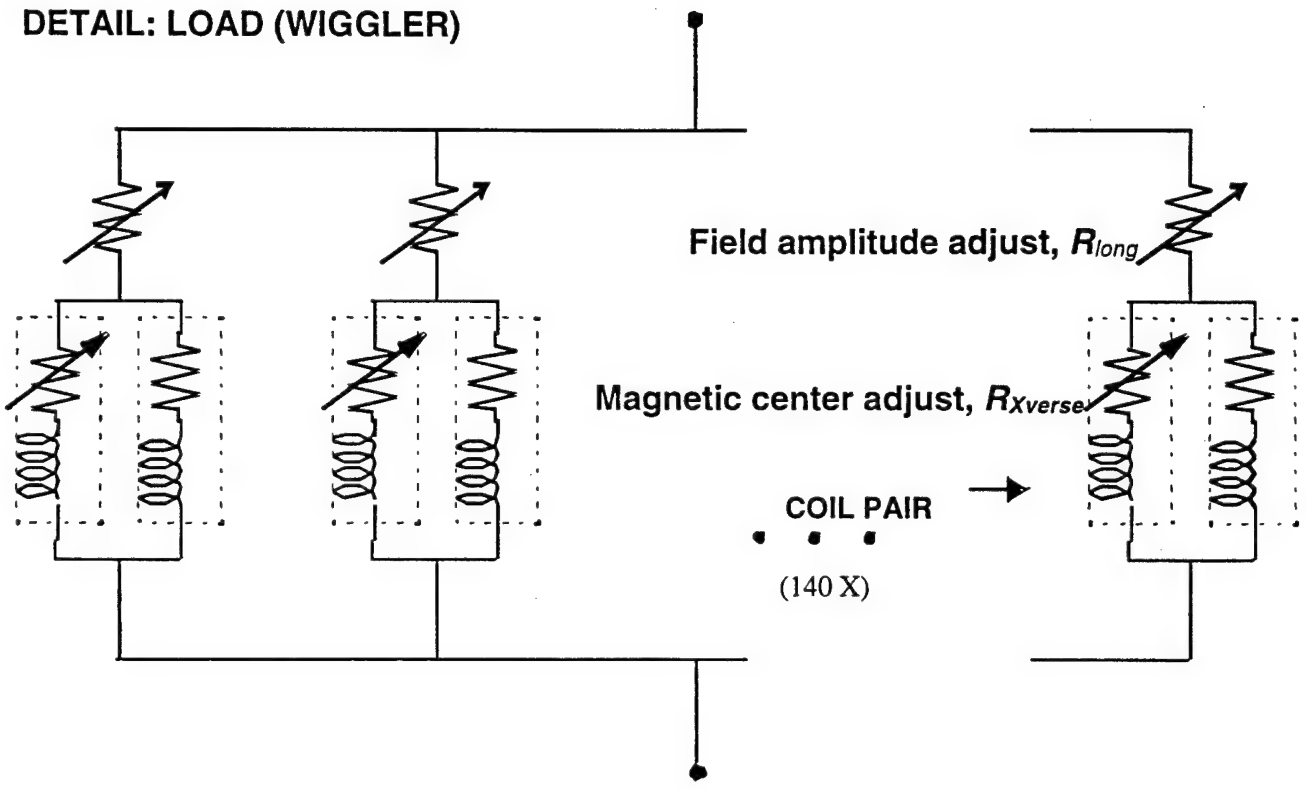

Figure 12. Wiggler equivalent circuit modified to include two-dimensional tuning. *A simple modification to the wiggler circuit would permit control of the magnetic centers as well as peak amplitudes. An additional variable resistance added to one arm of a pair of facing coils shifts the current distribution from one coil to the other and controls the boundary condition which determines the position of the magnetic center.*

References (Chapter 2)

[1] R. Stoner, "Radiation from relativistic electron beams in periodic structures," Ph.D. thesis, Massachusetts Institute of Technology (1994).

[2] R. Stoner and G. Bekefi, "A 70-period high-precision microwiggler for free electron lasers," *IEEE J. Quantum Electron*, **31**(6), 1158-65 (1995).

[3] Suggestion from Cyrus Biscardi.

[4] G. Ramian, "The new UCSB free electron lasers," *Nucl. Instr. & Meth.* A, **318**, 225-229 (1992).

[5] J. W. J. Verschuur and R. W. Warren, "Tuning and characterization of Twente wiggler," *Nucl. Instr. & Meth. A* **375**, 508-510 (1996).

[6] R. W. Warren and C. M. Fortgang, "Fabrication of high-field short-period permanent magnet wigglers," *Nucl. Instr. & Meth. A* **341**, 444-448 (1994).

[7] C. M. Fortgang and R. W. Warren, "Measurement and correction of magnetic fields in pulsed slotted-tube microwigglers," *Nucl. Instr. & Meth. A* **341**, 436-439 (1994).

[8] Suggestion from Bob Malone.

[9] Suggestions from Cyrus Biscardi and Bill Cahill.

[10] Suggestion from Rick Stoner.

[11] Discussions with Professor H. A. Haus

[12] K. W. Berryman, "Design, operation and applications of a far-infrared free electron laser (optical klystron)," Ph.D. thesis, Stanford Univeristy (1995).

[13] A. Lumpkin, B. Yang, Y. Chung, R. Deju, G. Voykov and G. Dattoli, "Preliminary Calculations on the Determination of APS Particle-Beam Parameters Based on Undulator Radiation," *Proceedings of the 1995 Particle Accelerator Conference*, 2598 (1995).

[14] Suggestion from Professor H. A. Haus.

CHAPTER 3: EXPERIMENTS IN BEAM CHARACTERIZATION

3.1 Introduction:

A desire to implement wiggler-based diagnostics has been expressed in the literature for many years. The application is appealing because wigglers are common in beamlines, and the most direct way to extract the information about the beam behavior identically at the wiggler position is from the wiggler itself. Moreover, given a sufficiently high quality field profile, the beam exits the wiggler intact for downstream use with an easily calculable transformation from input to output, enabling it to join a small class of beam diagnostic devices which are non-perturbative.

3.1.1 Strengths and weaknesses of wiggler-based diagnostics. There are areas in which wigglers can outperform other diagnostics. We demonstrate experimentally that single shot techniques are a particular strength of a wiggler for the regime in which we were operating, and provide single shot information about the characteristics of a single micropulse down to very low charge levels (50pC). By comparison, the user facility diagnostics available for parameters such as bunchlength and divergence were integrated measurements with several additional disadvantages. They were physically dislocated from the position of interest. The emittance measurement was performed in another beamline. Sometimes the beam experienced changes in the beamline before reaching the wiggler. In the case of bunchlength, a slit collimated the beam differently during the experiments than during the diagnostic measurement. Finally, the standard procedures required substantial changes to the beam tune. It is also worth noting that the extensive tunability and efficient control over

the field profile of this microwiggler may provide special advantages for beam diagnosis which as yet remain unexplored.

It is correct to argue that every diagnostic has its own area of particular strength. The compactness and economics of construction of this microwiggler was a considerable achievement by the designers[1]. However, one should consider whether the size and cost of building a wiggler and the effort to provide good alignment and matching of the beam into the wiggler makes it harder to manage than another device for the measurement some given parameter. In spite of this, there are arguments for expanding the wiggler's repertoire to include as many parameters as possible, irregardless of whether companion techniques are available. All too many times, two diagnostic techniques which both appear to be set up properly will produce different numbers for the same parameter. In the end it is most prudent to perform or at least to debug absolute calibrations with multiple techniques which have as different an underlying basis as possible. Looking at the other side of the coin, the analogy which exists between wiggler radiation other Cerenkov-type devices will permit diagnostic procedures developed with wigglers to carry over to other devices. Each may be more or less suited for a given range of parameters according to its construction and other singular qualities.

3.1.2 The opposing arguments. The full potential of the wiggler as a diagnostic has not yet been reached experimentally. In fact, during the course of this work, the pursuit of quantitative diagnostic applications of this wiggler met with skepticism. One argument voiced was that the opening angle of the spontaneous emission in the first harmonic was too broad compared with typical beam divergence to make a precise measurement. In fact, this is the reason why wiggler harmonics are used for diagnostic purposes, as the opening angle scaling

with harmonic number n goes as $1/\sqrt{n}$. The second opposing argument put forth was that the two largest contributors to the spontaneous emission broadening for the 40-55 MeV regime, beam divergence and energy spread are comparable in magnitude and similar in appearance in the spatial profile. The reason for the similarity can be seen from the fact that beam divergence in the *1-d* model is included by transferring the spread in angle to the spread in parallel velocity of the vector projection onto the longitudinal axis. This is completely indistinguishable from a spread in longitudinal velocity due to energy spread. To make matters worse, beam divergence is not the only effect which can be modelled this way; wiggler errors is another example.

We show in this chapter how these arguments were overcome and describe single macropulse experiments on beam characterization with the spatial profile of the emissions at 48 MeV.

3.2. Theory

3.2.1 Basic scalings. Many of the basic characteristics of the spatial and spectral profiles of the wiggler spontaneous emission are determined by the characteristic phase matching condition of Cerenkov radiation:

$$\lambda = \frac{\lambda_w}{2\gamma^2}\left(1+\frac{a_w^2}{2}+\gamma^2\theta^2\right)$$

The reasons for this are fundamental[2] and the condition describes the emissions of a entire family of devices. Some examples are Smith Purcell radiation, in which surface charge oscillates down a grating as the beam passes over it, transition radiation from a thin foil of high dielectric constant or metal, and other experiments specifically labelled Cerenkov radiation, in which the electron beam propagates through various media. Because almost all of the diagnostic properties of the wiggler radiation which are developed in this chapter can be estimated very simply from the phase matching condition common to these devices, it follows that the techniques developed for wiggler diagnosis may be adapted to other members of this family, which, like wigglers, are frequently found in beamlines. Part of the strength of this measurement relied on the fact that the emissions were set in the visible, and for other ranges of beam parameters, one or another of these devices may be more suitable.

The detailed expressions governing synchrotron radiation have been derived and discussed comprehensively by K.-J. Kim. The full expression for the spectral flux density of wiggler emissions is [3]:

$$\frac{\partial^2 F_{\sigma,\pi}}{\partial^2 \Omega} = \alpha \frac{\Delta\omega}{\omega} \frac{I}{e} \left(\frac{K\gamma}{1+\frac{K^2}{2}} \right)^2 \left(\frac{\omega}{\omega_1(0)} \right)^2 N_w^2 S_N \left(\frac{\omega}{\omega_1(\theta)} \right) B_{\sigma,\pi}^2(\omega,\varphi,\psi)$$

$$\text{where } S_N\left(\frac{\omega}{\omega_1(\theta)} \right) = \left(\frac{\sin\left(\pi N_w \frac{\omega}{\omega_1(\theta)} \right)}{N_w \sin\left(\pi \frac{\omega}{\omega_1(\theta)} \right)} \right)^2$$

$$\omega_1(\theta) = \omega_1(0) \frac{1}{1+\gamma^2\theta^2/(1+K^2/2)} \text{ and } \omega_1(0) = \frac{2\gamma^2}{1+K^2/2}\omega_u$$

$\frac{\partial^2 F_{\sigma,\pi}}{\partial^2 \Omega}$ is the number of photons per second per solid angle Ω, α is the fine structure constant, and $\frac{\Delta\omega}{\omega}$ is the percent bandwidth. I is the electron beam current and e the electron charge. As before, N_w is the number of periods in the wiggler and $K=a_w$ is the wiggler parameter. $\omega_1(\theta)$ is the phased matched frequency at a radial angle θ, within which ω_u is the frequency defined from the wiggler period. The azimuthal dependence is expressed in terms of the wiggle plane (subscript σ) and non-wiggle plane (subscript π), for which the angular variables are ϕ and ψ, respectively. The radial angle θ is equal to $\sqrt{\phi^2+\psi^2}$.

The essential scaling of the amplitude term is proportional to ω^2, for dipole radiation, and inversely proportional to γ^2, reflecting that intensity drops off as the electron traverses the magnetic pole in a shorter time and therefore experiences less of a deflection. The grating term arises from the periodic structure of the wiggler, and simplifies to a sinc function for small changes around each harmonic. Its maximum is determined by the phase matching condition and its width by the length of the wiggler, N_w. The sinc function also describes the concentration of the emissions into the $1/\gamma$ cone. The term $B_{\sigma,\pi}$ contains the azimuthal dependence of the radiation lobes, which is important at radial angles on the order of $1/\gamma$, and can be evaluated as a sum of Bessel functions. Because the spectrum is narrow and the energy spread sufficiently small, the amplitude factor is slow varying. The Bessel functions are approximately constant for small angles. Thus, the fastest varying term in this expression for small radial angles arises from the phase matching condition.

We now consider the behavior of narrow bandwidth cones as a function of the cone angle and beam parameters. The radius of the cone can be controlled by varying the beam

energy or filter central wavelength, as can be seen from Figure 1, which shows the phase matching condition for our experimental parameters and an intercepted cone. The cone width depends on the number of wiggler periods, and is further broadened by the beam energy spread, the beam divergence and the filter bandwidth. One nanometer bandwidth filters are available at conveniently spaced wavelengths across the visible spectrum, essentially furnishing a coarse adjustment knob over a range of beam energies. Fine tuning of the cone angle for a desired beam energy can be achieved by reasonable adjustments of the filter tilt and/or wiggler field strength.

The dependence of the cone radial angle, θ_{cone}, on wavelength, beam energy and wiggler field strength is given by phase matching condition. At a fixed wavelength, the contribution to the cone width scales differently with cone angle for the various broadening mechanisms. Simple expressions for the contributions of natural linewidth ($\sigma_{cone,nat}$), energy spread ($\sigma_{cone,\gamma}$), and divergence ($\sigma_{cone,x'}$) to the cone width in the wiggle plane are:

$$\sigma_{cone,nat} = \frac{1}{4N_w}\frac{1+\frac{a_w^2}{2}}{\gamma^2\theta_{cone}}, \qquad \theta_{cone} >> \frac{1}{\sqrt{N_w}\gamma},\ N_w >> 1$$

$$\sigma_{cone,\gamma} = \frac{\sigma_\gamma}{\gamma}\frac{1+\frac{a_w^2}{2}}{\gamma^2\theta_{cone}}$$

$$\sigma_{cone,x'} = \sigma_{x'}$$

The wiggle plane corresponds to the x-z plane, where z is the direction of propagation of the beam. σ_γ and $\sigma_{x'}$ are the widths of Gaussian distributions in energy spread and x divergence,

θ_{cone} is the angle at the which the resonance condition is satisfied for a fixed wavelength, N_w is the number of wiggler periods, and a_w is the wiggler parameter. For comparison with the preliminary data, analysis assumes transverse beam size small compared with the cosh variation of the magnetic field, and neglects the contribution from betatron motion.

The scaling of these equations can be explained qualitatively with a simple sketch of the phase matching condition for perturbations in beam energy and propagation angle (Figure 2). The parabola will shift vertically for a new co-directional electron with energy $\gamma_0+\delta\gamma$ and will shift horizontally for a new electron with the identical energy, but travelling at an angle $\delta\theta$ with respect to the wiggler axis. A sense of the broadening can be obtained by noting the width intercepted between a pair of parabolae which are shifted by energy (upper plot) and a pair which are horizontally shifted by divergence (lower plot) for different conditions. Any change which moves the operating point away from the bottom of the parabola decreases the intercepted width. For the case of two electrons with different energy, the radial angle θ_{cone} increases if the filter wavelength increases with respect to the on-axis wavelength, or if gamma increases. The contribution to the width from the natural linewidth also approaches a delta function as the cone angle becomes large. However, for divergence, the broadening in the spatial profile will be strong on-axis, but does not drop out as θ_{cone} increases. Thus, the contributions of natural linewidth and energy spread to the width decrease with cone angle, and for sufficiently large angles, the width is dominated by the distribution in divergence. In our case, the resolution in divergence is good above 2.5-3 mrad for reasonable energy spreads (0.6-1%). Note that the requirements on the collection angle of the system are easy to

implement for N_w=70, being only a few mrad. This is one of the advantages offered by a long microwiggler with good uniformity for this type of application.

To include some additional effects beyond those described by the analytic expressions, a code was written which convolves the full spectral flux density for a single electron with Gaussian distributions in energy spread, and x and y divergence. Computation of the Bessel function term was optional. The code calculates the slice of the cone in the wiggle plane for an array of any two of the energy spread, x divergence and y divergence, and generates a contour plot of χ^2 for theory compared to either laboratory or synthetic data. In this way, the relative sensitivity to two fit parameters can be observed graphically. The same code, modified appropriately, was incorporated into a multi-parameter fitting routine.

3.2.2 A comment on the sensitivity of the spatial profile vs. the spectrum.

The use of the spatial profile and spectrum for beam diagnosis from parameter-induced broadening is not equivalent. This is because the natural linewidth of the spectrum off-axis is defined by the length of the emission train and does not depend on angle. By contrast, the natural linewidth in the spatial profile arises from the angular change required to produce destructive interference at a given wavelength, which reduces with angle of observation. It is the scaling with angle which gives the spatial profile an advantage in sensitivity over the spectrum when each is viewed off-axis.

3.3 Experimental Setup

The core of the experimental setup is shown in Figure 3. The electron beam passes through the microwiggler, the spontaneous emission is outcoupled and intercepted by the interference filter, and the remaining narrow bandwidth constituent is focussed onto a CCD camera. The interference filter parameters were chosen to have a central wavelength of 532 nm and a bandwidth of 1 nm, which is sufficiently narrow to produce negligible broadening compared with other sources. A 10 nm bandwidth filter at the same wavelength was also available for comparison. The wiggler bore, made of smooth stainless steel waveguide, has dimensions 3.5 by 7 mm, and the wiggler length is about 0.6 meters. This limits to 4 mrad the collection angle at which emissions can pass out of the bore without experiencing any reflections.

3.3.1 The Accelerator Test Facility. The experiments with electron beam were performed in collaboration with researchers at the Accelerator Test Facility, a linac-based Users Facility at BNL. The ATF injector consists of a 1 ½ cell photocathode RF gun driven by an S-band klystron, and a focussing solenoid. The cathode is illuminated by a 10 ps Nd:YAG laser. The cathode material was originally copper (Gun 1B) and later interchangeable with magnesium (Gun III). As a rule of thumb in this thesis, the macropulse measurements were performed with Gun 1B and the single micropulse measurements with Gun III. The beam is accelerated to its full energy by two sections of SLAC-type linac and transported to one of

three beamlines. An overview of the transport line from injector through the end of the Experimental Hall, where the experiment was installed in beamline 3, is included in Figure 4.

A bending dipole separates the electron beam and optical emissions about 1 meter downstream from the wiggler, and the optical emissions are outcoupled with a coated silver mirror and a glass vacuum port. A multi-position diagnostic port 0.5 meters downstream from the wiggler contains a phosphor coated target for monitoring beam spot size and position, a thin pellicle for alignment use which generates some weak transition radiation, and a through hole for beam passage under normal operation. The beam continues about 5 meters downstream and is terminated onto a Faraday cup for charge measurement.

First studies on emission-based beam diagnosis were done with a beam energy of 48 MeV and a train of 20 microbunches at 150-200 pC each. Later, spatial profile measurements were performed on a single micropulse at 44 MeV, which will be described in a subsequent chapter. Nominal figures for energy spread and emittance for this chapter were 0.5% full width, and a few π mm-mrad, respectively.

The diagnostic system on the beamlines was built up over many years by ATF personnel and consists of measurements based on a variety of techniques. A collimating slit in the front end in a dispersive region following a bending dipole is used to monitor energy spread. Large changes in energy spread were deliberately introduced either by closing down this high energy slit, reducing the transmitted fraction of the beam, or by dephasing the second section of the linac to produce a chirp on the beam much larger than the local energy spread and maintaining a constant transmitted fraction of the beam. Emittance is usually measured in the front end with the quadrupole scan technique. It was difficult to measure emittance at the position of the wiggler with good resolution with this method. As a result, quadrupole scan

emittance measurements in the Experimental Hall took place in an adjacent beamline. Faraday cups and stripline monitors were positioned at various locations along the line. All the charge measurements cited here were obtained from either the Faraday cup at the end of beamline 3 or the one immediately following the gun. The beam profile was usually viewed with phosphor screens.

3.4 Experimental results

The dependence of the S.E. cones was studied as a function of beam energy, interference filter incident angle, beam energy spread, wiggler field strength, misalignment, and various beam optics.

3.4.1 Cone-angle scan. A scan comprised of a series of cones which systematically scan cone radius is particularly rich in information, both qualitative and quantitative, and demonstrates effectively why the S.E. cone is such a powerful tool. The cone provides immediate, visual feedback with a change of nothing more than a fraction of a percent in the mean beam energy, as can be seen in Figure 5. Eight cones of increasing cone angle (radius) are shown, each differing by only 0.5% in beam energy. The nominal beam energy was 48 MeV. The distinction between the cones at 0.995, 1.000 and 1.005 times the nominal beam energy at which the on-axis first appears are particularly easy to identify visually. In practice, the qualitative attributes of the cone were enough to earn it a natural role in the tuning process.

The scaling laws predict that a cone angle scan will be characterized by specific features. Among these are the familiar intrinsic width of the on-axis emissions, an asymptote leading to the value of beam divergence in the off-axis emission, and calibration information about beam energy (or angular calibration). There are two ideally equivalent ways to implement such an experiment: by varying the beam energy and by varying the filter tilt. Both were performed. The γ scan in figure will be used below to test for the presence of these features.

Calibration of beam energy. The reason that a good calibration of the beam energy is a product of the cone angle scan is because most of the contributing errors can be made very small: the angular calibration can be measured very accurately by standard optical techniques, the filter tilt can be measured with low error given enough data points with stable beam, and the curve is less sensitive to a_w when $a_w^2/2 << 1$.

Such an analysis is shown in Figure 6, where cone angle, θ_{cone}, is plotted against beam energy along with a fit to the phase matching condition. The filter tilt, which determines the filter central wavelength was determined directly from the spontaneous emission by looking for the turning point in the cone radius as a function of angle. The wiggler parameter was determined as described in the previous chapter and has an error bar of 5-10%. An independent measure of the beam energy was provided by the facility with a calibrated bending dipole and is cited to about a percent. When this data set was analyzed, the fit parameter values (μrad/CCD pixel, γ, filter tilt and a_w) all fell within the error bar of independent measurements. This type of scan offers a competitive measure of the beam energy.

Single shot calibrations of beam energy can be performed given good measurements of the accompanying parameters from a single cone, or, for more accuracy, from a double cone formed with two filters of different wavelength.

Comparison with beam energy calibration based on spectral measurements. One can calibrate beam energy with a measurement of the peak wavelength using a spectrometer. The spatial profile has the following advantages: The co-alignment of the emissions with a potentially long optical transport line is not an issue. The spatial profile provides visible reassurance that nothing in the system caused a change in direction of the emissions, a frequently observed drift. In Figure 5, all the cones are concentric and digression from this state would be easy to detect. Although the cones included in the set are more or less symmetric, asymetric cones were often observed, particularly in the non-wiggle plane, which was probably caused by jitter in the pointing of the electron beam. In the spectrum, such jitter would translate into small shifts in the spectral peak, and it would be much harder to resolve its origin without further information.

Test for expected behavior on-axis. A straightforward and familiar limit to examine in the data set of Figure 5 is the behavior of the on-axis emissions, where theory predicts the unbroadened half width of $\sim 1/(\sqrt{N_w}\gamma)$. The measurement exceeds this value, consistent with inhomogeneous broadening. More detailed fits, described below, confirm that the on-axis behavior is reasonable.

Test for the predicted asymptote in the off-axis cone width. Cone width in the wiggle plane was analyzed systematically as a function of γ, or, equivalently, θ_{cone}, in order to compare the predictions of the analytic expressions with the observed features. In Figure 7, two curves recording FWHM are shown, one starting at the forward emissions and the other in the regime where there is no on-axis emission. The former defines the FWHM from cone outer edge to outer edge and is most interesting at small angles. The latter corresponds to the FWHM of the cone ring width, which loses meaning when the on-axis null starts to fill up. A distinct asymptote in FWHM2 is observed in the data as the cone radial angle increases. The scaling expressions predict such an asymptote when θ_{cone} is greater than 1.3 mrad, which agrees with the data, and that this asymptote should converge to the value beam divergence. The measured one-σ width at this asymptote is 0.3 mrad. At θ_{cone} = 2.6 mrad, equations 1-3 predict the natural linewidth to be 0.16 mrad and the width due to energy spread to be negligible for typical energy spreads, which yields an estimate for $\sigma_{x'}$ of 0.25 mrad from the data. A least squares contour plot (Figure 8) which compares the experimental data with the code for an array in energy spread and x divergence confirms a best fit at 0.25 mrad. The fit, which was performed for a slice in the wiggle plane, was found to be insensitive to the values of energy spread and y divergence. The solid curve fitting the experimental data in Figure 7 was computed with the divergence extracted above, and a full width energy spread of 1% (0.25%, one-σ) and fits the entire data set well, including the on-axis emissions.

A qualifying remark is interjected at this point. Two imaging setups were used during the course of these scans. In one, the plane at infinity was focussed onto the CCD chip. The

imaging used in the present chapter focussed a plane 9 cm in front of the wiggler onto the camera. We have neglected the contribution of transverse beam size in the analysis here and in reference 4. When it is taken into account, the estimate for beam divergence changes from 0.25 mrad to 0.35 mrad. The value of x divergence extracted from the spontaneous emission is reasonable for the beam tune, and corresponds to a beam emittance of about 8π mm.mrad.

The correct way to image the emissions if the goal is to extract beam divergence in a single shot is to focus the plane at infinity onto the camera. Examples of data taken with such imaging are contained in Chapter 5, where the single micropulse cone measurements are described. The influence of the transverse beam size in the off-axis emissions close to the wiggler is useful. Imaging the near field at a sufficiently large angle so that the diffraction limited spot size is small compared with the beam spot size is one way to separate the information of transverse spot size from other effects. Further directions in which this idea may be taken are discussed in the section on future work at the end of this Chapter.

3.4.2 Energy spread scans. There are several ways to test for the reduced effect of energy spread as a function of angle which is predicted by the scaling laws. The most simple is to vary the energy spread and to compare the effect on large and small cones. The assumption is made that the change induced in energy spread dominates any change in the beam divergence. The energy spread was added by imposing an energy chirp to the beam by dephasing the second section of linac and keeping the percentage of the beam which passed through the slit constant. Cones were measured for energy spreads ranging from 0.5% full width to 2% full width for cone angle of 1.5 mrad. The results, shown in Figure 9 show marked variation with energy spread. An experiment was also performed in which the energy

spread was varied for a cone of large radius, and negligible changes in the cone width were observed.

The effect of energy spread was also monitored with measurements of the spectra and the sensitivity of the cones and the spectra to a similar range of energy spread can be seen by comparing Figure 9 with Figure 10. Because of jitter, and the cones and spectra are sorted for highest intensity and best symmetry (implying similar alignment on the high energy slit, and otherwise minimizing the complications of jitter), and regular trends are clear as a function of the induced energy spread.

3.4.3 Slice information from cones. S. E. cones may be used to complement studies of slice emittance. The head, middle, and tail slice of the beam are typically separated by placing an energy chirp on the beam and using the high energy slit as a selector. Marked changes in cone width (θ_{cone}~1.5 mrad) were observed when different portions of the beam (without change in chirp) passed through the high energy slit. A comparison of the integrated emittance and energy spread to the central slice was made by keeping the high energy slit fixed and increasing the chirp on the beam, so that a smaller percentage of the beam passed through the slit. Cone width sharpened noticeably. Thus spontaneous emission measurements indicate that a better quality of the beam in the central slice compared with the total beam exists at the location of the wiggler.

3.4.4 Wiggler field strength scans. *A few ways to measure the Twiss parameters.* In principle, the Twiss parameters, similar to the q parameter in optics which defines the

envelope of a Gaussian beam, in the wiggle plane can be estimated from a measurement of a cone at large angle and measurements of the beam spot size on BPM 1 and 2. Part of the reason why effort was delegated to using the wiggler to estimate Twiss parameters was that the nearest two positions at which emittance measurements could be set up with quadrupole scans were in an adjacent beamline, or substantially upstream from the wiggler.

The quadrupole scan technique for measuring Twiss parameters can be applied to the wiggler emissions in two ways: from the beam spot size downstream from the wiggler, or from the cone measurements. The equations for the quadrupole scan need to be modified so that the wiggler is modelled as a thick lens, rather than thin. The standard procedure can then be used on the beam spot size measured downstream from the wiggler. In order to extend this technique to S.E. cone measurements, we suggest that divergence be monitored instead of spot size as a function of field strength using large angle cones. This can be implemented by maintaining the radius of the cone constant with a small tilts of the interference filter(s) while the wiggler field strength is varied, or better yet, to set an operating point where all the measured cones would lie in the off-axis emissions. The standard analysis is modified by substituting the measured vector of beam divergences for the measured vector of spot sizes. Both of these variations on the quadrupole scan require that field quality remains sufficiently good over the entire range of variation, and the beam size in the wiggler be sufficiently small that it experiences a linear restoring force from the variation of the wiggler longitudinal field.

As a first benchmark, the response of S.E. cones and downstream spot size to a sweep in a_w was measured experimentally without adjustment of the other beam parameters. A family of profiles, shown in Figure 11, was recorded for ten values of a_w. The variation in cone

radial angle, similar in appearance to the γscan, as well as a difference in the cone width in the wiggle and non-wiggle plane are expected features which are observed in the data.

Scans of the spot size downstream from the wiggler as a function of field strength similar to those accompanying the cone measurements in Figure 11 were recorded during previous runs for two different beam tunes (Figure 12), and the modification to the quadrupole scan described above was applied to this data. The estimated emittance from both runs was 6π mm.mrad, which comes within a factor of two of the facility measurements. The spot size on the phosphor preceeding the wiggler agreed with that calculated from the extracted Twiss parameters to 15% in one case. During some runs it was difficult to maintain acceptably low error bars due to machine jitter and the difficulty of recording the behavior at the waist. The measurement error would have been improved by sending the beam fully through a waist during the scan. This condition was satisfied for our present target position at a lower beam energy.

Using the onset of the on-axis null. The following expressions give the percent change in beam energy and wiggler field strength required to shift the single frequency emission pattern for a single electron from a peak on axis to the first null, which give a sense of the relative sensitivity in these two parameters:

$$\frac{\Delta a_w}{a_w} = 2\frac{\left(1+\frac{a_w^2}{2}\right)}{N_w a_w^2}$$

$$\frac{\Delta\gamma}{\gamma} = \frac{1}{2}\frac{1}{N_w+1}$$

For our parameters, the numbers work out to $\Delta\gamma/\gamma_0 = 0.7\%$ and $\Delta a_w/a_w = 20\%$ at $a_w = 0.37$ and nominal beam energy $\gamma_0 \sim 100$. The corresponding radial angle shift is from 0 mrad to 1.3 mrad. In practice, these values are changed by a few tens of percent by the distribution in beam parameters. For an 8-bit CCD camera, a 100% change in intensity is monitored to better than 1 part in 200. Thus, our parameters are such that the cones are much more sensitive to relative changes in the mean beam energy than in the wiggler field strength, but enough resolution is still available to make use of the wiggler field strength effects. The former has good consequences for applications such as beam energy calibration. As an application of the latter, we carried out an in-vacuum change in the length of the wiggler using the onset of the on-axis null.

The sensitivity of the cone radius and null to field strength was used to set the new operating point for the wiggler field strength without the luxury of a field measurement. Later, once a vacuum break was possible, it turned out that the field strength was set properly to within 1%. As our angular resolution provided about 1 part in 20 resolution of the measured shift in the peak at the first null of ~1.3 mrad, corresponding to a shift of 20% in a_w, this measurement is consistent with the preceeding estimate. The ability to make an in-vacuum change in the wiggler was a useful time-saver.

3.4.5 Alignment directly from the spontaneous emission. The effect of misalignment on both the spontaneous emission spectra and spatial profiles was recorded. In Figure 13 the beam was misaligned deliberately in the plane of field variation by the maximum amount allowed by the 3.5 mm wiggler bore, and broadening in the 1 nm spatial profile all but

washed out the cone interior. The sensitivity of the spectra to misalignments in the non-wiggle plane is shown in Figure 14. It was possible to obtain significant reductions in the width of the spectra by adjusting alignment systematically with the spectra as a guide. Single shot spectra diagnostics were set up to make such optimization procedures more efficient and to reduce integrated effects.

The narrow bandwidth emissions were found to provide useful information about cavity alignment. A filter was placed at the output of the cavity and the emission profile was examined for various filter tilts. It was found that the sensitivity to tilt was almost as good as the Fabry-Perot-based technique, which requires coherence. This technique had the advantage that it aligned the cavity directly to the spontaneous emission, rather than the alignment HeNe. At the time, the direction of best optical alignment was did not coincide with the Fabry-Perot technique. The subsequent discovery of multiple pieces of magnetic material in the beamline was consistent with this observation.

3.5 Application of wiggler emission – based diagnosis: identifying and understanding startup.

The information provided by wiggler emission - based diagnostic techniques is important to the proper experimental identification of the early stages of startup. When a system is complex, and effects are small, it is essential to study and characterize the effect in as many ways as possible. Even more basically, the properties of spontaneous emission must be carefully considered when determining system requirements for startup. For example,

theoretical work was performed in support of these experiments[5] which determined a new criterion for the length of the pulse train required for FEL startup for our parameters.

The original goal of this project, which began in 1989, was to build an FEL oscillator in the green, and ultimately UV wavelengths. Early attempts to lase with the oscillator at 532 nm were not successful. Progress was made in the system, increasing the length of the pulse train and switching to a Magnesium cathode for higher quantum efficiency. The wavelength was switched to 1064 nm, as gain would be higher with the longer wavelength and the requirements on the electron beam quality reduced. Startup with the oscillator was not observed at 1064 nm. However, because single bunch production could be implemented with higher currents than those available with a pulse train, searches for single pass amplification took place, and self amplified spontaneous emission was demonstrated at 1064 nm.

Understanding the physics of self amplified spontaneous emission has been a subject of considerable theoretical effort in recent years[6,7]. However, experimental work has until now been limited to long wavelengths, the most recent reported results being those of CLIO at 10 and 5 microns[8]. Moving studies toward shorter wavelengths is technically challenging because of tighter demands on the quality of the system. Furthermore, the longer wavelength experiments are favored by higher gain and a larger ratio of wavelength to bunchlength, which can provide coherent enhancement of spontaneous emission without gain. Levels of coherent enhancement of four orders of magnitude have been reported by several groups[9,10] working in the far-infrared, which provided beneficial reductions in the startup requirements for their experiments. Our experiments differed from the previous experiments in the frequency, which

at 1.064 microns was a factor of five higher than previous work, and the short period of the microwiggler, which made it possible to perform the measurements at 632 nm at a lower beam energy than the recent reported results at 5 microns.

3.5.1 The experimental setup. The experimental setup is shown in Figure 15. The CCD camera was replaced with an avalanche photodiode and a 23 nm BW interference filter at 1.064 microns was substituted for the 1 nm BW interference filter at 532 nm. The emissions into an opening angle of 0.87 mrad, defined from the wiggler center, were focussed onto the photodiode for charge variable from 0 to 800 pC. Charge was scanned by closing down the high energy slit in the front end and was measured with the Faraday cup at the end of beamline 3 simultaneous with each wiggler emission measurement. Note that because of jitter, the correspondence between the high energy slit width and the charge is not one-to-one. The beam energy for the data at 1.064 microns was 34 MeV. The wiggler was operated at a length of 60 periods for the runs with Gun III.

3.5.2 Description of the data. A scan of emissions vs. charge is contained in Figure 16a, and shows a superlinear dependence of emission power on beam charge, with a final increase over the initial slope of about a factor of two. Figure 16b shows the corresponding temporal profile of the electron beam, taken with the chirped beam technique, described in more detail in chapter 4. Further description of the beam parameter measurements can be found in reference[11], which cite 2.4π mm.mrad and 1.2π mm.mrad

emittance for the full beam and an 80 pC slice, respectively. The high energy slit full width of about 0.7% in energy typically allowed most of the beam to pass.

In order to test for coherent effects at the wavelength of 1 micron, transition radiation 0.55 meters upstream from the wiggler was measured as a function of beam charge. The emissions were limited to the same wavelength range as the wiggler emission scan using the 23 nm BW filter centered at 1.064 microns. The results are shown in Figure 16c, and exhibit a linear dependence on charge. An assumption is made that the beam properties did not change between this measurement and the measurement of enhancement (Figure 16a) which followed.

Later, during a cone measurement run at 44 MeV, a wiggler emissions vs. charge scan with a similar appearance was recorded, as shown in Figure 17. The experimental setup for this data was changed in significant ways from the runs at 1.064 microns. The bandwidth of measured emissions was different, being changed to the narrow bandwidth of 1 nm required for good diagnosis. Off-axis emissions were recorded rather than on-axis. The cone scan itself indicated that the on-axis wavelength was 593 nm, 40 nm shorter than the filter wavelength of 633 nm. Spectrometer measurements on the next run day were centered at 593 nm. An estimate of the power level is indicated on the figure. The superlinear curve exceeded the initial slope by about a factor of two. The fact that the operating point was 40 nm off-axis would lead one to worry. However, emission vs. charge curves of similar superlinear shape were observed almost at the on-axis wavelength in similar experiments.

Finally, in an early run with Gun 1B, spatial profiles were monitored as the beam energy was reduced from 48 MeV to 34 MeV, using the superelement to modify the energy over this enormous range and only one beam tune. The full single pass spontaneous emission from the wiggler at 70 periods length was incident on the CCD camera (no interference filters).

Saturated profiles were recorded all the way from just under 48 MeV to 34 MeV with a 20 micropulse train of 200 pC bunches of 7 ps bunchlength, full width. At 34 MeV, three micropulses were still sufficient to require the full dynamic range of the CCD camera. It should be strongly emphasized that this data has never been published because it was never reproduced and because for the most part it involved saturated signals. We will not comment on the shape of the spatial profile. However, one comment can be made with assurance. A Watec 902A CCD camera, which is optimized for visible response (0.03 lux at 30% video), attenuates strongly in the IR wavelengths and offers less than a few percent sensitivity at 1.064 microns. A 10 nm filter was placed in the emissions, and some, but not all of the emissions, which peaked on-axis without the filter, were found to be at the second harmonic. The effect was also seen a beam energies in the visible wavelengths, which sets the second harmonic well outside the spectral response of the CCD camera. The observation of any signal at all either at the fundamental or the second harmonic is completely inconsistent with spontaneous emission and is even more surprising given the unoptimized matching into the wiggler at 34 MeV during this run.

3.5.3 Evidence of self-amplified spontaneous emission at 1.064 microns.

It is important to compare the ability of various models to fit the data, since the observed enhancement is small (~ a factor of two) and the experimental system is complex. Caution is required in the interpretation because other experimental effects can create data of the form observed in the emissions vs. charge scans, on which the main arguments for SASE rest. Consideration of error bars is essential.

Theoretical modelling of the data at 1064 nm. Theoretical modeling was performed by L. H. Yu which showed that the data at 1.064 microns could be explained with SASE theory. Further details of his analysis can be found in reference 11. This modeling did not include coherent effects. The contribution of coherent effects due to a Gaussian bunch envelope is expected to be negligible at 1.064 microns and the scan of transition radiation at 1.064 microns did not provide any evidence of microbunching.

The modeling did not include the variation in beam parameters caused by closing down the high energy slit to scan the beam charge. Such variation comes into play because there are limited collection elements (limited spatial aperture and BW); limiting the collection of the spontaneous emission was the basic principle behind building the diagnostic setups of the previous chapter. Another uncertainty in the model is the assumption that the charge scan is identical to a current density scan.

In response, the spontaneous emission baseline was studied for various rules linking variation in energy spread and divergence with charge. Bandwidths and apertures were tried separately and together. In this modelling, the central wavelength of the filter was assumed identical to the on-axis resonant wavelength, the high energy slit was assumed to close symmetrically down on the charge, and misalignments were assumed small enough to neglect. These computations were compared with a subset of the data at 1064 nm in which the power levels could be legitimately compared. A collection of emissions vs. charge scans which were linear with charge were set against two scans which exhibited superlinear behavior.

It was found that the initial slopes were the same across this set of data, and the enhancement lay above the initial slope. The initial slopes in both cases were at a reasonable level for spontaneous emission. It then becomes impossible to explain the superlinear curves

with the spontaneous emission model. Degradation of beam parameters will cause the scan to lie below that obtained when the parameters remain constant. Significant curvature occurs when the initial slope is considerably smaller than the ideal case. Neither of these characteristics is seen in the data. This argument supports the claim of SASE at 1064 nm.

Open directions at 1.064 microns. The data was difficult to reproduce at 1064 nm, and the cause remains a mystery. It is possible that it was related to the way in which the emissions were scanned. However, a variety of functional forms were observed in the high energy slit scans at 1064 nm with the 23 nm filter and 3 mm aperture: linear, superlinear, two linear slopes, sub-linear with threshold followed by linear, as well as the inverse: concave up followed by concave down. This variation indicates two things: that the machine parameters were indeed changing from run to run and that the emission measurement setup was capable of responding to this level of change. The source of the changes was undetermined. It might have been linked to how the laser cleaning was done and how long after the cleaning the data was taken, but it was difficult to determine a consistent pattern. Best results were most often obtained right after a cleaning, but were also observed late in a run, or to diminish with time.

Coherent effects due to microbunching are a particularly important factor in startup at long wavelengths. Anomalously high power which was successfully modeled with coherent effects has been reported at the ATF for the front end Smith Purcell experiment. A recent long wavelength study of microbunching has also occurred in the facility in conjunction with the IFEL experiment. A new user experiment was proposed by D. Nguyen at the July, 1997 ATF User's Meeting to develop a bunchlength monitor from measurements of coherent enhancement in off-axis Smith Purcell radiation. In the present experiments at 1064 nm, the

test for microbunching consisted of transition radiation emissions recorded as the beam was being focussed into the wiggler slightly upstream, which were linear with charge. Since coherent effects have been observed in other experiments at the facility, documentation of the presence and subsequent disappearance of microbunching at the ATF as the wavelength gets systematically shorter over a large wavelength range would support the present data. As a tangent benefit, the dependence of long wavelength coherent effects on the laser cleaning parameters and the time from laser cleaning to data taking might provide some illuminating clues on what controls the reproduction of the most favorable operating conditions.

Why SASE and no oscillator? The question of why SASE could be observed at 1064 nm, while multi-pass gain was not demonstrated is a relevant one. A possible explanation lies in the superior parameters of a single bunch compared with the bunch train. Engineering difficulties in producing a long bunchtrain with homogeneous parameters are considerable. Two examples are beam-loading induced problems and the challenge of producing a flat RF envelope at both the gun and the linac sufficiently long to satisfy startup requirements. The overall system for an FEL is also much more complex, requiring the precise setup of a cavity, with matching and stability issues which become more critical with increase in the number of passes.

In sum, the experimental evidence is consistent with the claim of startup of SASE at 1064 nm and at present cannot be explained by models which do not include gain. In general the data-taking can be improved by providing more angles of view (such as spatial profile/spectrum), and by including more beam diagnosis, especially at the position of the

wiggler. It goes without saying that saturation or a substantially larger enhancement would improve the problem of analysis and correct interpretation, but that the modifications required are extensive at this wavelength.

3.5.4 Open questions raised by the data at 632 nm. The interpretation of the data at 632 nm is not as clear. All of the emissions vs. charge scans at 632 nm were accompanied by shifts of a various nature, yet to be described and studied thoroughly. There are some principal differences in the way the experiments were done at the two wavelengths. Unlike the data at 1064 nm, the scans at 632 nm were performed with a bandwidth much less than $1/N_w$ (1 nm instead of 23 nm) and at times recorded the power characteristics of an off-axis cone of up to 40 nm from the on-axis resonant wavelength. The reason why the data at 632 nm was recorded with these changes in the apparatus is that the effects were remarked after the fact using setups designed for beam diagnosis during single shot measurements of the following chapter. As a result, these measurements are more prone to extraneous sources of curvature in the spontaneous emission baseline than those at 1064 nm. The observation of the same maximum level of enhancement at 632 nm as at 1064 nm is a little odd, as well as the same level of enhancement for different shifts of the central wavelength relative to the on-axis resonant wavelength. However, at times, power levels were higher than those expected from spontaneous emission. It may yet turn out that gain was observed and a supporting explanation was suggested in which off-axis enhancement results from bunching due to gain. A study of the intensity of the cone angle scan as a function of radius will clarify given sufficiently accurate calibrations. At this time, further analysis is needed before a claim of SASE should be made from the emissions vs. charge scans at 632 nm.

3.5.5 Application of the wiggler-based diagnostic techniques.

The non-perturbative beam diagnostic techniques with the wiggler developed in this thesis are one way to provide a better handle on this complex system when other information is not available. The techniques described in this chapter can be applied to off-axis spontaneous emission during searches for SASE. Performing double cone scans and single shot spectra studies in the visible wavelengths with the fundamental or with the 2^{nd} harmonic would provide essential information on the modifications to the beam parameters induced by the high energy slit. Significant new diagnostic information was already provided during the first study of the effect of the high energy slit on fluctuations in the single shot spectra.

An assumption made in the quantitative comparison with the SASE model at 1064 nm is that current density varies linearly with charge during the high energy slit scan. Measurements of the single shot spectra performed in Chapter 4 during the bunchlength monitor development raises a question about the validity of this assumption. Unfortunately, with the addition of an uncertainty in bunchlength to the uncertainty in variation in other beam parameters, one can imagine many variations to the final form of the emission vs. charge curve. One is: a first slope for spontaneous emission, a second slope for gain, increasing linearly as more charge is added to the bunch as the bunchlength gets longer, and then becoming sublinear as the beam quality and matching degrades with the addition of the head and tail. This makes the quantitative analysis more difficult and should be addressed in the absence of stronger effects by studying the enhancement in as wide a variety of ways as possible. Comprehensive beam diagnostic techniques at the position of the wiggler will give more strength to the claims made.

3.6 Some suggestions for future directions

The information which can be extracted in a single shot from the spatial profile could be increased with the following modifications to the S.E. cone measurements: the "double cone profile" and the "wishbone profile."

3.6.1 The double cone profile. The double cone profile has the purpose of extracting both the information of beam divergence and energy spread in a single shot measurement. The setup in Figure 18 is one way to implement a multiple cone profile. The emissions are passed through filters at central wavelengths λ_1 and λ_2, chosen to select a cone at large angle and one at an angle close to the first onset of the on-axis null. Divergence is estimated from the large angle cone, and this value is used when fitting the small angle cone against energy spread. A setup designed for experiments at 44 MeV gives a feel for typical numbers: the on-axis wavelength was chosen to be 622 nm, and λ_1 and λ_2 were 632 nm and 676 nm, as 1 nm BW filters are stock items at these three wavelengths.

It is also possible to chose the separation between cones to provide a second "pseudo-null" in between the two cones, now tunable through small tilts in the filters. This is useful because one can optimize the setup to be most sensitive to the beam parameters under study. One thing to look into is the choice of the double cone outside the region in which there is sensitivity to energy spread. In other words, by choosing a double cone at large angle, divergence would cause a filling in of an artificially produced valley, and the measurement would be converted to a peak to valley ratio instead of a width, which is easier to respond to

visually. The separation between the two cones should be adjusted empirically for maximum sensitivity and the final values of the two composite radii calibrated independently.

3.6.2 Wishbone profile. The wishbone profile is proposal for a way to record a full cone angle scan in a single shot. This is motivated by the success of the cone angle scan in providing a large quantity of information, which made it ideal as a benchmark procedure during the experiments. A possible implementation is shown in Figure 19. The output is limited to one axis of measurement. The emissions in this axis are selected by a narrow slit aperture. The remaining far field emissions are incident on a grating with the groves oriented parallel to the slit aperture and the two dimensional profile measured with a CCD camera. A theoretical profile is shown in Figure 19, where one axis of this profile is wavelength and the other angular position. All of the measurements descibed with the cone angle scan can now be performed: beam energy calibration, divergence estimate (with a slice at the longest wavelength), energy spread estimate (with a slice near shortest wavelength) but without the uncertainties arising from changing the superelement or drifts in the machine. If the number of photons and resolution were sufficient, one could estimate the number of transverse modes in two ways: from the divergence of the on-axis emissions and from the dependence of fluctuations with angle, building on the techniques tested in Chapter 5.

3.6.3 Application of radon transform to cone measurements. Finally, it is clear that since all of the quantitative analysis in this chapter relied only on a single slice of the two-dimensional cone, that considerably more information is contained in each shot. In order to extract this information, the radon transform can be used. Each slice of a large angle

cone in the far field is the projection of $\sigma_{x'}$ and $\sigma_{y'}$ onto that slice. With slices sampled at many angles, one can perform a Radon transform to obtain the full distribution in $\sigma_{x'}$ and $\sigma_{y'}$. A similar procedure is applicable to the near field for the distribution in σ_x and σ_y.

3.7 Conclusions

A systematic series of experiments was performed to demonstrate that a 50 MeV beam may be characterized with the spontaneous emission from a microwiggler. Simple analytic expressions have been derived to quantify broadening of spontaneous emission into a 1 nm bandwidth cone of chosen radius. With fixed frequency and a large angle radiation cone, simple theory predicts that divergence broadening will dominate over natural linewidth and energy spread broadening, so that at sufficiently large angles, a direct, single-shot measurement of beam divergence can be obtained. Studies of the spatial profile showed useful sensitivity to variations in the machine parameters, and an estimate of beam divergence in the wiggle plane was extracted from the data. Suggestions for the refinement of the diagnostic method have been described.

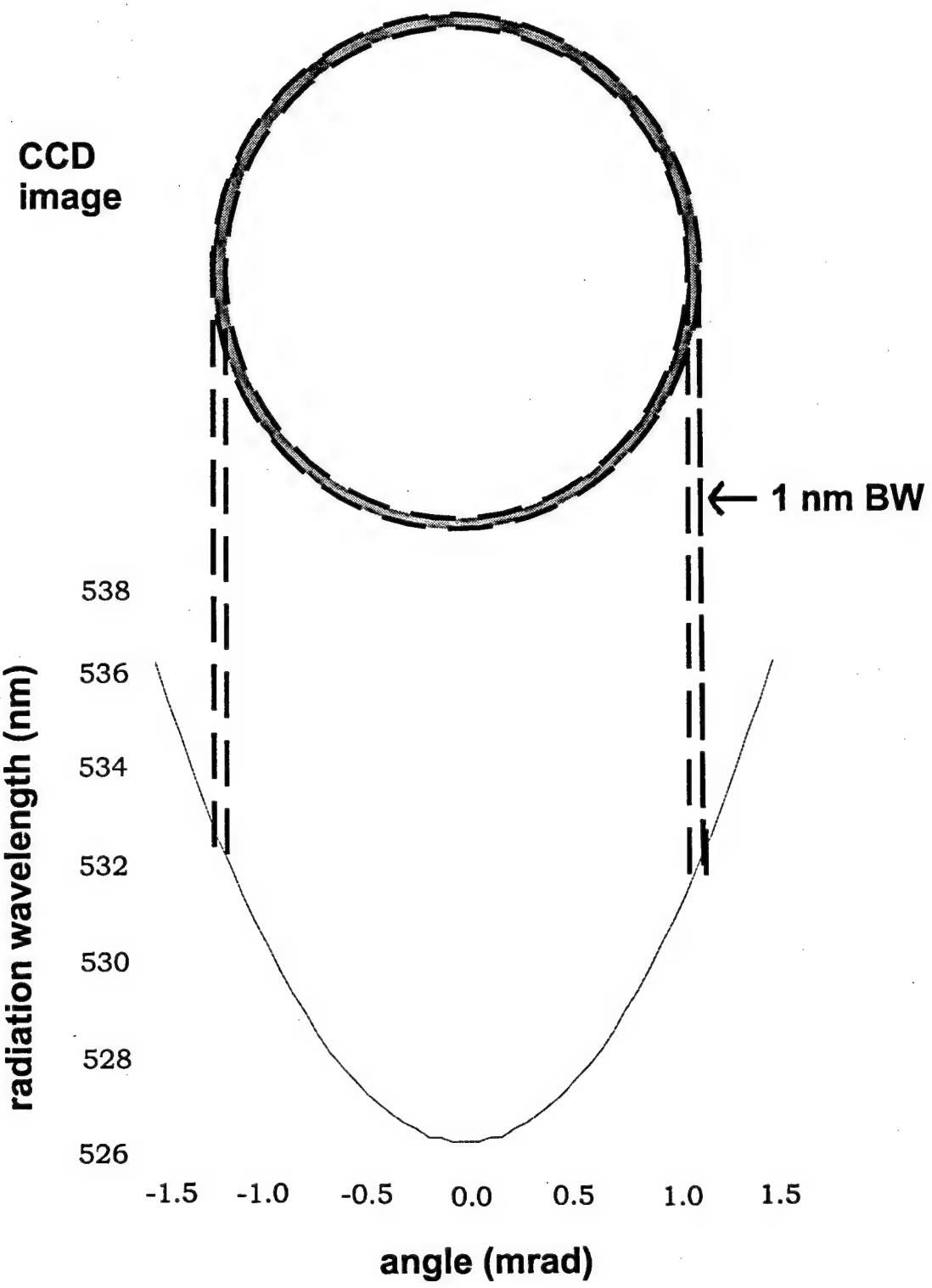

Figure 1. Phase matching condition and narrow bandwidth spatial profile of the wiggler spontaneous emission in the far field.

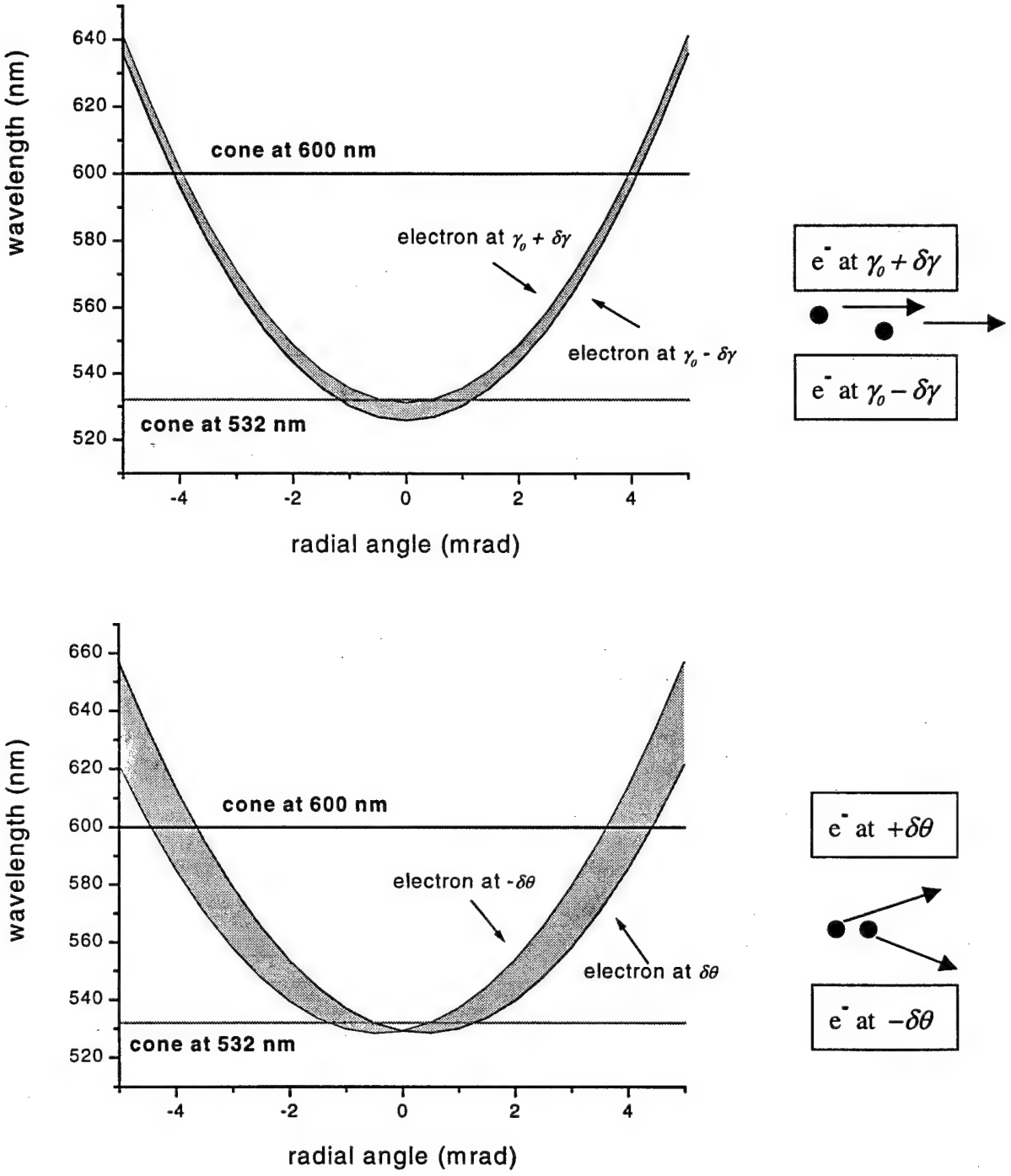

Figure 2. Physical picture of scaling of cone width with beam parameters. *The phase matching condition for a pair of electrons co-propagating at two beam energies separated by* $\gamma_0 \pm \delta\gamma$ *and a pair of electrons with the same energy propagating at angles* $\pm \delta\theta$ *with respect to the wiggler axis are shown. The cone width scalings predicted by the analytic expressions can be seen easily with this diagram. Realistic values of* $\delta\gamma$ *(0.25%) and* $\delta\theta$ *(0.4 mrad) are plotted.*

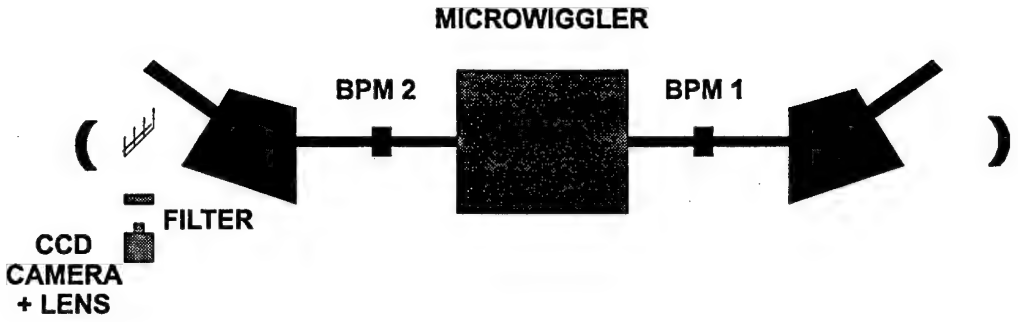

Figure 3. Experimental setup for the spatial profile measurements. *Emissions are outcoupled from the beamline with a silver mirror, intercepted by a 1 nm BW filter, and focussed onto a WATEC 902A CCD camera. The setup is simple and economical.*

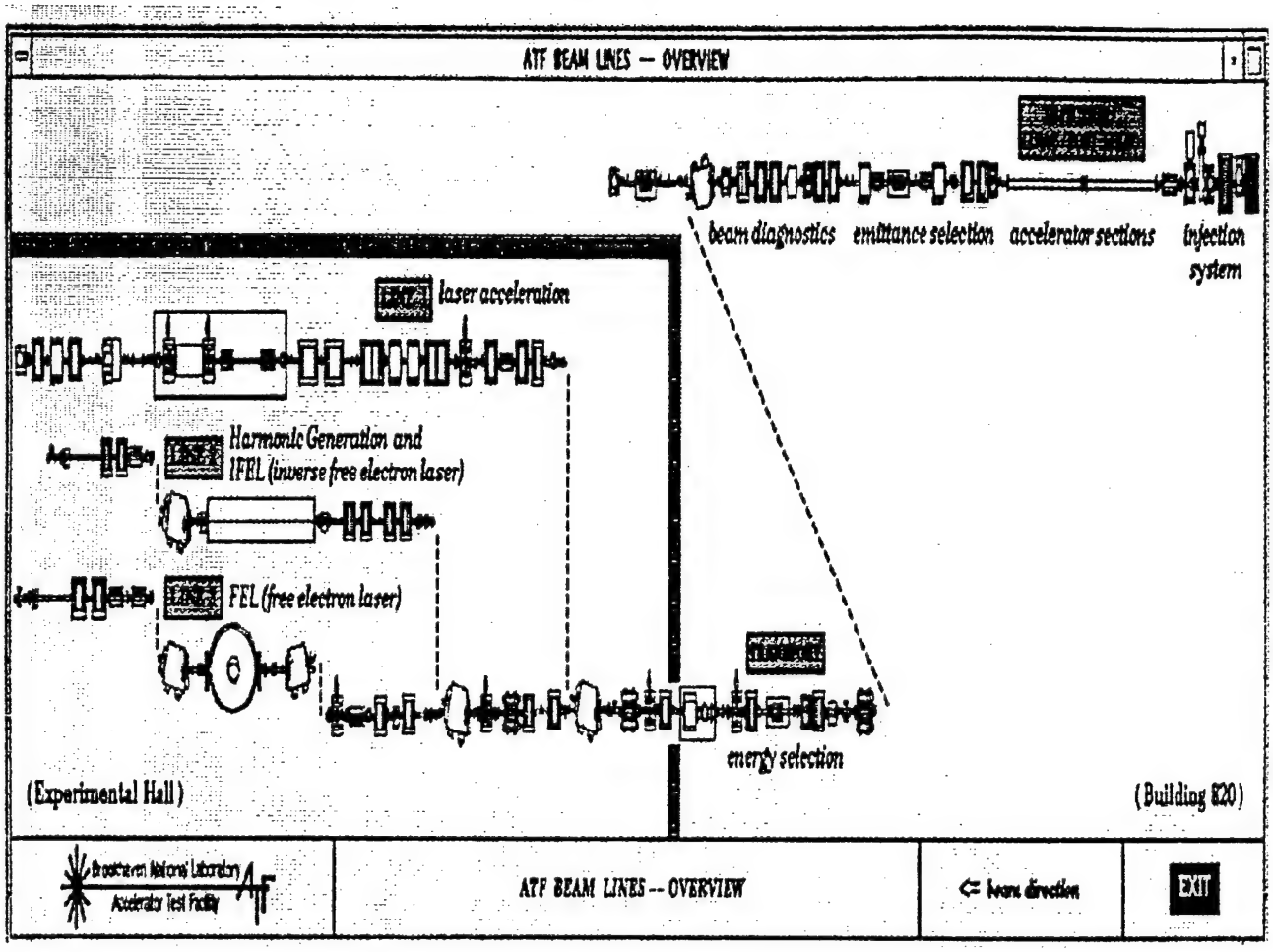

Figure 4. Overview of the Accelerator Test Facility injector and transport optics.

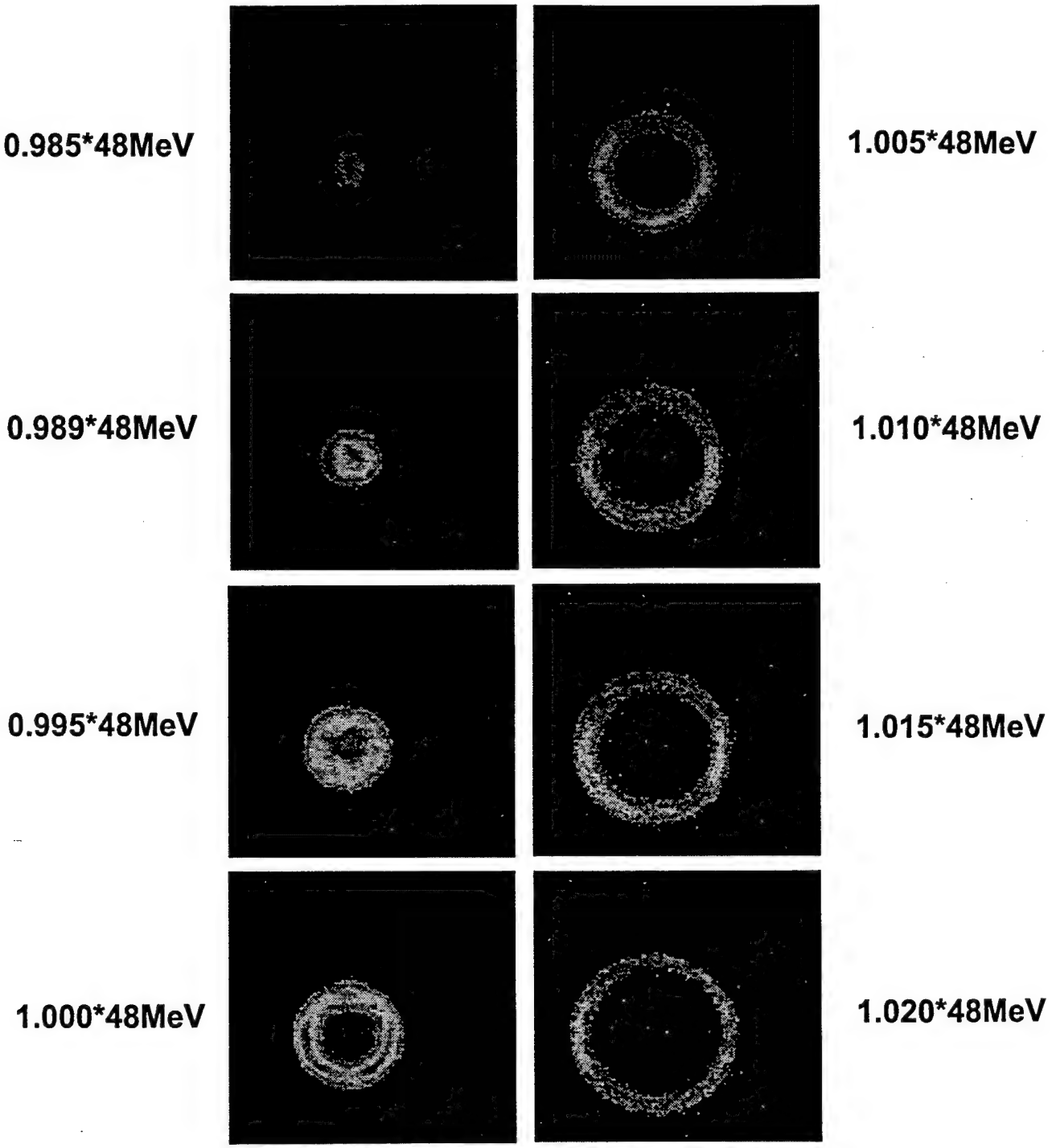

Figure 5. Cone angle scan. *The scan was performed by adjusting the beam energy over a range of +/- 2% in increments of 0.5% with a superelement – a collection of beam optics whose values are automatically scaled for the change in the beam energy. Note the excellent sensitivity to small changes in beam energy for the smaller cones.*

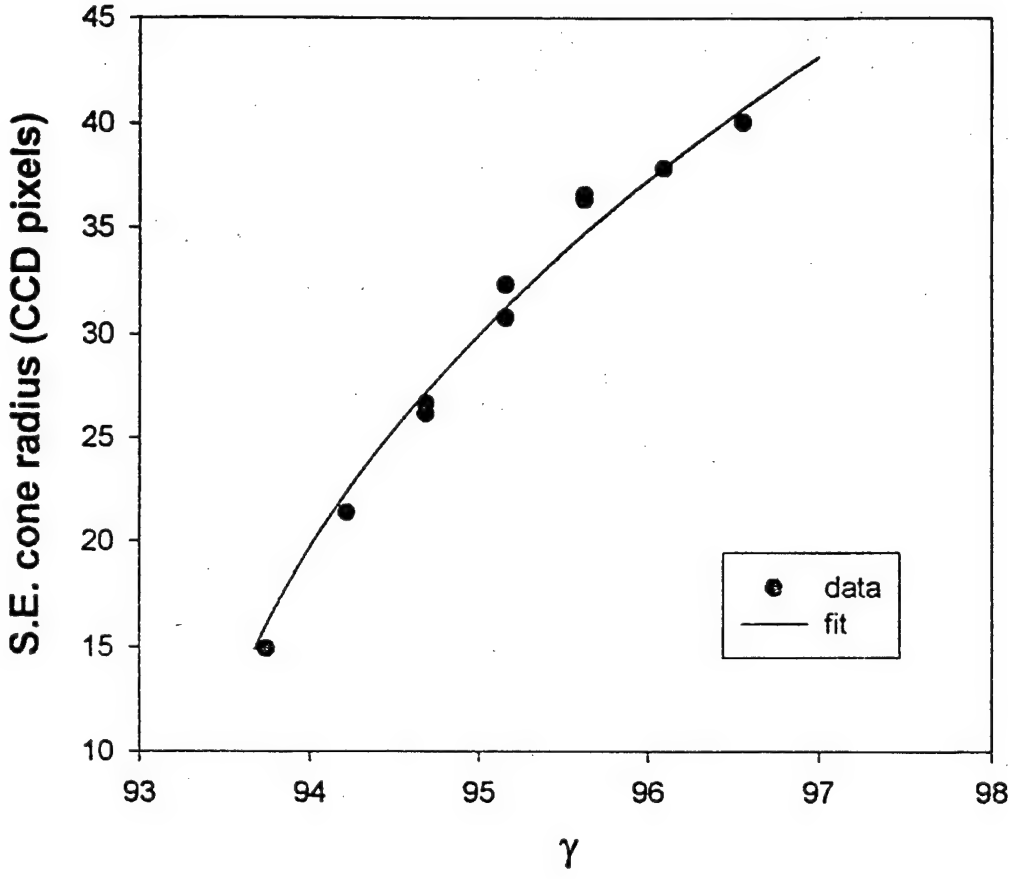

Figure 6. S.E. cone radius as a function of beam energy *obtained from the data in Figure 5 and theoretical fit to the phase matching condition. This information provides an absolute calibration of the beam energy, given independent calibrations of the radial angle and the wiggler field strength.*

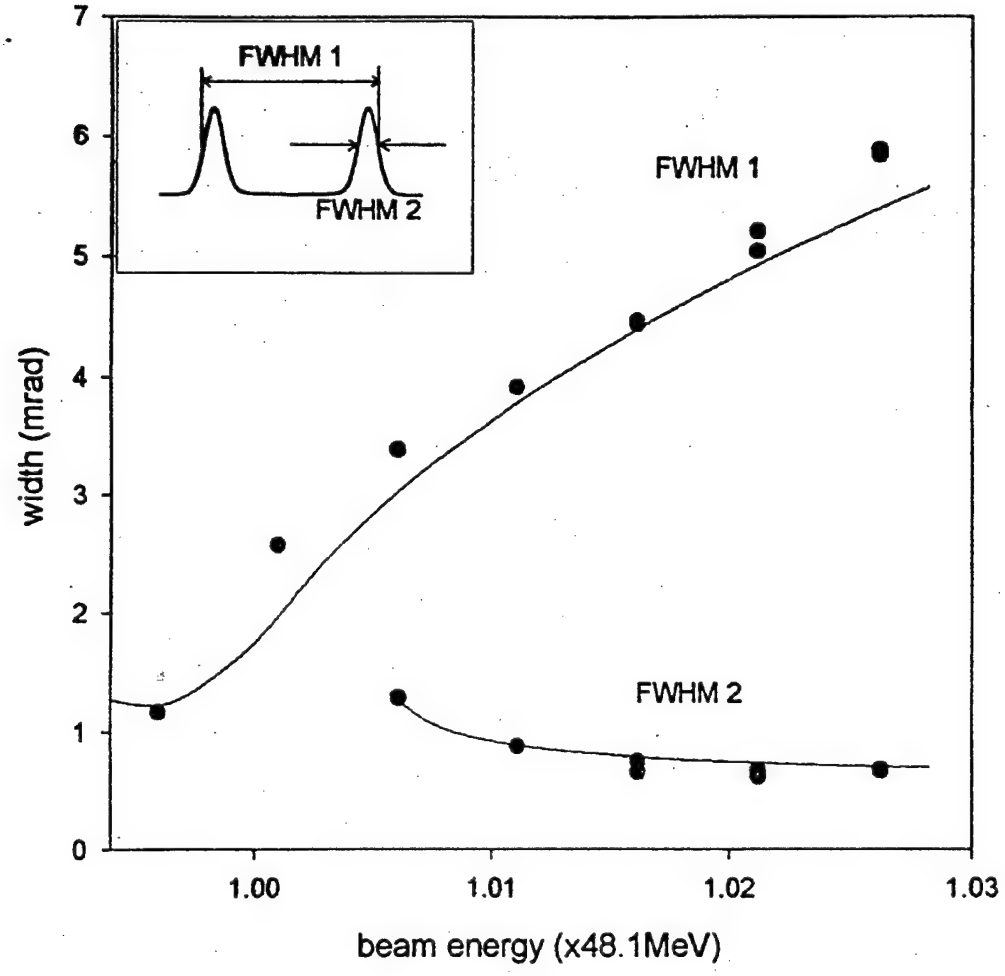

Figure 7. Study of S.E. cone widths as a function of beam energy. *The solid line was computed with parameters $\delta\gamma/\gamma$=1% FW, $\sigma_{x'}$ = 0.24 mrad, $\sigma_{y'}$ = 0.35 mrad, and a_w, N_w, γ, and λ_w and radial angle calibrations are identical to those used in the fit in Figure 6. Note the asymptote in the lower curve as γ increases, from which the estimate for divergence was extracted.*

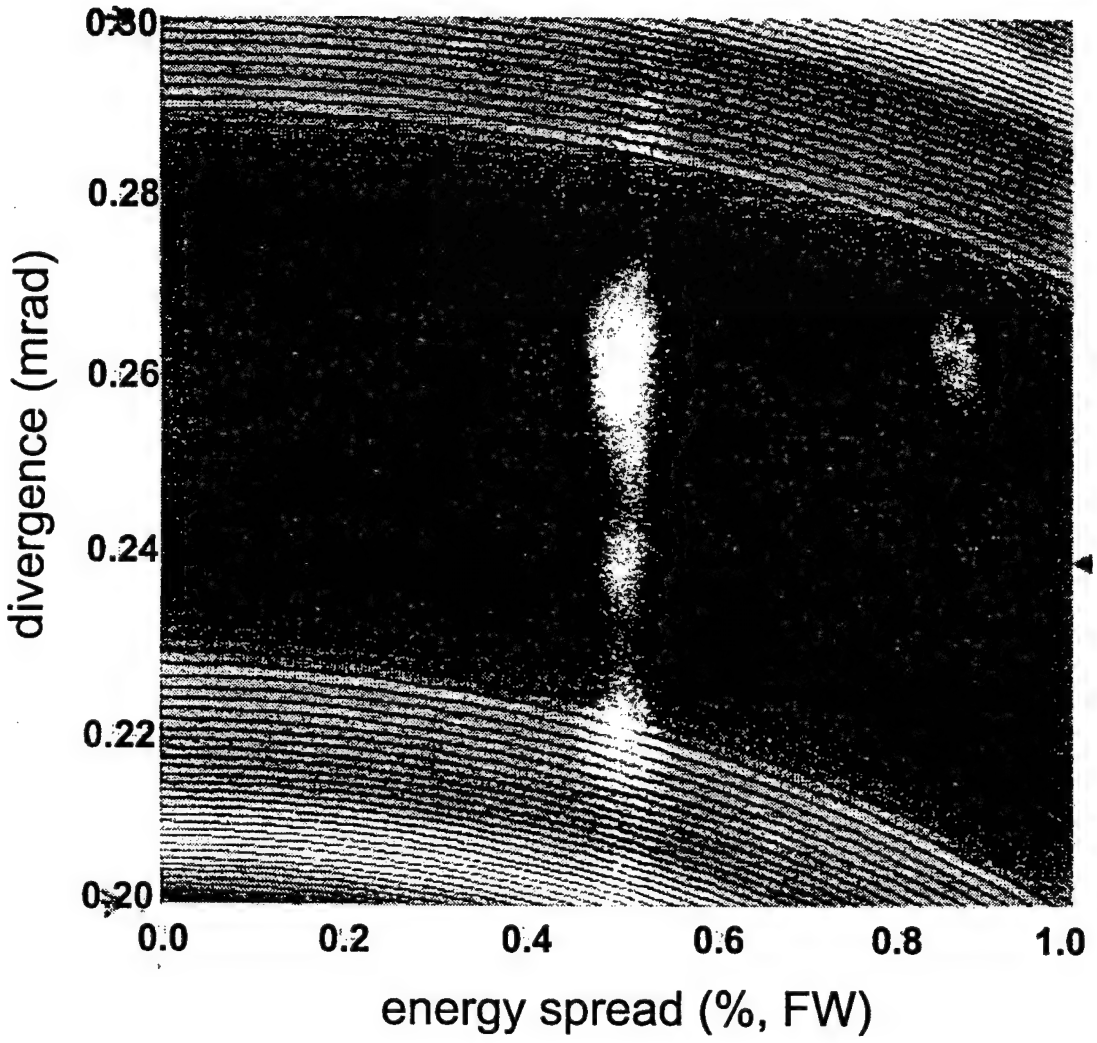

Figure 8. χ^2 plot indicating the region of best fit between the data and simulation for a S.E. cone at θ_{cone} = 2.6 mrad. *The intensity as a function of angle in the wiggle plane was computed for the array of energy spreads and divergences shown, with $\sigma_{y'}$ at 0.35 mrad. The best fit to the data lies at $\sigma_{x'}$ = 0.25 mrad and is relatively insensitive to energy spreads below 1% FW. This difference in sensitivity is consistent with the scaling expressions.*

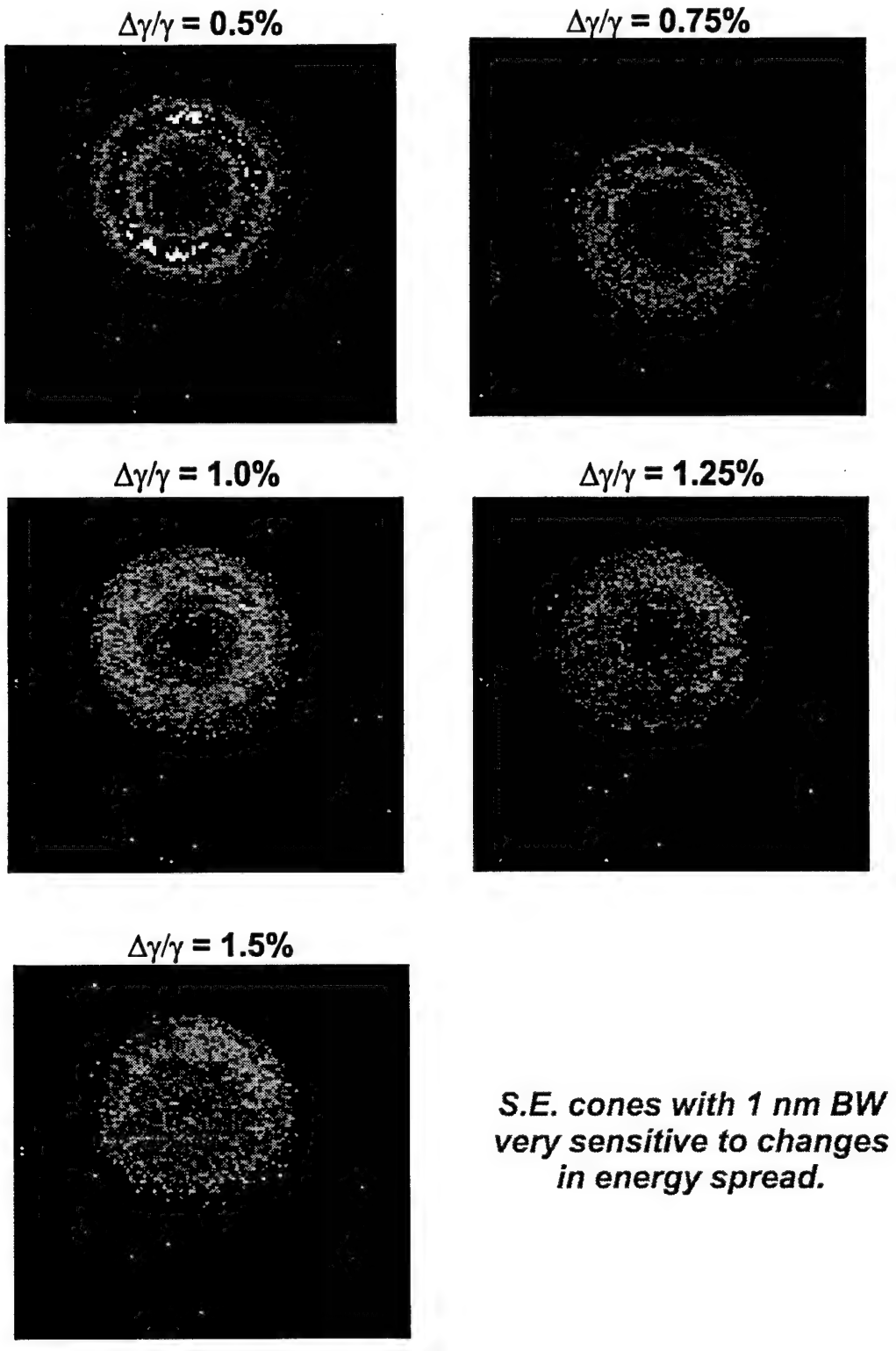

Figure 9. S.E. cone scan in energy spread. *The cone radius was adjusted to be most sensitive to the energy spread range of 0-1.5% FW, with marked success.*

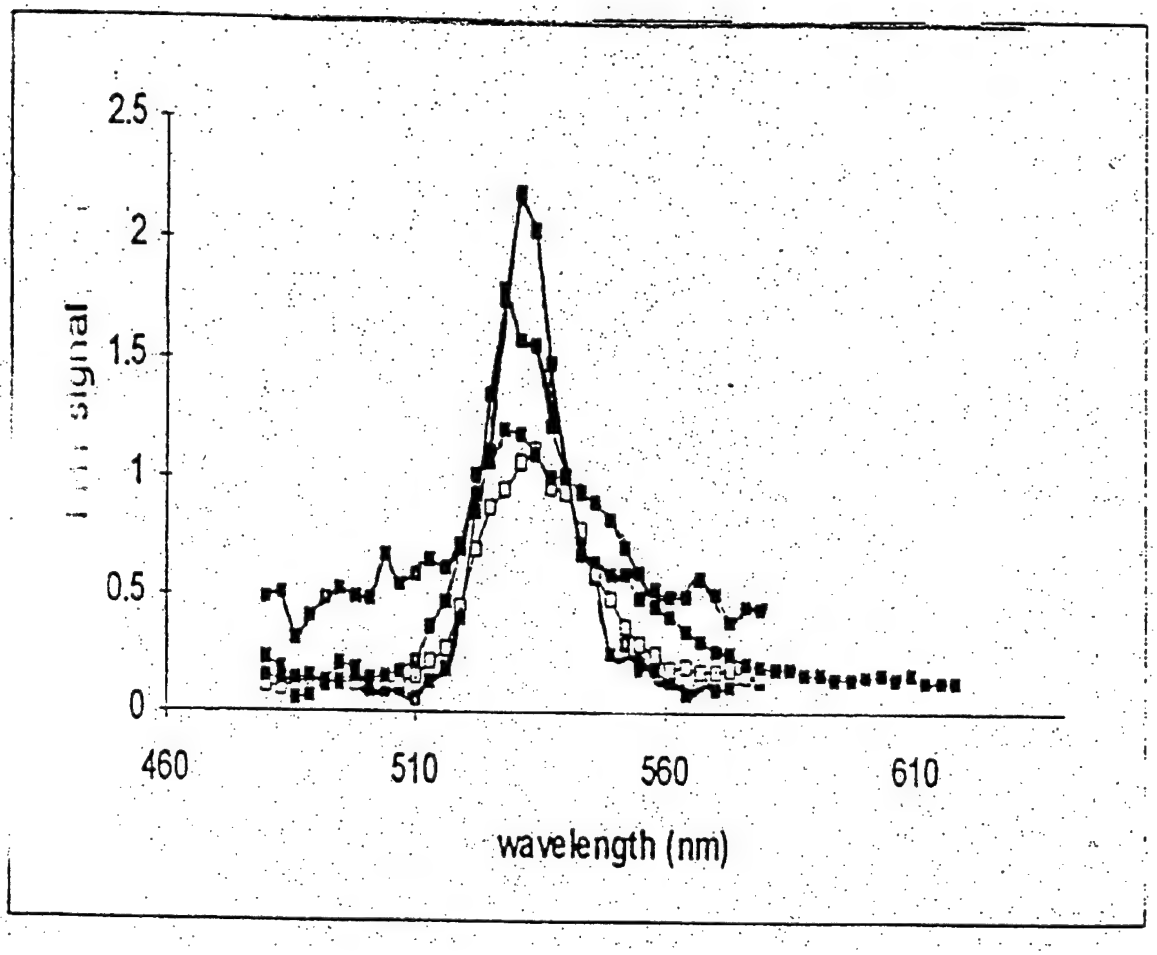

Figure 10. Dependence of spontaneous emission spectra on energy spread. *Four spectra are shown with the beam energy spread ranging from 0.25% to 2%. Compare with Figure 9.*

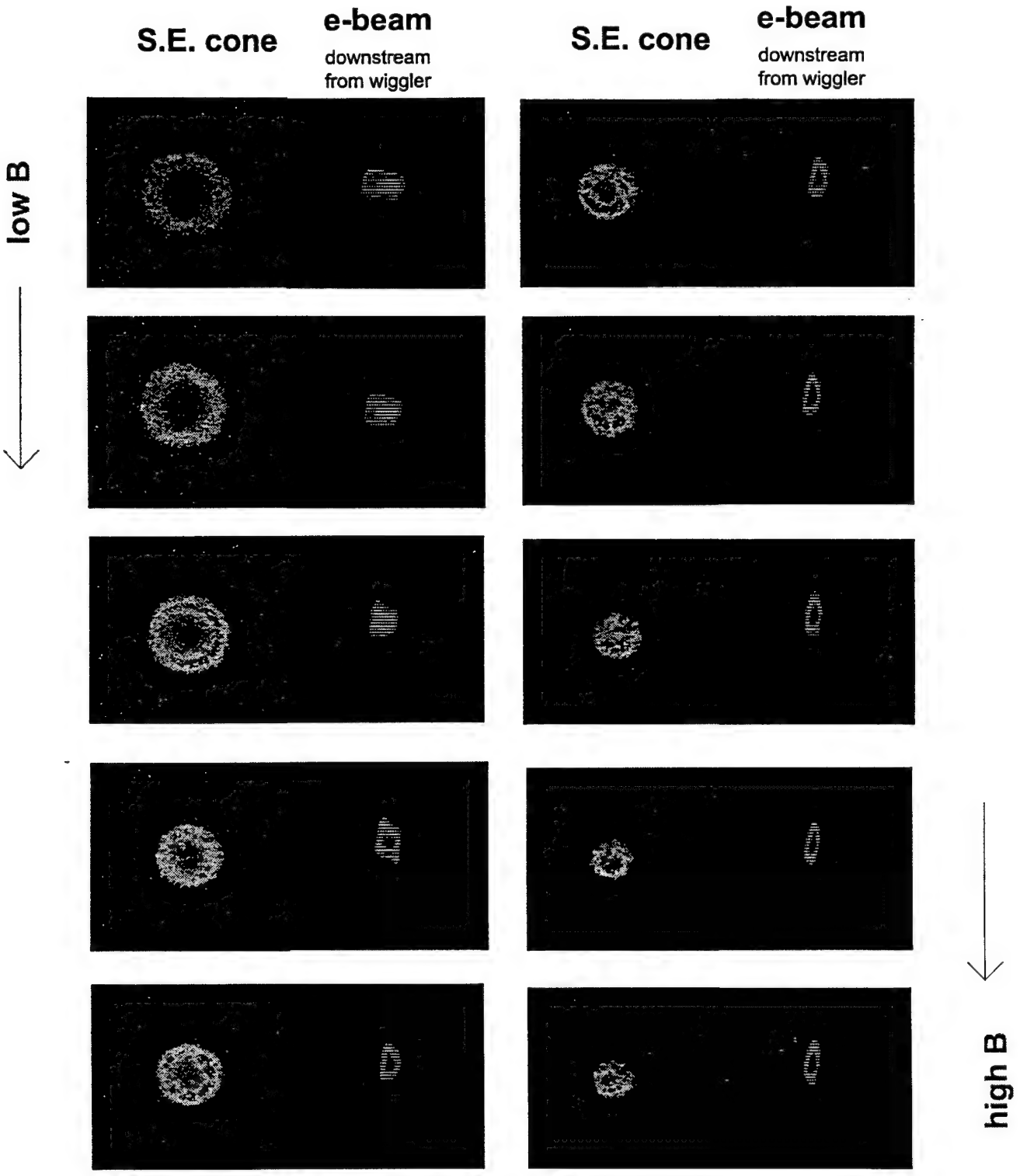

Figure 11. S.E. cone scan as a function of wiggler field strength and accompanying beam profile downstream from the wiggler. *This scan shows that for aw~0.37, the cones respond visibly to changes in the wiggler field strength. Possible applications of such a scan are estimation of the Twiss parameters and in-vacuum adjustments to the wiggler.*

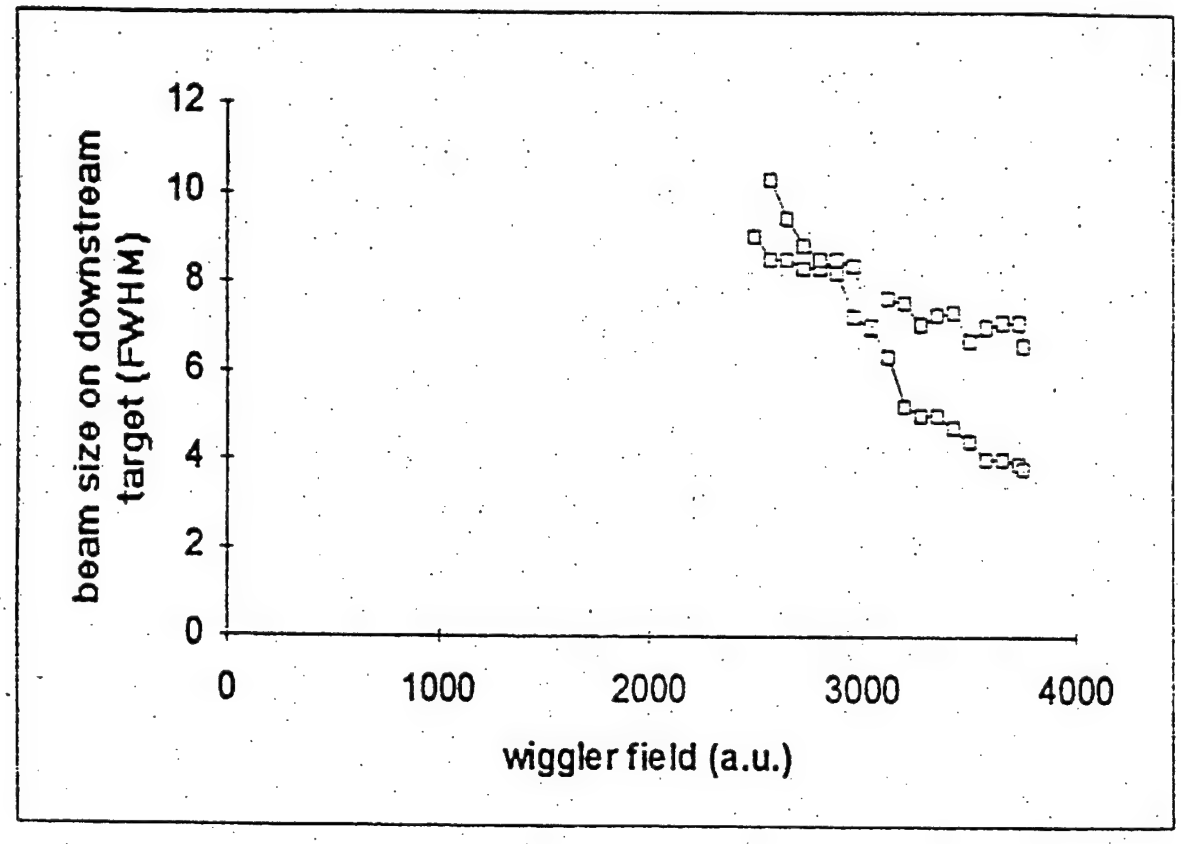

Figure 12. Use of wiggler focussing to estimate Twiss parameters. *Spot size in the non-wiggle plane downstream from the wiggler was recorded as a function of wiggler field strength for two beam tunes in a procedure similar to a quadrupole scan.*

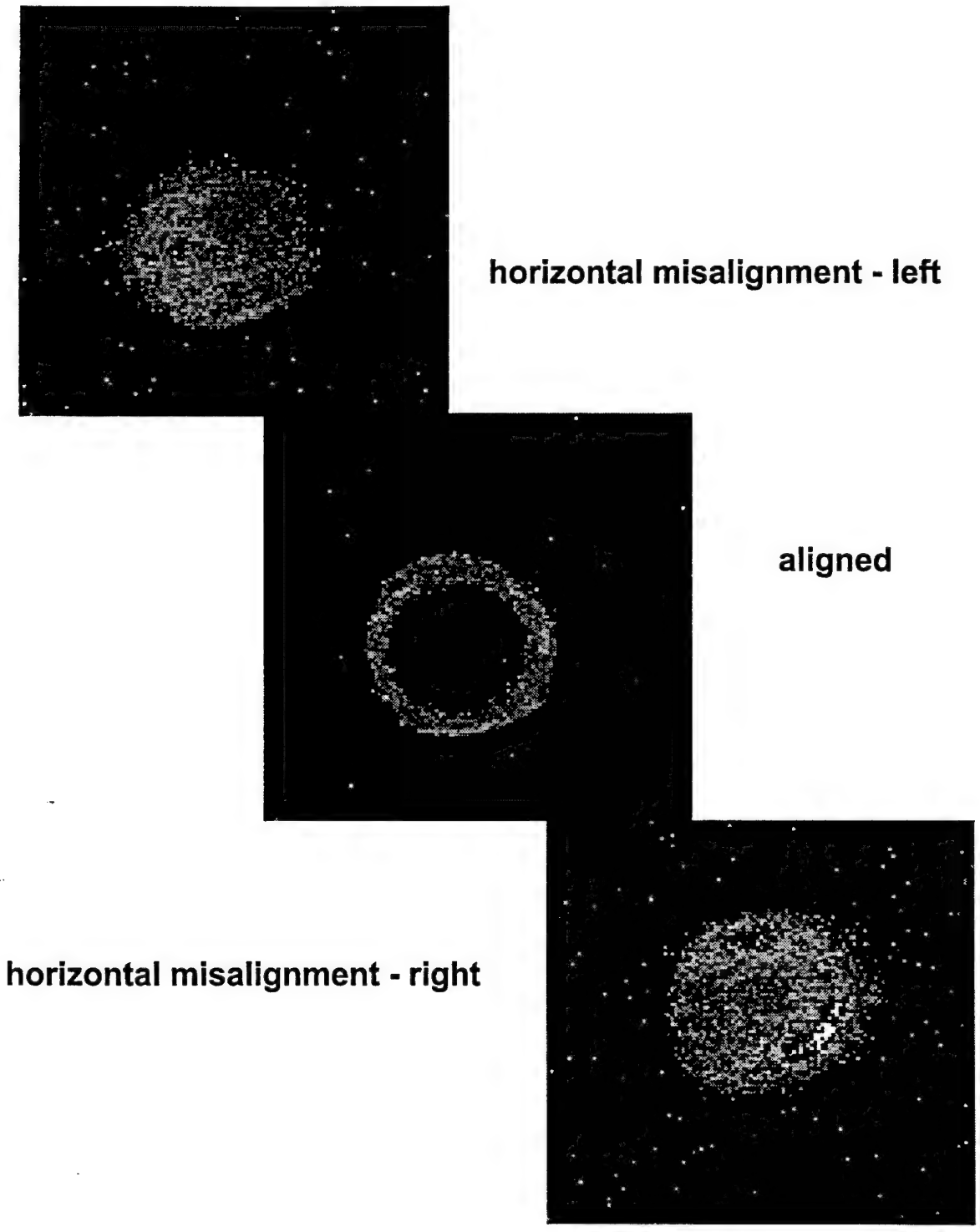

Figure 13. Effect of large beam misalignment in the non-wiggle plane on the S.E. cone. *(Note that the wiggle plane is vertical for this wiggler.) With the selection of a narrow bandwidth portion of the spontaneous emission, sensitivity to misalignment increases in a useful way.*

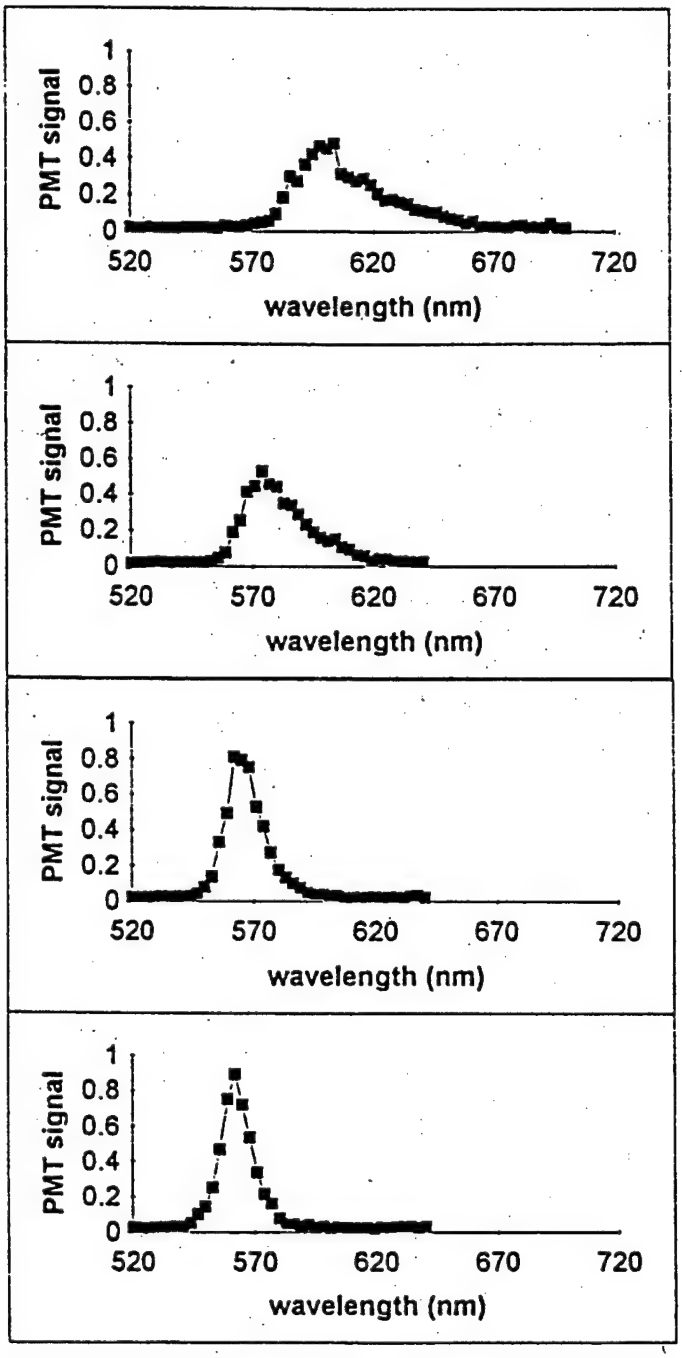

Figure 14. Effect of beam misalignment in the non-wiggle plane on the spontaneous emission spectra. *In the wiggle plane, misalignment was harder to see until the angles became large. In this case, clipping could be favoring the off-axis emissions.*

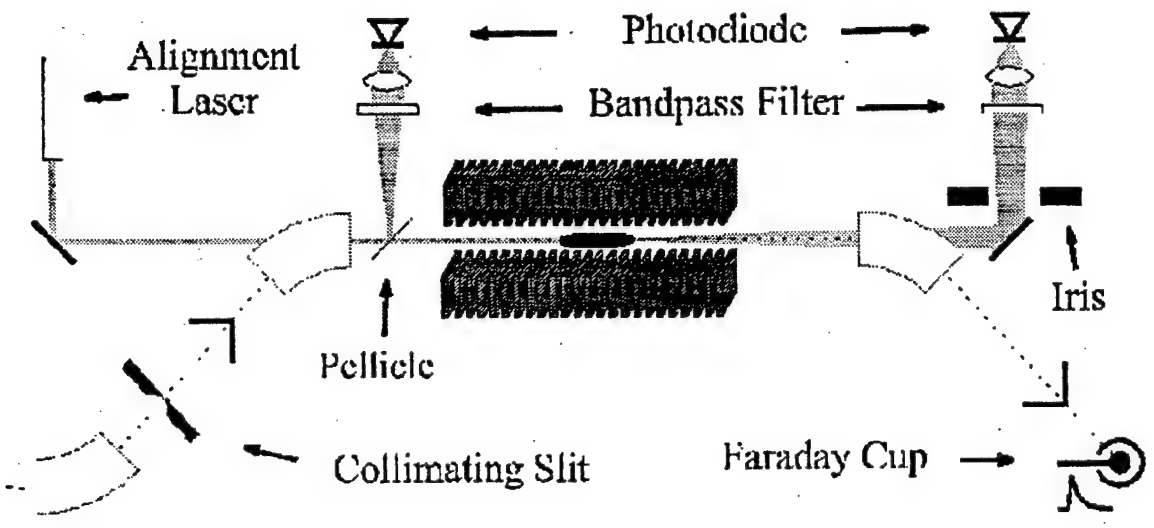

Figure 15. Experimental setup for search for self-amplified spontaneous emission at 1.064 microns.

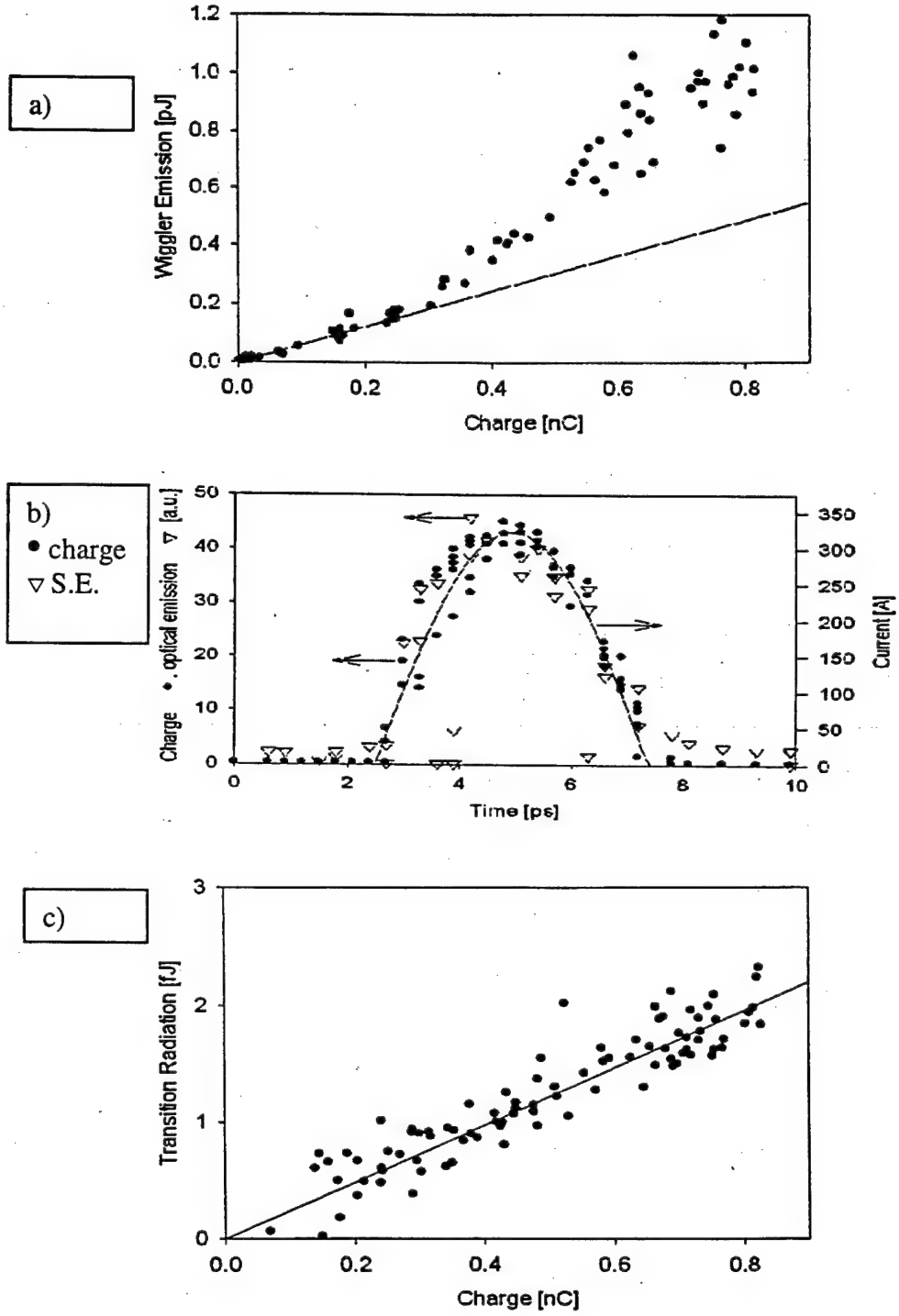

Figure 16. Experimental results indicating evidence of SASE at 1.064 microns. *The upper curve (a) is the beam temporal waveform. The middle plot (b) is the dependence of the wiggler emissions on beam charge into a limited collection angle and bandwidth, and is followed by the dependence of transition radiation on beam charge for the same bandwidth.*

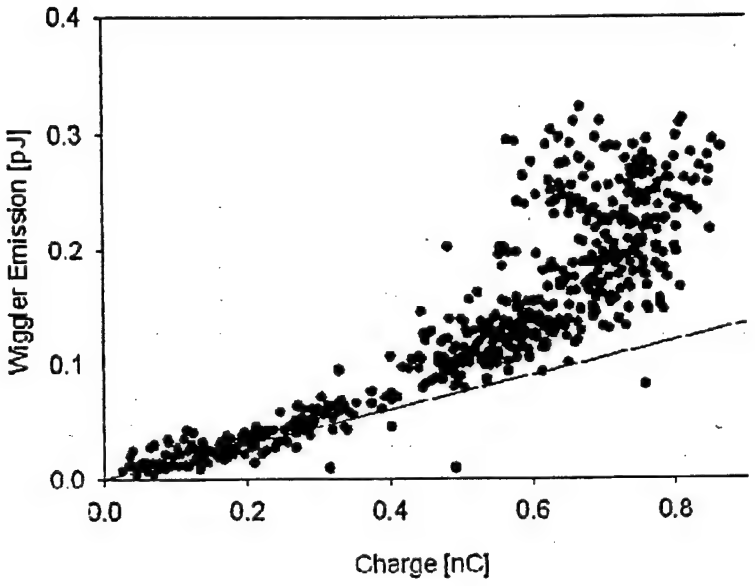

Figure 17. Off-axis wiggler emissions as a function of beam charge measured into a 1 nm BP interference filter centered at 632 nm.

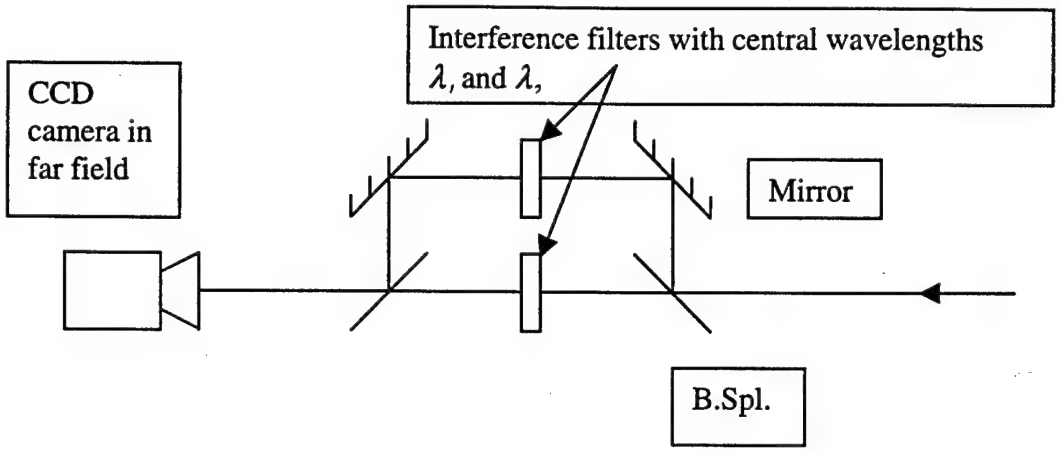

Figure 18. Experimental setup for double cone measurement. *The goal of this setup is to extract an estimate for both energy spread and divergence in a single shot.*

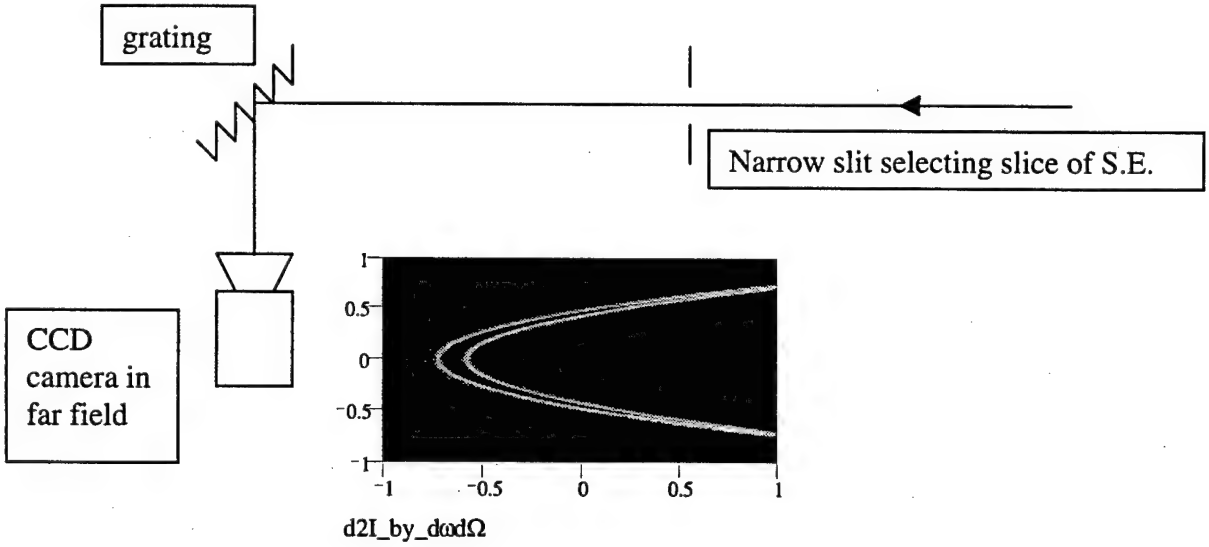

Figure 19. Experimental setup for "wishbone" profile. *The goal of this setup would be to perform a cone angle scan in one axis in a single shot. This will increase the number of parameters which can be extracted in a single shot, and improve the accuracy of fits, as a continuous fit can be performed over data which previously included the shot to shot jitter of the machine. A theoretical profile (no bradening included) is shown.*

References (Chapter 3)

[1] R. Stoner and G. Bekefi, "A 70-period high-precision microwiggler for free electron lasers," *IEEE J. Quantum Electron*, **31**(6), 1158-65 (1995).

[2] H. A. Haus, "On the radiation from point charges," *Am. J. of Phys.*, **54**(12), 1126-9 (1986)

[3] Kim, Kwang-Je, "Characteristics of synchrotron radiation," *AIP Conference Proceedings* **184**, Vol. 1, 565-632, (1989)

[4] X. Qiu, P. Catravas, M. Babzien, I. Ben-Zvi, J.-M. Fang, W. Graves, Y. Liu, R. Malone, I. Mastovsky, Z. Segalov,, J. Sheehan, R. Stoner, X.-J. Wang, J. S. Wurtele, "Experiments in nonperturbative electron beam characterization with the MIT microwiggler at the accelerator test facility at BNL," *Nucl. Instr. & Meth. A* **393**, 484-489 (1997).

[5] G. Shvets and J.S. Wurtele, "Temporal and spectral structure of an FEL oscillator during start-up," *Nucl. Instr. & Meth. A*, **393**, 273-6 (1997).

[6] Kwang-Je Kim, "Three-dimensional analysis of coherent amplification and self-amplified spontaneous emission in free-electron lasers," *Phys. Rev. Lett.*, **57**(15), 1871-4 (1986); Kwang-Je Kim, *Nucl. Instr. & Meth. A*, **393**, 167 (1997).

[7] R. Bonifacio, C. Pellegrini, and L. M. Narducci, "Collective instabilities and high-gain regime in a free electron laser," *Optics Commun.*, **50**(6), 373-8 (1984).

[8] R. Prazeres *et al. Phys. Rev. Lett.* 78(11) 2124-2127, (1997); T. Orzechowski *et al., Nucl. Instr & Meth. A* **250**, 144, (1987); D. Kirkpatrick *et al., Nucl. Instr & Meth. A*, **285**, 43, (1989); S. Okuda *et al. Nucl. Instr & Meth. A* **331**, 76-78, (1993); D. Bocek *et al. Nucl. Instr & Meth. A*, **375**, 13-16, (1996)

[9] K. W. Berryman *et al. Nucl. Instr & Meth A*, **375**, 526-529, (1996)

[10] D. A. Jaroszynski *et al., Phys. Rev. Lett.* **72**, 3798, (1993)

[11] M. Babzien, I. Ben-Zvi, P. Catravas, J.-M. Fang, T. C. Marshall, X. J. Wang, J. S. Wurtele, V. Yakimenko, L. H. Yu, "Observation of Self-Amplified Spontaneous Emission in the Near-Infrared and Visible," Accepted by *Phys. Rev. E.*, 1998.

CHAPTER 4: MEASUREMENTS OF THE FLUCTUATIONAL CHARACTERISTICS OF THE WIGGLER EMISSIONS FROM A SINGLE MICROPULSE

This chapter contains measurements of the single shot characteristics of emissions from a single micropulse. Both spectral and spatial profile data were taken. The measurements were motivated by a proposed technique for bunchlength diagnosis from

fluctuations in the wiggler emissions arising from shot noise on the electron beam, introduced in references 1 and 2.

4.1 Theory [3]

The model. An electron beam of Gaussian shape and bunchlength τ_b is considered, with an assumption that there are no interactions between the electrons in the bunch. The electron density is sufficient that at any point in time the number of electrons with overlapping emission trains is large. The length of the wavetrain emitted by a single electron is much shorter than the beam bunchlength. The emissions reaching the detector are assumed to be transversely coherent, and the number of available photons large enough to neglect quantum effects.

Shot noise on the electron beam creates fluctuations in the incoherent emissions, with which are associated specific properties. Each fraction of the beam contains an average of $\overline{N}$ particles with a deviation of $\sqrt{\overline{N}}$. The radiation can be computed by summing over their random amplitudes and phases, yielding a distribution of final amplitudes and phases proportional to $\exp(-\frac{E^2}{\langle E^2 \rangle})$. This distribution determines some important attributes of the emissions. First, fluctuations in the temporal envelope are expected to be 100%, as the probability of finding a composite electric field with a given amplitude has a maximum at zero electric field. Second, it is possible to find the fields adding in such a way as to produce a very large resultant field, but not probable. The

timescale on which the variation from 0 to 100% occurs in the temporal envelope of the emissions depends on the bandwidth of the emissions, which is inversely related to the length of the train of emissions from a single electron. Thus, in the case of a wiggler, the emission envelope varies on a timescale proportional to $1/N_w$, where N_w is the number of periods in the wiggler.

Because of the finite length of the bunch train, fluctuations in the spectrum occur not as white noise, but with upper and lower bounds in frequency. The lower bound in the width $\omega_{\min}$ of a spike in the spectrum is set by the inverse of the pulse length.

$$\omega_{\min} \sim \frac{1}{\tau_b}$$

A laboratory observation of a spike in the spectrum with a width shorter than $1/\tau_b$ would imply that contributions at the spike frequency added in phase over a longer period in time than the electrons were available to emit, and would indicate an error in the experimental setup or a violation of the assumptions made about the beam. The upper bound in frequency can be estimated from the extreme case of a bunch formed of a train of uniformly spaced electrons.

$$\omega_{\max} \sim \frac{N_e}{\tau_b}$$

where N_e is the total number of electrons in the bunch.

Condition on transverse coherence. Transverse coherence exists when the spot size of the source is less than or equal to the diffraction limited spot size d.

$$\theta_{rad} = \lambda/(2\pi d).$$

θ_{rad} is the divergence angle or collection angle, λ is the emission wavelength. This condition is satisfied if the beam is matched into the wiggler. However, if the emittance of the beam is too large, the emission characteristics scale as the average of contributions from independent sources, the number of which is the ratio of source area to diffraction limited area.

Degeneracy. In order to determine the importance of the contribution of quantum fluctuations, one must evaluate the magnitude of fluctuations arising from Bose-Einstein statistics. These scale as $1/\sqrt{\langle n \rangle N}$, where $\langle n \rangle$ is the degeneracy and $N = \tau_b / \tau_{coh}$, the ratio of the beam bunchlength to the coherence time associated with the width of the measurement bin: $\tau_{coh} = 1/\Delta\omega$. In order to implement a bunchlength diagnostic without considering the contribution of quantum fluctuations, this term must be small compared with $1/\sqrt{N}$. In sum, the measured fluctuation level in the total number of photons N_{ph} is:

$$\text{total photons} = N_{ph}\left(1 \pm \frac{1}{\sqrt{N}} \pm \frac{1}{\sqrt{\langle n \rangle N}}\right)$$

N is assumed small compared with unity. The form of the expression for degeneracy comes from the number of photons in the coherence volume defined by the diffraction limited size d and the coherence time τ_{coh} and a reduction factor to account for the difference in the size of the transverse size and opening angles of the optical mode and electron beam.

In practice, τ_{coh} is a design parameter and N is computed from the data. The bunchlength is estimated from the ratio. To make an instant estimate, one uses the minimum spike width in the data.

4.2 Experimental setup and parameters

Basic experimental setup. The wiggler emissions are outcoupled from the beamline after the beam is separated from the emissions with a bending dipole. The emissions are apertured, and transported out of the Experimental Hall to the diagnostic room where they are focussed into a spectrometer, which contains an open output port at which the full spectrum impinges on an image intensifier. The power at various points along the path was measured with an avalanche photo diode.

Diagnostic specifications. The spectrometer used was a model Spex 270M with a focal length of 0.27 m and 1200 groove per mm visible grating. The manufacturer rated resolution was 0.062 nm. The spectrometer offers the choice of axial and lateral output ports, the latter with an adjustable slit, the former completely open. A PMT placed at the slit exit to recorded reference spectra integrated over many shots. An image intensifier was positioned at the open output port to record the full single shot spectrum. The image intensifier was Gen IV, fiber optically coupled, with a GaAs photocathode with Q.E. of 35-40% in the visible. Gating down to 100 ns was optional.

The intensifier was sometimes placed directly at the focal plane at the spectrometer output; sometimes, additional optics was added to change the magnification. This permitted the signal to noise ratio and resolution to be optimized and instrumental broadening sources to be determined empirically. In particular, the resolution limitation caused by instrumental broadening was checked. The intensifier line transfer function was 62 lp per mm. A HeNe spectrum recorded with the intensifier at magnifications of 7 pixels/nm, 19pixels/nm and 25 pixels/nm was 2.5 pixels wide and identical in all three cases. This confirms that the resolution was limited by the intensifier and not by the spectrometer, in agreement with the manufacturer ratings of both devices. The usable portion of the full spectrum was limited to the bandwidth over which the image was well focussed in the plane defined by the photocathode. Furthermore, an intensity reduction factor exists in part of the spectrum. For this reason, the single shot spectra profiles are not the same as their companion measurement of integrated spectrum measured with the PMT wavelength by wavelength at the exit slit at the lateral port. However, the spectra are true in a specific portion of the image, which is sufficiently large for statistics to be performed, and the signals in the region have good signal to noise. Gating to 100 ns was available, but the dark current levels were not found to be an issue for the experiments reported here.

Data acquisition. The video signal from the intensifier was digitized with one of two 8-bit frame grabbers, one located in the control room, and the other, a Spiricon, in the FEL room. The path length for the video signal in the latter case was a meter or two, and this setup provided the cleanest signals. The distance to the more powerful frame grabber

in the control room was many tens of meters, and after care was taken to minimize noise pickup, a signal was obtained which was almost as clean as that obtained adjacent to the signal.

Experimental parameters. The parameters for the experiments were chosen so that the wavelength would be in the region of highest quantum efficiency of the detector in order to reduce quantum fluctuations as much as possible. Emissions were in the red wavelengths, near 632 nm, corresponding to a beam energy of 44 MeV. The bunchlength was varied from <1 to 8 ps, and an independent measure of the temporal profile, as described in reference 4, accompanied the spectral measurements. Unlike the measurements in reference 4, in which the charge was monitored immediately following the high energy slit, for these measurements the charge transmitted past the wiggler and intercepted with the Faraday cup at the end of beamline 3. Total charge varied with bunchlength within a range of 50 pC to 800 pC.

Measurements with the Magnesium cathode showed that a range of about 1 to 8 ps (defined by charge/peak current) was available for the experiments. As the operating time after a laser cleaning lasted about 30 hours, the charge at the crest diminished with time during the course of a run. The dependence of bunchlength with phase/charge relative to the crest for two values of the crest was not the same: for a higher value of the crest, the same relative point on the charge curve corresponds to a longer bunchlength. This could be caused by bunch lengthening due to space charge effects. Each collection of spectral measurements was accompanied by a record of the operating point from charge levels at the gun and a chirped bunchlength measurement.

4.3 Single shot spectral measurements

In order to test the proposed bunchlength monitor, a variety of scans were performed, along with accompanying measurements designed to test if assumptions made were satisfied. A collection of single shot spectra were recorded for each of a number of bunchlengths, alternating with a pair of integrated measurements - one the measurement of bunchlength, the other the measure of the integrated spectrum with the PMT, normalized to the charge at the Faraday cup. The charge at the crest was recorded, as well as the charge just after the gun. The results will be divided into two sections. In the first section, an individual single shot spectrum is analyzed in detail and examined for the presence of the vital features predicted by the theory. In the second section, the sources of error and some related experiments are described.

4.3.1 Analysis and estimate of bunchlength. A sample individual single shot spectrum was singled out for detailed analysis. The accompanying bunchlength measurement performed with the chirped beam technique was 4 ps FWHM. For this particular spectrum, the HES was closed down to a full width of 0.35%, permitting only a very low level of charge passed through (60-120 pC). Although the emittance was not measured explicitly for this bunch, typical number cited by the facility are 2π or 3π mm mrad, and improvement of the beam emittance for the central portion of the beam has been repeatedly observed.

Shown in Figure 1 is the full single shot spontaneous spectrum of a single micropulse, below the 2-D intensity plot as recorded by the intensifier. The wavelength

bin was 1/19 nm per pixel. 12 rows of CCD pixels were added together to reduce the read noise of the CCD chip. The mean noise level was determined from a blank portion of the image and subtracted from the spectrum. Several things are notable about this spectrum. First, fluctuations approach 100%, and the resolution is sufficient that each individual spike is recorded by a group of 10-15 data points. These are features predicted by the theory when resolution is sufficient for a given bunchlength.

As the wavelength bin increases, or multiple pulses are integrated, the spectrum is expected to approach the familiar smooth spectrum of characteristic width greater or equal $1/N_w$. In Figure 2, an integrated result is shown, where the sample spectrum and the 4 consecutively recorded spectra are summed together. Figure 3 contains the sample spectrum plotted with different wavelength bin widths, including 30-pixel binning. In both these sets of data, a smoother spectrum of Gaussian-like shape clearly takes form. Note that the actual spectra may be a little broader than those shown because of an attenuation factor, which was not included.

Bin size post-processing was used to analyze the data in more detail. The residuals to a fit performed to the spectrum as a function of pixel number for the three bin sizes plotted in the previous figure show a clear trend toward reduced fluctuations. The residuals are normalized to the mean value and the regions of the spectrum in which the mean value was low are not included in the analysis. This calculation was repeated for all 30 bin sizes, and the standard deviation was taken for each set. The resulting rms value are plotted as a function of bin size in Figure 4. It is satisfying to find an asymptote at small bin sizes, which is predicted by the theory when the resolution exceeds that required to record the fastest fluctuations associated with a given bunchlength.

The bunchlength may now be estimated using the relation ... The dependence of bunchlength on bin size is predicted to be flat by this theory. When the bin size increases by some factor n, the rms fluctuations decrease by $\sqrt{n}$, and the estimated bunchlength remains the same. The bunchlength estimated from the sample spectrum is shown in Figure 5, plotted against bin size, which shows a constant dependence except at the lowest few bin sizes. This is reasonable for the intensifier broadening measured earlier to be 2.5 pixels. A single shot value of bunchlength (2ps) was estimated from the constant portion of this plot.

At this point in the analysis, cited numbers are estimated within a factor of two or 2π. This is because some straightforward detail work remains to be done, including a check on the fit used to compute the mean value, which can change the final estimated value, particularly if there are small deviations in the sloped region of the spectrum. Also, as we will show in the section to follow, another factor comes from a possible reduction in the bunchlength caused by the high energy slit itself, since the independent measure of bunchlength given by the chirped beam technique does not include any such high energy slit effects.

Systematic measurements of fluctuations with variation in beam bunchlength from less than 1 ps to 8 ps were performed. This data will provide an opportunity to check scaling of the fluctuation-derived bunchlength with that provided by the chirped beam technique.

4.3.2 Sources of error.

Emittance and matching. Emittance measurements cited by the facility are well below what is required for this experiment. The collection angle was limited, ensuring that emissions from less than the diffraction limited spot size would be included. Spot sizes before and after the wiggler looked reasonable. This leads us to believe that the emittance and matching requirements were satisfied. During some runs, the width of the spectrum would increase for an unknown reason to a value much larger than could be explained by inhomogeneous broadening, and the most legitimate analysis is performed using the narrowest, and shortest wavelength spectra. Should there be significant sources of error, the most likely ones are matching such that the spot size be too small and the divergence too large, or misalignment. Both of these effects would tend to reduce the fluctuations and overestimate the bunchlength.

It was important to take a complete family of measurements before a jump in phase at the gun (and therefore a changed bunchlength) occurred and desirable to take a complete systematic scan before the cathode Q.E. changed too much. Therefore, detailed studies of the matching were not done during the first stage of this experiment. The next stage for these measurements is to accompany the fluctuation data with direct evidence of the beam divergence, alignment and other parameters at the wiggler position with the techniques worked on in Chapter 3. Once again, the usefulness of single shot wiggler-based diagnostic techniques is indicated by the improvement in the thoroughness an experimental study could achieve with such instant feedback without degrading the results with measurement delays.

Number of photons. Measurements of the number of photons incident in a given bandwidth using a photodiode confirmed that a sufficient number were incident on at the intensifier photocathode that the fluctuations reported above were not quantum fluctuations. In practice, the most difficult source of a reduction in photons to address was change in the emission broadening from run to run from undetermined origin.

Modification of the bunchlength by the high energy slit. The consequences of a possible modification to bunchlength by the high energy slit are significant both for the results in this chapter and those of the previous chapter. The bunch arriving at the wiggler may be shorter than that measured with the integrated technique and the form of its profile modified. This could cause an increase in the fluctuation level. Furthermore, the possibility that the high energy slit modifies the bunchlength requires a complete rethinking of the emissions vs. charge curve defined by the high energy slit, as mentioned in Chapter 4.

Because the change in bunchlength originates from a velocity chirp on the beam created by the RF curvature at the gun, it is not clear that the high energy slit does not modify the bunchlength. In order to test this hypothesis two tests were performed. The first was to compare the fluctuations for a spectrum centered at the shortest possible wavelengths, and one which was red-shifted. This occurs when the beam is clipped at the high energy slit because of jitter which moves the central portion of the beam to the right or left side of the slit, which may be jitter in central energy, or steering. A comparison showed that the red-shifted estimated bunchlength was smaller than that of the blue

shifted spectrum. For the second test, single shot spectra were taken for two widths of the high energy slit, and one of the spectra performed at the lower charge (smaller width) was analyzed as the sample spectrum above. Both measurements were performed at low charge and current. The charge for the wider high energy slit opening was 300 pC, and the narrower was 60-120 pC. During the same run, at a bunchlength which produced more charge, a slightly superlinear emissions vs. charge scan was recorded. Choosing the data at lower charge simplifies the experimental conditions as much as possible.

To perform the comparison between the two values of the high energy slit a collection of spectra for the HES open to a full width of 0.35% and one for the HES open to double that value were recorded. A substantial reduction was observed in the spectral width when the HES was closed down, indicating a significant improvement in the beam quality. A shift in the central wavelength was also observed. The fluctuational characteristics changed significantly for the widths. All of these significant differences can be seen in Figure 6. A quantitative comparison of the ratio for the two spectra is shown in Figure 7 as a function of bin size, computed as for Figure 5, which defines a ratio of 3:1 in estimated bunchlength using the spontaneous emission model. This confirms that there is a marked difference between the fluctuations when the high energy slit is closed down and when it is open.

One explanation for this observation is a modification of the bunchlength by the high energy slit. Another plausible explanation is that the wavelength shift was caused by the measurement of off-axis emissions, which would be accompanied by a decrease in the rms fluctuation level. A number of sources which could have affected alignment or matching. However, it is important that the alignment and initial optimization was not

performed using the partial beam (HES open to 0.35%), but with the full beam (HES open to 0.7%). If a drift in the phase occurred in between the two measurements, a shift in mean beam energy could occur, as well as alignment and other matching problems and the bunchlength would also change. In light of the observation of superlinear curves under some conditions at the same emission wavelength, two additional alternatives are given. 1.SASE present in the central portion of the beam, where the quality of the beam was better. By closing down the HES, this portion of the beam is favored, resulting in different fluctuation characteristics. 2. A combination of modification to the bunchlength by the high energy slit and some SASE.

Correlations among the electrons. The presence of gain can modify the final value of bunchlength extracted from fluctuation measurements. The presence of gain-induced enhancement in any of the 632 nm data taken with the Magnesium cathode is still an open question. For the specific data selected for the sample spectrum and the high energy slit study, the low charge level is consistent with spontaneous emission only and inconsistent with SASE only. The observed wavelength shift with the closing of the high energy slit together with a very small difference between the resonant on-axis wavelength and the 1 nm filter central wavelength can explain superlinear emissions vs. charge scans very easily given only spontaneous emission. When the hypothesis includes both the bunchlength change and SASE, also taking into account the evidence that the beam quality changes as the slit is closed down and the absence of another measurement of the current density, one can arrive at many forms of the high energy slit scan using handwaving arguments. Calculations are in progress to look for more direct evidence for

correlations among the electrons using the single shot spectral measurements themselves, comparing them under different operating parameters.

Deviation of the bunch temporal profile from Gaussian distribution. Comparison of data with theory has been done assuming a Gaussian temporal distribution of the electron bunch. With the chirped beam technique (a typical example is contained in the paper in Chapter 4) the measured bunch profile deviated from Gaussian in the direction of a square profile. A non-Gaussian profile modifies the fluctuational characteristics.

4.4 Single shot cone measurements and applications

The fluctuation measurements were taken in a new direction: from the spectrum to the spatial profile.

One possible application spatial profile measurements is a test of the listed assumptions. Regarding transverse coherence, a series of narrow bandwidth cones should exhibit a reduction in fluctuations which is related to the diffraction limited spot size at the cone angle. Supporting data has been taken with single shot cones (Figure 8 and Figure 9) which show a marked increase in fluctuations with decrease in cone radius. This effect is directly calculable, and can be used to prove that a sufficiently small collection angle was used for the final spectral measurements. Regarding the assumption of independence of electrons, this scan can be used to test for the presence of either microbunching or SASE gain. Either of these will modify the intensity of the spatial

profile compared with spontaneous emission, the former favoring the off-axis emission and the latter the forward emissions.

The following application has been suggested[15a5]: the extraction of emittance from measurements of fluctuations in the cones. This can be implemented with a single shot cone angle scan. The statistical quantities which describe the fluctuations depend on beam emittance. The limiting case for small emittance occurs when the criterion on emittance and wavelength which ensures good spatial overlap between an electron beam and a Gaussian optical mode is satisfied. The number of transverse modes and the beam emittance are closely related. Fortuitously, a measurement of the width of the narrow bandwidth cones also provides a simultaneous, independent measurement of both the number of transverse modes and the beam divergence for comparison. When the angular profile is measured on-axis, the number of transverse modes on-axis can be calculated by a standard method: it is the ratio of the measured divergence to that of a diffraction limited source of the same wavelength, spot size and location. The estimate of the beam divergence can be obtained from the series of cones by methods developed elsewhere in the thesis.

4.5 Conclusions

The wiggler emissions of a single micropulse were measured with a resolution sufficient to record their fluctuational characeristics in a single shot. The analysis of a sample spectrum reveals features predicted by shot noise theory and a bunchlength of 2

ps was estimated from the rms fluctuation level. Single shot measurements of narrow bandwidth cones in the spatial profile were also performed, showing greater fluctuations at small cone radii, as expected.

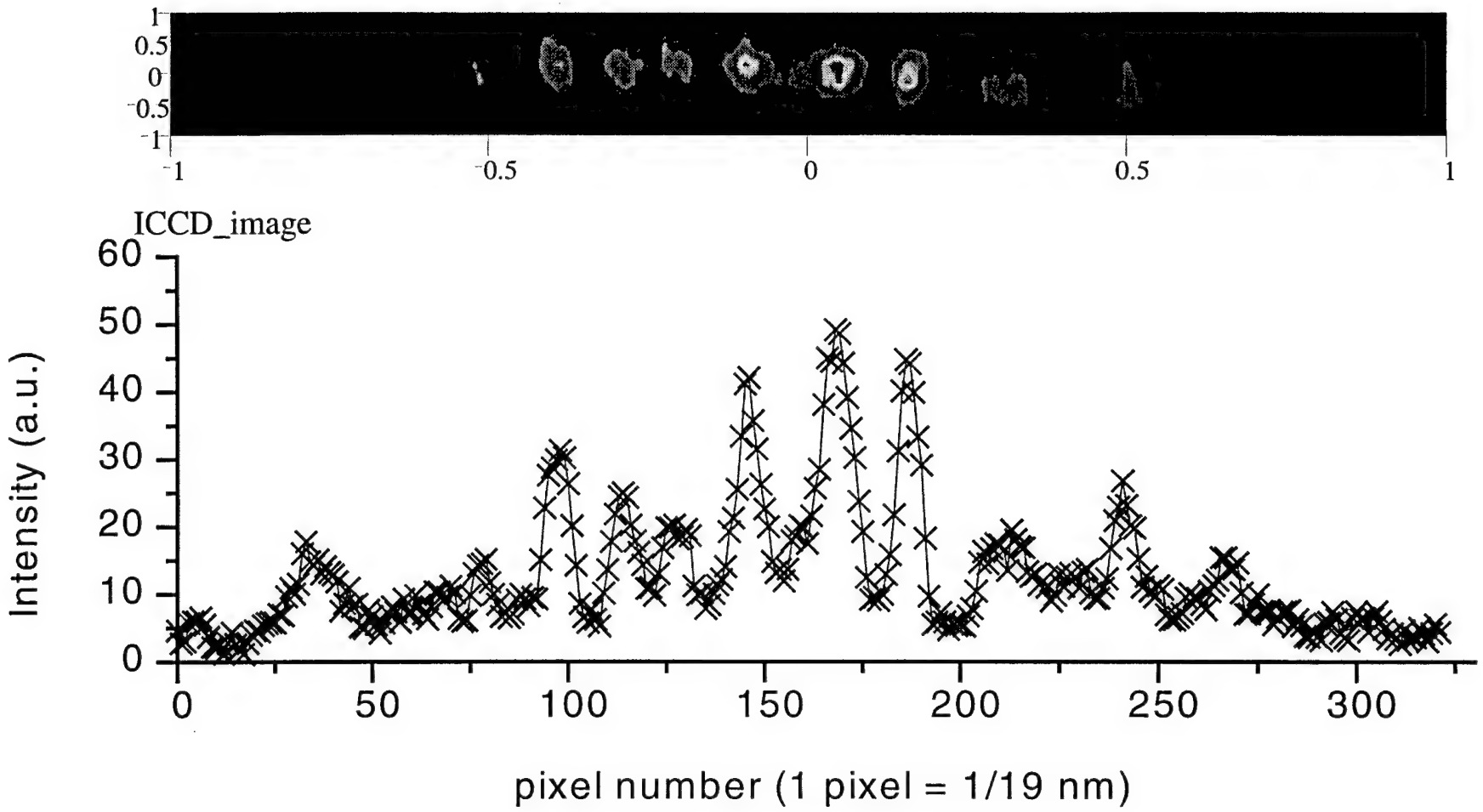

Figure 1. Single shot spectrum of wiggler emissions from a single electron micropulse. *The intensity pattern was recorded with an image intensifier (upper plot) installed at the output port of the spectrometer. In the corresponding spectrum (lower plot), the resolution of 1/19 nm per pixel was sufficient to record each spike in detail.*

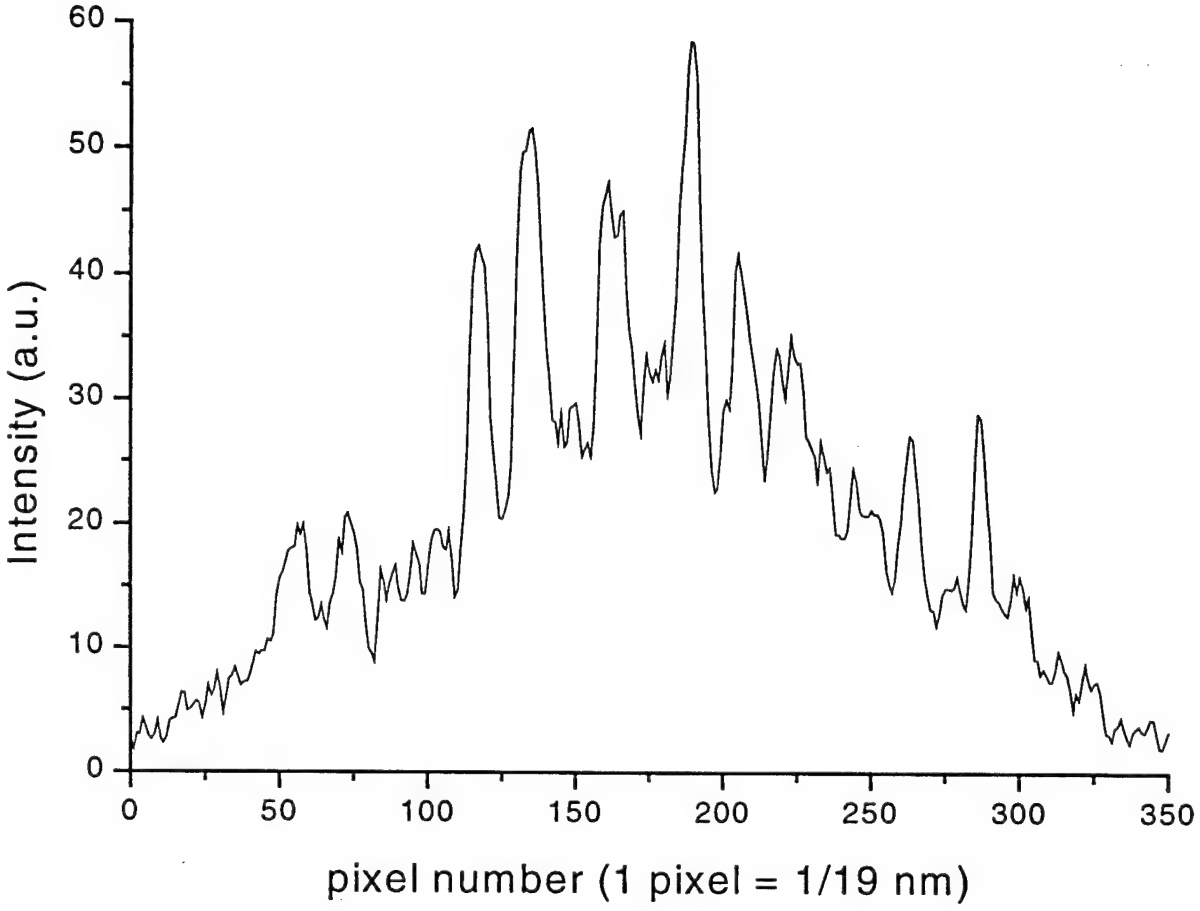

Figure 2. Integrated spectrum formed by summing five consecutive single shot spectra. *The resulting spectrum starts to approach the familiar, smooth wiggler spectrum of width* $>1/N_w$.

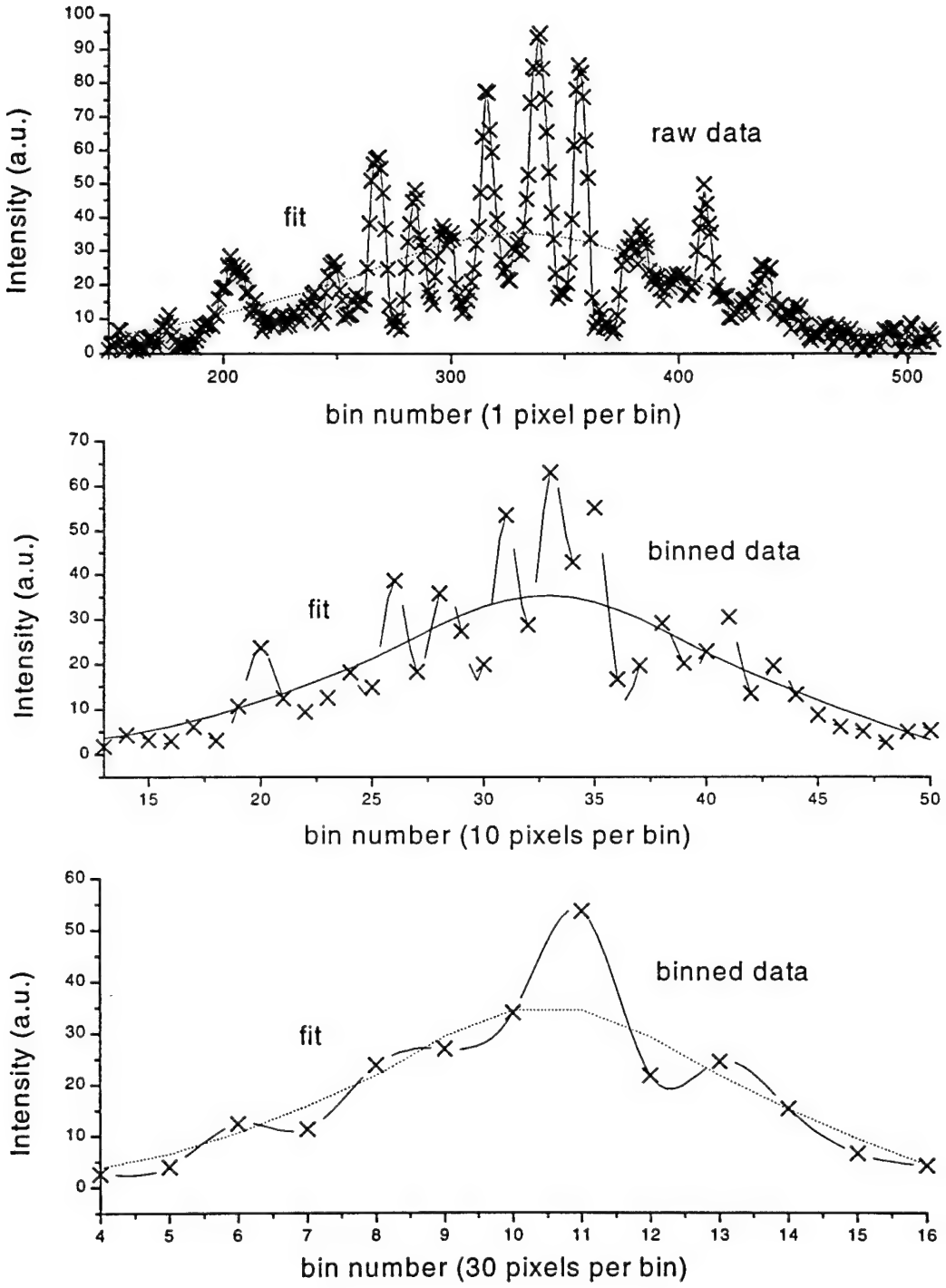

Figure 3. The single shot spectrum, as raw data, and with two different bin-sizes. *With a resolution of 30/19 nm/bin (lowest plot), the post-processed data takes the same shape as the integrated spectrum.*

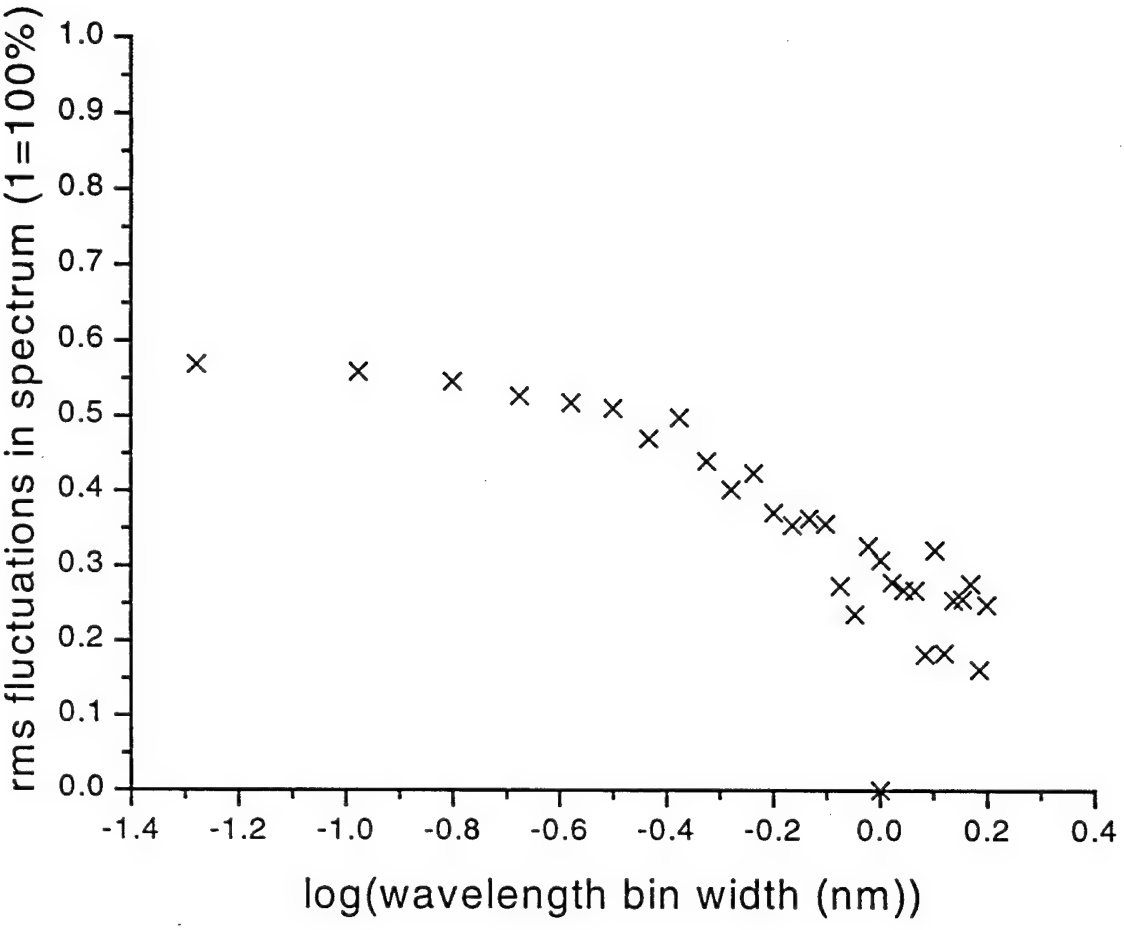

Figure 4. Dependence of rms fluctuations on wavelength bin width. *The log of the bin size in nm ($0 \leftrightarrow 1\,nm$)was taken in order to isolate trends with increasing resolution of measurement. An asymptote is observed, as expected with good resolution, corresponding to σ^2 of about 0.3. One can see the error bar increasing with bin size, as the number of points determining σ^2 decreases.*

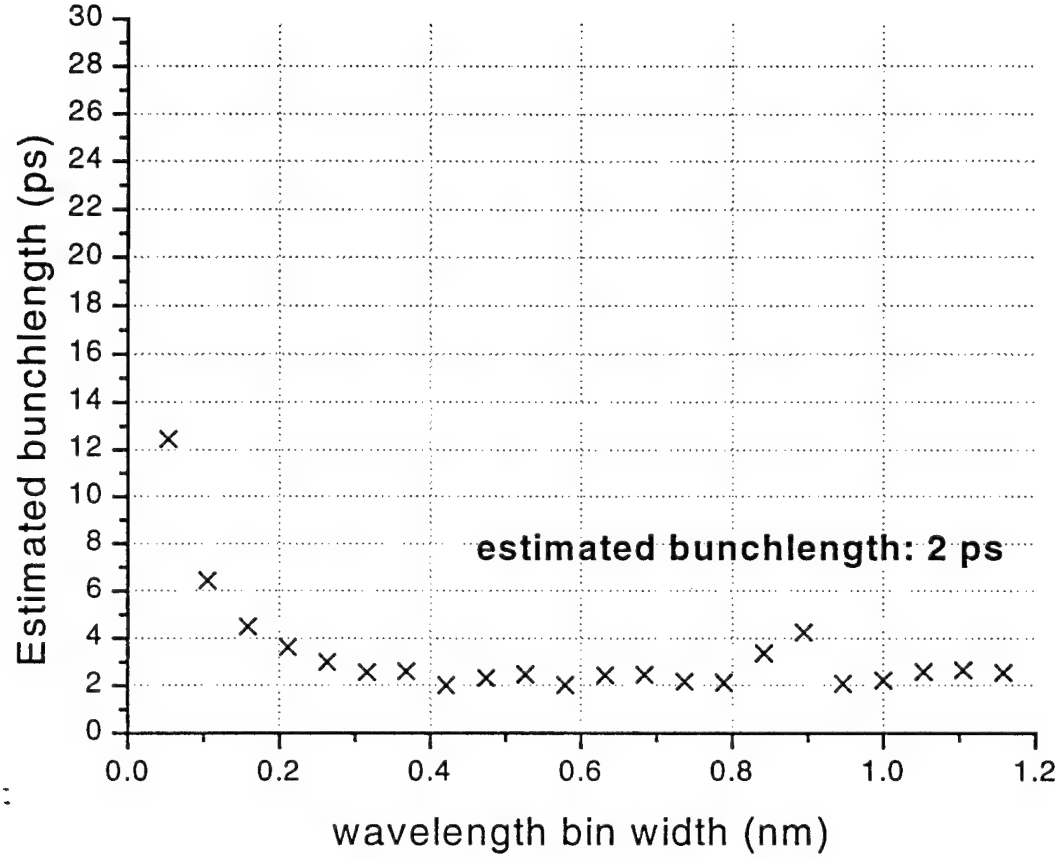

Figure 5. Bunchlength estimated from fluctuation measurements calculated for each wavelength bin size. *For the same single shot spectrum, bunchlength was estimated separately for each bin size from 1 to 22 pixels wide, corresponding to a resolution range of 1/19 nm to 1.2 nm. Bin sizes were limited to those for whom there were at least 10 fluctuation values in order to reduce extraneous error. For resolutions of better than 0.2 nm, the estimated bunchlength is flat with frequency bin, as predicted by theory, and lies at about 2 ps. This is an excellent result.*

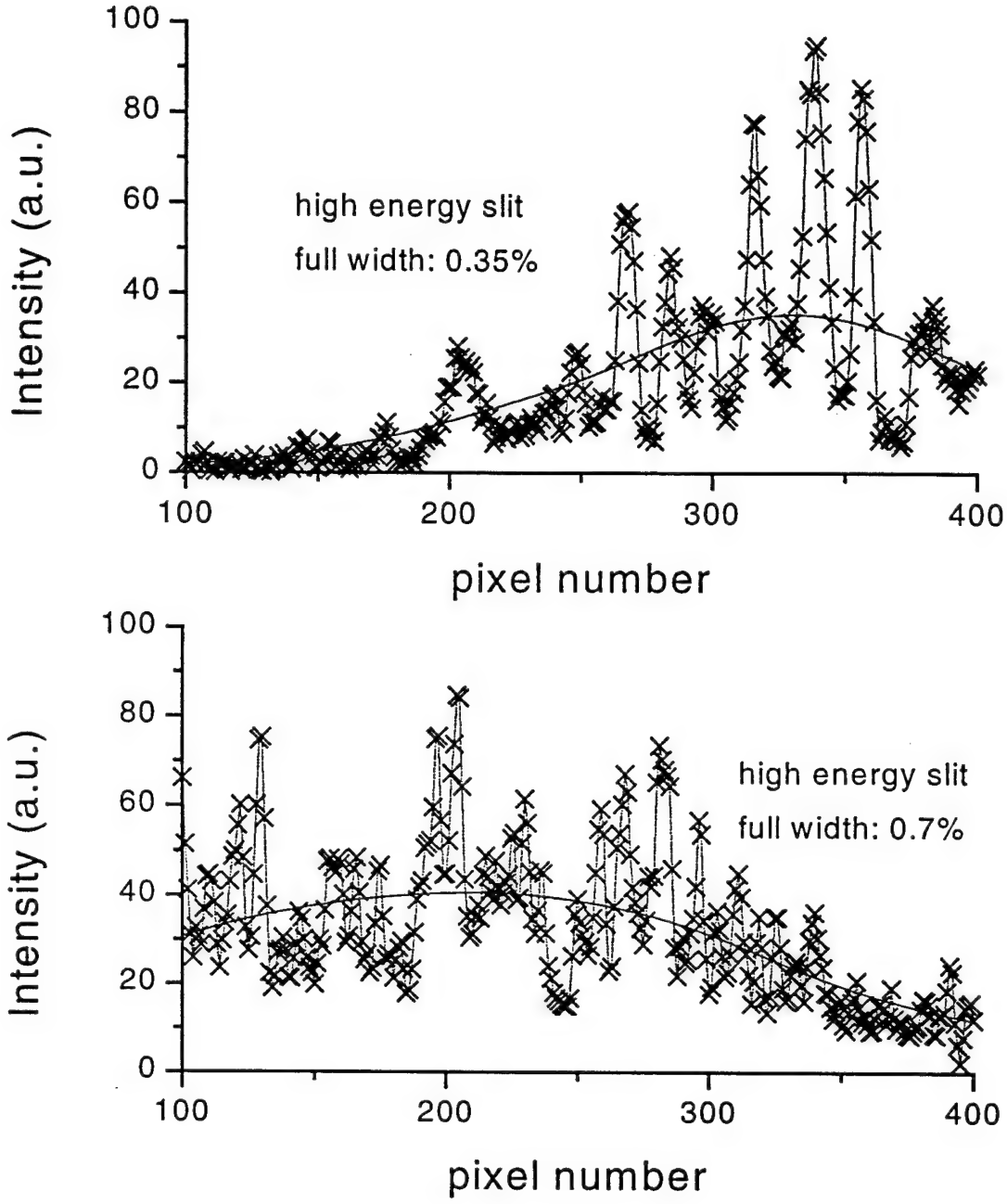

Figure 6. Comparison of single shot spectra for two widths of the high energy slit. *The spectra show a number of features which are important: a change in the fluctuational characteristics, a shift in the central wavelength, and a change in the width of the mean spectrum. Possible consequences are discussed in the text.*

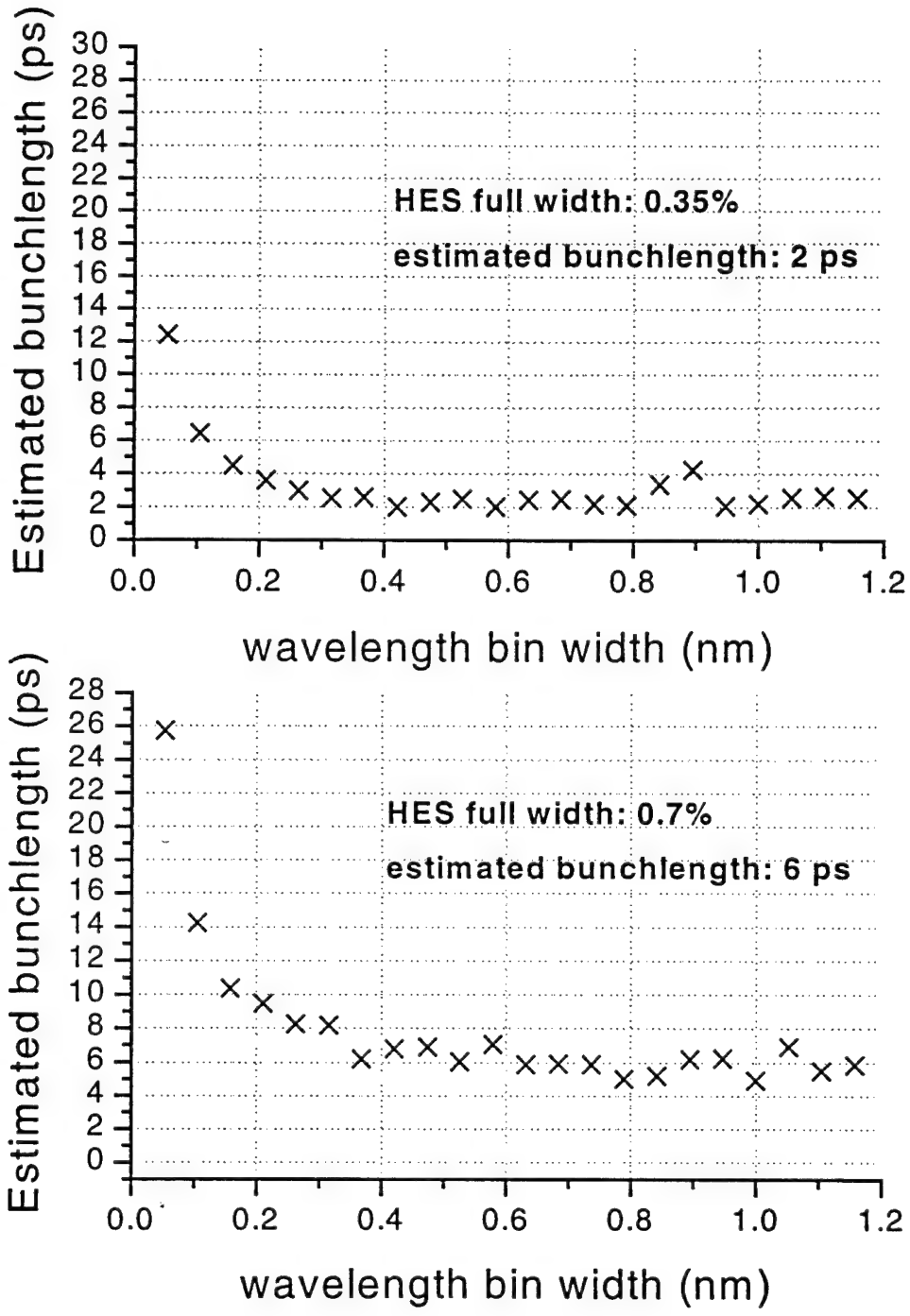

Figure 7. Bunchlength estimated from fluctuations for two widths of the high energy slit. *This calculation quantifies the difference in the fluctuational characteristics observed as a function of high energy slit width.*

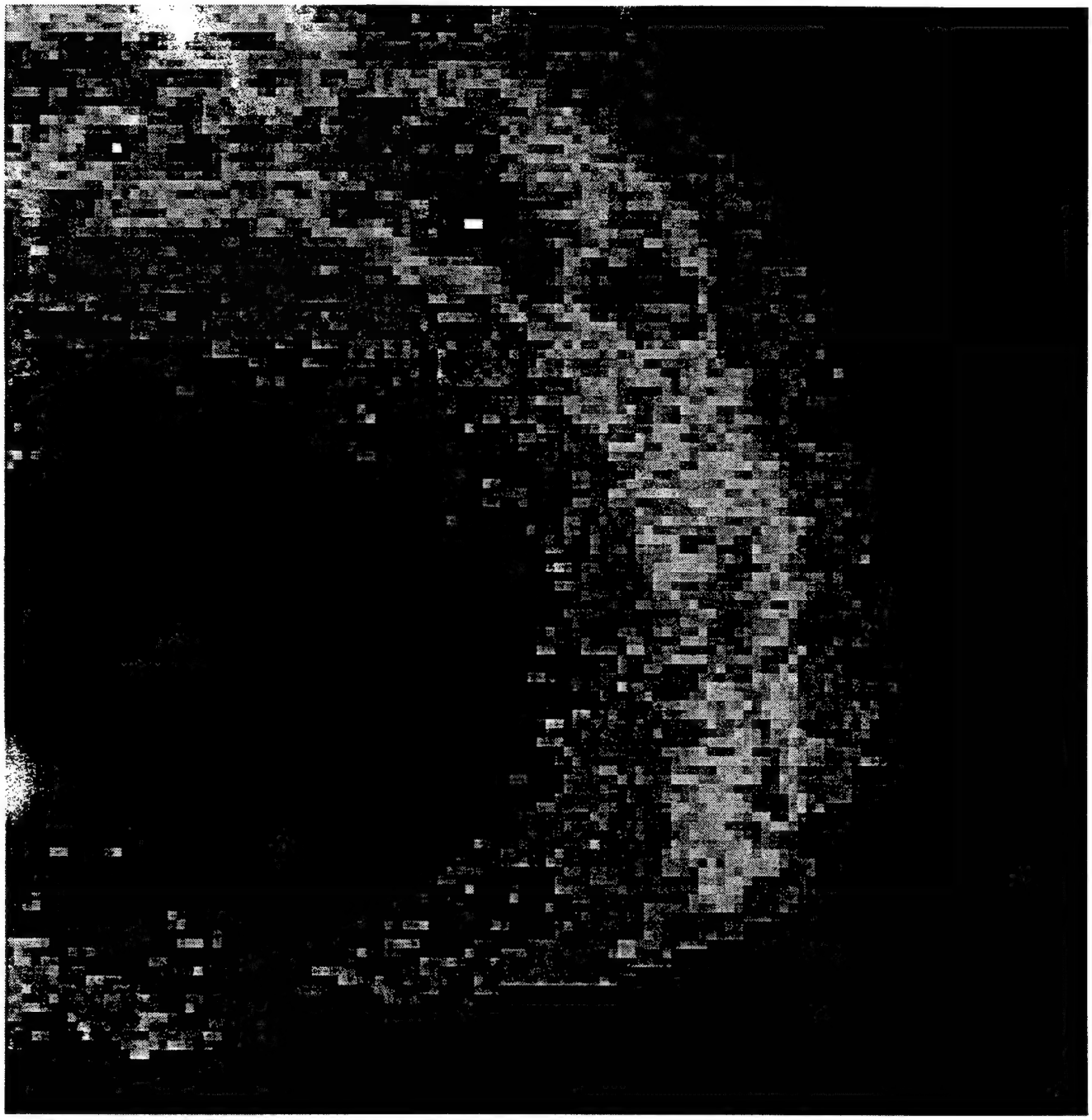

Figure 8. Single shot cone measurement. *Emissions were intercepted by a 1.5 nm bandpass filter at 676 nm, and imaged onto the intensifier with a camera lens focussed at infinity. Note the absence of fluctuations in this large angle cone where the corresponding diffraction limited spot size is small.*

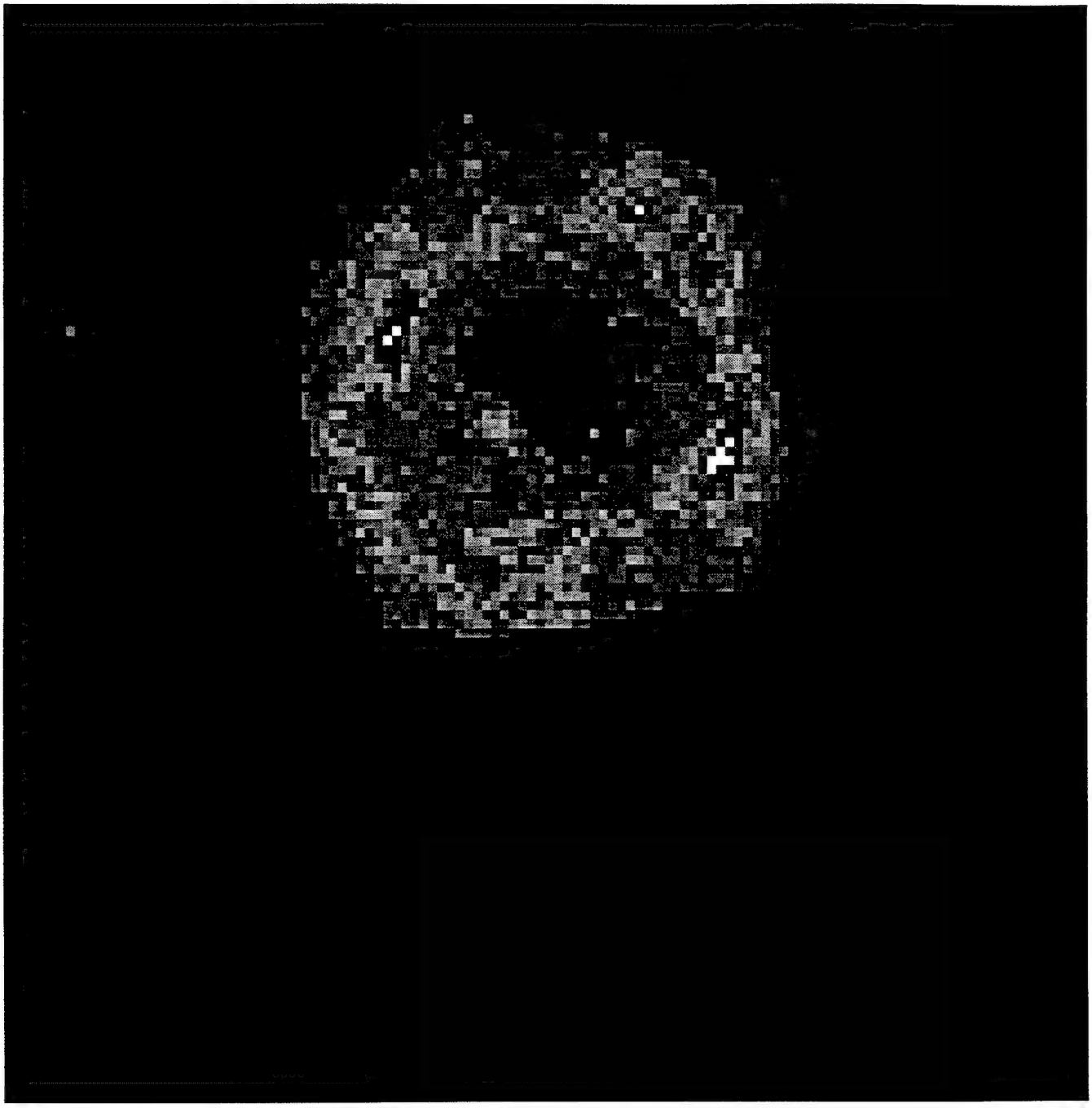

Figure 9. Single shot cone measurement. *Emissions were intercepted by a 1 nm bandpass filter at 632 nm, and imaged onto the intensifier with a camera lens focussed at infinity. Note the appearance of fluctuations in the spatial profile as the cone radial angle decreases and the conditions for transverse coherence are better satisfied.*

References (Chapter 4)

[1] M. S. Zolotorev and G. V. Stupakov, "Fluctuational interferometry for measurement of short pulses of incoherent radiation," SLAC-PUB-7132 (March, 1996)
[2] M. S. Zolotorev and G. V. Stupakov, "Spectral fluctuations of incoherent radiation and measurement of longitudinal bunch profile," submitted to the 1997 Particle Accelerator Conference.
[3] This section is based on discussions with M. Zolotorev (June, 1997) in preparation for the experiment.
[4] X. J. Wang, X. Qiu, and I. Ben-Zvi, "Experimental observation of high-brightness microbunching in a photocathode RF electron gun," *Phys. Rev. E*, **54**(4), pt. A, R3121-4 (1996)
[5] Suggestion from J. Wurtele, October, 1997.

CHAPTER 5: CONCLUSIONS

We have described experiments in non-perturbative electron beam diagnosis using a microwiggler. The MIT microwiggler has an opportunity to contribute in this area because it provides emissions in the visible at 40-55 MeV accompanied by an appropriate combination of field quality, field strength, short period, total length and high long term performance level.

First efforts were devoted to the wiggler itself, building on the success of past work to bring the wiggler to its best level of field quality. We report a field uniformity of ~0.08% in rms peak amplitudes, which is the first time a spread of less than 0.1% has been achieved in any sub-cm period wiggler. It was obtained consistently over two years of extensive demand on wiggler time. Through measurements, this new figure was placed in the full context of the limits of the measurement system, spread in pole integrals, field quality off-axis, and coil-to-coil variations, and exceeded the criteria developed for each of these.

Much of the thesis time was spent on setting up an FEL oscillator experiment in the visible. While startup of the oscillator was not achieved, evidence of self amplified spontaneous emission was obtained at 1064 nm with enhancement of a factor of two over spontaneous emission. Results with a similar form in the visible have proven more complicated to analyze and are still under study.

The need for more comprehensive and less time consuming techniques for beam diagnosis was demonstrated repeatedly during the course of the work. One of the difficult issues to handle in claiming a demonstration of startup was how to model a complex system in which not all of the parameters could be monitored. We describe experiments which provide additional diagnostic information about the beam in single shot measurements with the advantage of reflecting the beam behavior directly at the wiggler position.

Narrow bandwidth Cerenkov cones in the spontaneous emission spatial profile were studied systematically as a function of beam energy, energy spread, wiggler field strength, filter wavelength and misalignment and were found to be sensitive to realistic changes in the machine parameters. Full two-dimensional images of the spatial profile were recorded in a single shot, both for a macropulse containing 20 micropulses and a single micropulse. Analytic expressions were derived for the dependence of the cone width when energy spread is significant, and beam divergence was extracted from a large angle cone in a single shot measurement.

The fluctuational characteristics of the wiggler emissions were recorded in both the spectrum and the spatial profile. Experiments were motivated by a technique proposed in the literature to extract bunchlength information from the fluctuations in the incoherent emissions arising from shot noise on the electron beam. Single shot spectra were measured systematically along with an independent but integrated gauge of beam bunchlength. Features predicted by the theory were found to be present in the experimental data, and a quantitative analysis produced excellent results.

Office of Naval Research

DISTRIBUTION LIST

Charles W. Roberson
Scientific Officer

Code: 1112AI — 3 copies
Office of Naval Research
800 North Quincy Street
Arlington, VA 22217

Administrative Contracting Officer — 1 copy
E19-628
Massachusetts Institute of Technology
Cambridge, MA 02139

Director — 1 copy
Naval Research Laboratory
Attn: Code 5227
4555 Overlook Drive
Washington, DC 20375-5326

Defense Technical Information Center — 2 copies
8725 John J. Kingman Road, STE 0944
Ft. Belvoir, VA 22060-6218